



저작자표시-비영리-변경금지 2.0 대한민국

이용자는 아래의 조건을 따르는 경우에 한하여 자유롭게

- 이 저작물을 복제, 배포, 전송, 전시, 공연 및 방송할 수 있습니다.

다음과 같은 조건을 따라야 합니다:



저작자표시. 귀하는 원저작자를 표시하여야 합니다.



비영리. 귀하는 이 저작물을 영리 목적으로 이용할 수 없습니다.



변경금지. 귀하는 이 저작물을 개작, 변형 또는 가공할 수 없습니다.

- 귀하는, 이 저작물의 재이용이나 배포의 경우, 이 저작물에 적용된 이용허락조건을 명확하게 나타내어야 합니다.
- 저작권자로부터 별도의 허가를 받으면 이러한 조건들은 적용되지 않습니다.

저작권법에 따른 이용자의 권리는 위의 내용에 의하여 영향을 받지 않습니다.

이것은 [이용허락규약\(Legal Code\)](#)을 이해하기 쉽게 요약한 것입니다.

[Disclaimer](#)

이학박사학위논문

말초조직의 에너지대사조절에서  
Cryptochrome 1 (CRY1)의 역할 규명

Roles of Cryptochrome 1 (CRY1) in the regulation of  
energy metabolism in peripheral tissue

2023 년 8 월

서울대학교 대학원

생명과학부

김 예 영

# 말초조직의 에너지대사조절에서 Cryptochrome 1 (CRY1)의 역할 규명

Roles of Cryptochrome 1 (CRY1) in the regulation of  
energy metabolism in peripheral tissue

지도교수 김재범

이 논문을 이학박사 학위논문으로 제출함

2023년 8월

서울대학교 대학원

생명과학부

김예영

김예영의 박사학위논문을 인준함

2023년 8월

위원장 \_\_\_\_\_ (인)

부위원장 \_\_\_\_\_ (인)

위원 \_\_\_\_\_ (인)

위원 \_\_\_\_\_ (인)

위원 \_\_\_\_\_ (인)

**Roles of Cryptochrome 1 (CRY1) in the  
regulation of energy metabolism in peripheral tissue**

**A dissertation submitted in partial fulfillment of  
the requirement for degree of  
DOCTOR OF PHILOSOPHY**

**To the Faculty of the  
School of Biological Sciences**

**At**

**SEOUL NATIONAL UNIVERSITY**

**By**

**Ye Young Kim**

**August, 2023**

**Data Approved**

---

---

---

---

---

---

# ABSTRACT

## **Roles of Cryptochrome 1 (CRY1) in the regulation of energy metabolism in peripheral tissue**

Ye Young Kim

Peripheral clocks are entrained by various external stimuli and play a crucial role in systemic energy homeostasis by regulating physiological rhythms and metabolic processes. Disruption of peripheral circadian clocks is closely associated with metabolic disorders such as obesity, insulin resistance and cardiovascular disease. Recently, it has been reported that circadian rhythm appears to be linked to mitochondrial dynamics to maintain mitochondrial health. Despite this, underlying mechanisms by which molecular clocks contribute to metabolic diseases and regulate mitochondrial homeostasis remain elusive.

In the present thesis study, I have examined the roles of CRY1, which is a core member of the circadian regulator, in the regulation of energy metabolism in peripheral tissue. In chapter one, I have shown that GSK3 $\beta$ -dependent hepatic CRY1 degradation contributes to hyperglycemia through the upregulation of hepatic glucose production. In the liver, I found that elevated hepatic FBXL3, ubiquitin E3 ligase, downregulated hepatic CRY1 protein in diabetic animals, eventually leading to excessive hepatic

glucose production through an increase in FOXO1. Furthermore, in liver of diabetic animals, activated GSK3 $\beta$ -induced CRY1 phosphorylation facilitated FBXL3-mediated CRY1 degradation, resulting in hyperglycemia. These findings suggest that the dysregulation of CRY1 protein stability through the GSK3 $\beta$  -CRY1-FBXL3 axis would be one of the etiological features of diabetic hyperglycemia.

In chapter two, I have demonstrated that CRY1 could exert important roles to maintain mitochondrial fitness in brown adipose tissue (BAT). Upon cold exposure, BAT becomes metabolically active with enhanced mitochondrial activity accompanied by quality control, which might be regulated by CRY1. During cold acclimation, CRY1 knockout (KO) mice showed cold-intolerant phenotypes with decreased mitochondrial contents. In particular, mitophagic flux was enhanced in CRY1-deficient mouse embryonic fibroblast (MEF) and BAT of CRY1 KO mice. Furthermore, restoring CRY1 specifically in BAT rescued the thermogenic activity of BAT of CRY1 KO mice, accompanied by an increase in mitochondrial abundance. These data suggest that CRY1 is a crucial factor in maintaining mitochondrial homeostasis and preserving thermogenic activity in brown adipose tissue.

Together, these findings suggest that the regulation of hepatic glucose production through hepatic GSK3 $\beta$ -dependent CRY1 degradation broadens the understanding of the pathogenesis of diabetes. In addition,

CRY1 in BAT has a novel role in preserving mitochondria fitness for thermogenesis. Therefore, this thesis proposes that circadian regulator CRY1 could function as a key regulator of energy metabolism in metabolic organs such as liver and BAT beyond its canonical function.

**Keyword :** Cryptochrome1, hepatic glucose production, liver, brown adipose tissue, thermogenesis, mitochondria quality control

**Student Number :** 2016-20377



4. Results .....	35
5. Discussion.....	84
<b>CHAPTER TWO : CRY1 participates in mitochondria quality control for thermogenesis in BAT .....</b>	<b>90</b>
1. Abstract.....	91
2. Introduction .....	92
3. Materials and methods .....	94
4. Results .....	101
5. Discussion.....	131
<b>CONCLUSION .....</b>	<b>139</b>
<b>1. CRY1 and hepatic glucose production in diabetes .....</b>	<b>140</b>
<b>2. CRY1 and mitochondrial quality control .....</b>	<b>142</b>
<b>ACKNOWLEDGEMENTS .....</b>	<b>144</b>
<b>REFERENCES .....</b>	<b>145</b>
국문 초록	156

# LIST OF FIGURES

Figure 1. Peripheral clocks coordinate external cues with physiologic output .....	3
Figure 2. Molecular mechanism of mammalian circadian clock .....	4
Figure 3. Hormonal and transcriptional regulation of hepatic glucose production .....	14
Figure 4. Mitochondria quality control in brown adipocyte.....	17
Figure 5. The phenotype of NC-fed and HFCF-fed mice and strategy of CRY1 binding proteins in the liver .....	36
Figure 6. Hepatic CRY1 protein is downregulated in mouse models of diabetes	37
Figure 7. Proteasomal degradation is a determinant of CRY1 protein.....	38
Figure 8. Hepatic FBXL3 interacts with CRY1 .....	41
Figure 9. FBXL3 expression is increased in mouse model of diabetes.....	42
Figure 10. Hepatic FBXL3 promotes polyubiquitination and degradation of CRY1 protein .....	43
Figure 11. FOXO1 target genes are highly expressed in liver of CRY1 KO mice .....	45
Figure 12. FBXL3 overexpression boosts hepatic glucose production with decreased CRY1 protein.....	50
Figure 13. Suppression of FBXL3 represses hepatic glucose production via an increase in CRY1 protein .....	51
Figure 14. <i>in vivo</i> FBXL3 suppression decreases hepatic glucose production ....	52
Figure 15. <i>in vivo</i> FBXL3 knockdown downregulates hepatic glucose production. ....	53
Figure 16. <i>in vivo</i> FBXL3 suppression ameliorates hyperglycemia in diabetic	

animals .....	54
Figure 17. CRY1 phosphorylation level is enhanced in the livers of <i>db/db</i> mice	57
Figure 18. The level of hepatic CRY1 protein is increased by the GSK3 $\beta$ inhibitor.....	58
Figure 19. Enzymatic activity of GSK3 $\beta$ is augmented in diabetic animals.....	59
Figure 20. GSK3 $\beta$ involves in CRY1 phosphorylation.....	60
Figure 21. CRY1 protein degradation is suppressed by GSK3 $\beta$ inhibitors.....	61
Figure 22. CRY1 phosphorylation by GSK3 $\beta$ facilitates FBXL3-mediated ubiquitination .....	62
Figure 23. GSK3 $\beta$ phosphorylates CRY1 protein at S280.....	65
Figure 24. GSK3 $\beta$ induces CRY1 phosphorylation at S280/S281 residues.....	66
Figure 25. GSK3 $\beta$ -induced CRY1 phosphorylation potentiates protein degradation.....	67
Figure 26. GSK3 $\beta$ -induced CRY1 phosphorylation promotes FBXL3-dependent polyubiquitination .....	68
Figure 27. GSK3 $\beta$ suppression downregulates hepatic glucose production with increased CRY1.....	70
Figure 28. Inhibition of GSK3 $\beta$ downregulates CRY1-mediated gluconeogenesis .....	71
Figure 29. GSK3 $\beta$ -induced CRY1 phosphorylation elevates hepatic glucose production .....	74
Figure 30. GSK3 $\beta$ modulates hepatic glucose production through FBXL3-dependent CRY1 degradation.....	75
Figure 31. CRY1 deficiency leads to glucose intolerance.....	77

Figure 32. CRY1 knockout mice exhibit elevated hepatic glucose production....	78
Figure 33. GSK3 $\beta$ inhibitors do not largely affect body weights .....	80
Figure 34. Increase in CRY1 protein by GSK3 $\beta$ inhibitors mitigates hyperglycemia in diabetic mice.....	81
Figure 35. GSK3 $\beta$ inhibitor mitigates hyperglycemia in diabetic animals .....	82
Figure 36. <i>in vivo</i> GSK3 $\beta$ suppression reduces hepatic glucose production in diabetic mice .....	83
Figure 37. Graphical summary of chapter one.....	89
Figure 38. Deficiency of CRY1 in BAT results in morphological mitochondrial defects .....	103
Figure 39. Deficiency of CRY1 in BAT decreases expression of mitochondrial proteins and mitochondrial contents. ....	104
Figure 40. Deficiency of CRY1 shows reduced OXPHOS protein abundance and mitochondrial contents in various tissues.....	105
Figure 41. MEF cells are established from WT and CRY1 KO mouse embryos .....	107
Figure 42. CRY1-deficient MEF shows downregulated OXPHOS and mitochondrial proteins abundances and mitochondrial contents .....	108
Figure 43. CRY1 deficiency in MEF is associated with dysfunctional mitochondria. ....	109
Figure 44. CRY1-deficient MEF exhibits defective mitochondrial function.....	110
Figure 45. Mitochondrial biogenesis gene expression in MEF is comparable between WT and CRY1 KO.....	112
Figure 46. CRY1 deficiency in MEF is associated with induced mitophagy ...	114
Figure 47. CRY1 deficiency in MEF is associated with induced mitophagy.....	115

Figure 48. In BAT, the expression of CRY1 is increased by cold exposure.....	117
Figure 49. In iWAT, the expression of CRY1 is increased by cold exposure.....	118
Figure 50. CRY1 KO mice show impaired heat generation.....	120
Figure 51. CRY1 KO mice exhibit decreased energy expenditure upon $\beta$ -adrenergic agonist CL316,243 injection .....	121
Figure 52. Thermogenic gene expression in BAT is comparable between WT and CRY1 KO.....	122
Figure 53. In BAT, deficiency of CRY1 decreases expression of mitochondrial proteins and mitochondrial contents after cold exposure.....	124
Figure 54. Deficiency of CRY1 in brown adipose tissue shows morphological defects in mitochondria upon cold exposure.....	125
Figure 55. PINK-Parkin pathway is activated in BAT of CRY1 KO mice after cold exposure .....	126
Figure 56. Mice with BAT-specific CRY1 overexpression potentiates thermogenic capacity.....	128
Figure 57. Mice with BAT-specific CRY1 overexpression exhibit increased mitochondrial contents and protein abundance.....	129
Figure 58. BAT-specific CRY1 restoration results in enhanced heat generation and mitochondria DNA contents.....	130
Figure 59. BAT-specific CRY1 OE increases mitochondrial protein abundance.....	131
Figure 60. CRY1 deficiency downregulates the ability to perform the exercise .....	136
Figure 61. CRY1 is enriched to mitochondria upon cold and $\beta$ -adrenergic stimulation.....	137
Figure 62. Graphical summary of Chapter Two .....	138



# LIST OF TABLES

Table 1. Metabolic phenotype of clock gene knock out mice .....	8
Table 2. Primers used for qRT-PCR in chapter one.....	32
Table 3. List of the putative binding proteins of CRY1 .....	39
Table 4. NP score of candidate genes in liver of CRY1 KO mice compared to WT .....	46
Table 5. Primers used for qRT-PCR in chapter two .....	101

# BACKGROUNDS

## 1. Circadian regulator and metabolism

### 1) Circadian clock

Circadian clocks regulate internal physiological rhythms and molecular processes throughout day and night cycle [1]. In mice, 43% of all protein-encoding genes exhibit circadian rhythms in the level of transcription somewhere in the body, predominantly in a tissue-specific manner [2]. The mammalian circadian molecular clocks consist of suprachiasmatic nucleus (SCN) located in hypothalamus, known as the central clock, as well as peripheral clocks found in numerous tissues such as liver, adipose tissue, muscle, intestine, and pancreas [3-5]. A range of 5% to 20% of tissue-specific genes are estimated to exhibit an oscillatory expression profile, which underscore the circadian control over the function of peripheral tissues [6-9]. The rhythmic signal produced by molecular clock has a period of approximately 24 hours, which is a circadian period. While central clock is primarily regulated by light, peripheral clock is also affected by hormonal signals (such as insulin, glucagon, melatonin, and cortisol), changes in body temperature, feeding/fasting cycle, and physical activity [10-12]. Also, many rhythmic genes in peripheral tissue are participate in their own physiological functions (Figure 1).

Central feature of circadian rhythm is dependent on transcription-translation coupled auto-regulatory negative feedback loops; BMAL1 (also

known as ARNTL), CLOCK (its orthologue NPAS2), Period (PER1, PER2 and PER3), and cryptochrome (CRY1 and CRY2) are core clock molecules that produce rhythmic oscillations in a cell-autonomous manner [13]. The transcription factors BMAL1 and CLOCK promote the expression of PER and CRY genes, which acts as transcriptional repressor complex to suppress the activity of BMAL1 and CLOCK, resulting in negative feedback regulation (Figure 2). Additionally, BMAL1 and CLOCK promote the expression of the orphan nuclear-receptor REV-ERB $\alpha$  (NR1D1, nuclear receptor subfamily 1 group D member 1) which negatively regulates BMAL1 transcription [13]. ROR $\alpha$  (retinoic acid receptor-related orphan receptors), a BMAL1 transcription activator, competes with REV-ERB $\alpha$  for BMAL1 binding elements [14]. In addition to transcriptional regulation, all these molecular clocks are regulated by post-translational modifications to finely tune rhythmicity and in turn trigger multiple responses in the cells [15].

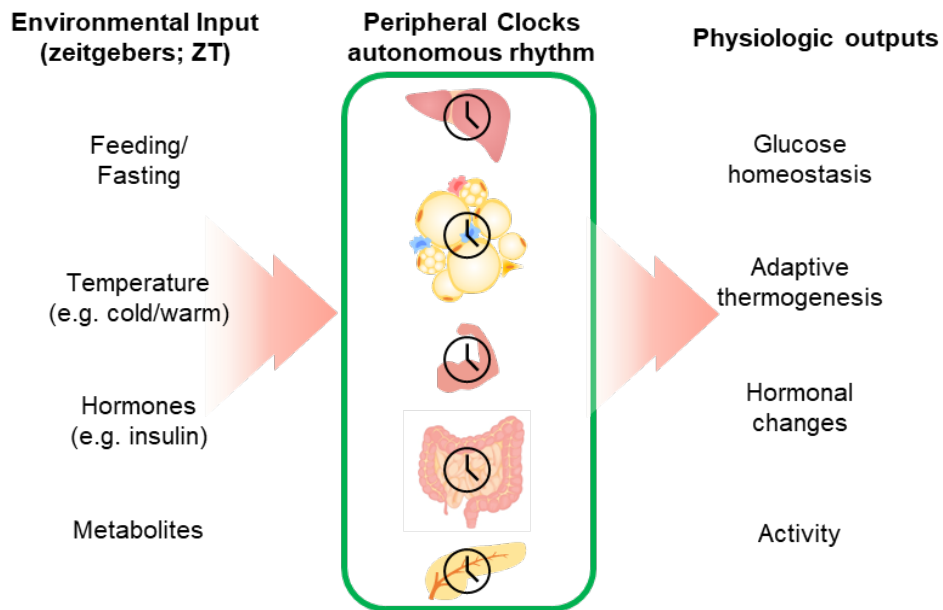


**Figure 1. Peripheral clocks coordinate external cues with physiologic output**

Peripheral clocks in liver, adipose tissues, muscle, gut, and pancreas, are entrained by various environmental cues such as nutrient cycles (feeding/fasting), changes in temperature, and hormones. Outputs of these peripheral clocks include glucose and lipid homeostasis, thermogenesis, and physical activity.

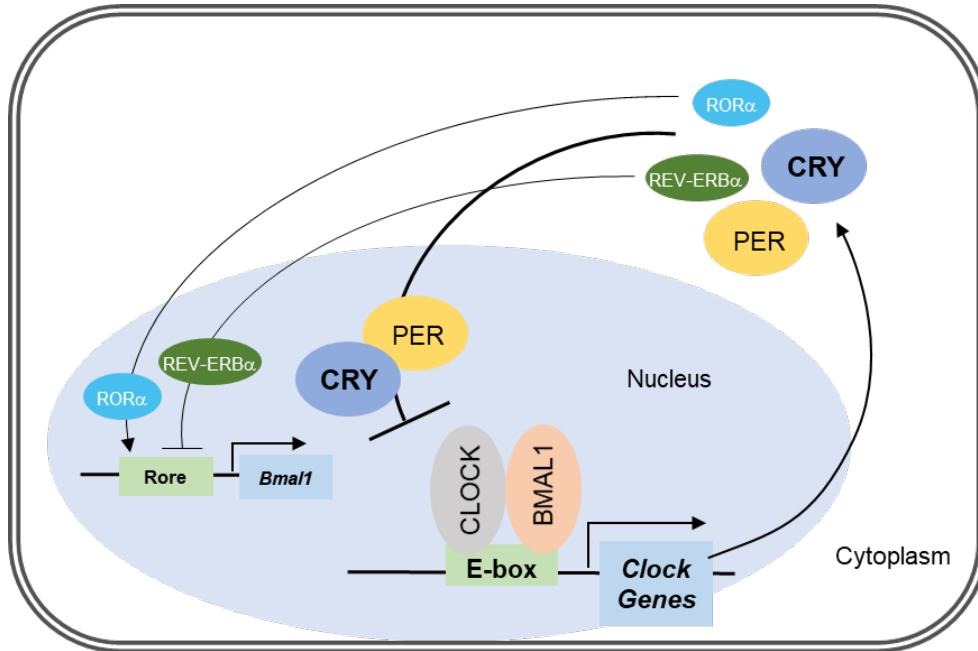


**Figure 2. Molecular mechanism of mammalian circadian clock**

Transcriptional-translational feedback loops of core clock genes. CLOCK and BMAL1 dimerize and activate transcription of other clock genes including CRY, PER, REV-ERB $\alpha$ , ROR $\alpha$ . After transcription of these clock genes they are translationally released in the cytoplasm. PER and CRY proteins heterodimerize and translocate back to nucleus to inhibit the transcription of their own genes by binding to BMAL1 and CLOCK. ROR $\alpha$  and REV-ERB $\alpha$  play a regulatory role in fine-tuning the expression of Bmal1. ROR $\alpha$  activates the expression of Bmal1, while REV-ERB $\alpha$  represses its expression.

## 2) Peripheral clock and metabolism

Besides serving as circadian regulators, peripheral circadian clocks serve as a crucial factor for metabolic homeostasis and their disruptions are associated with metabolic disorders, including obesity, diabetes, and cardiovascular disease [16]. For example, numerous knockout mice lacking clock genes exhibit various metabolic disorders (Table 1) [17, 18]. In humans, misalignment of circadian clock due to several factors such as shift work, eating at night, and social jet lag has been correlated with metabolic syndrome [19].

In liver, circadian rhythm is highly influenced by timing of food consumption, as alteration of the daily feeding pattern can cause an uncoupling from the central clock [20]. Clock genes in liver regulate several pathways involved in the control of glucose and lipid metabolism, as revealed by multi-omics data [9, 21]. In rodents, liver clock is essential for glucose homeostasis through controlling hepatic glucose production and glucose export [22, 23]. For instance, BMAL1 facilitates rhythmic glucose export in liver by modulating diurnal expression pattern of glucose transporter 2 (Glut2) [23]. Furthermore, clock genes in liver contribute to regulation of hepatic glycogen contents, insulin sensitivity, and mitochondrial dynamics [24]. During fasting, clocks in liver are involved in regulating the oxidation of glucose and fatty acids in mitochondria, thereby safeguarding liver from oxidative stress[25, 26]

In white adipose tissue (WAT), circadian clock is also entrained by

food intake [27]. WAT clock regulates diurnal insulin responses through retinol-binding protein receptor (RBP)/stimulated by retinoic acid 6 (STRA6) signaling axis [28]. CLOCK and BMAL1 modulate expression of key enzymes in the regulation of lipolysis such as adipose triglyceride lipase (ATGL), lipoprotein lipase (LPL) and hormone-sensitive lipase (HSL) [29, 30]. In addition, WAT and BAT in human and rodents have circadian rhythmicity in glucose uptake [31, 32].

Recent studies have shown a correlation between circadian rhythm and mitochondrial function [33, 34]. For example, various aspects of mitochondrial biology, including its contents, dynamics, and functions such as respiration, ATP production, and reactive oxygen species (ROS) production are regulated by circadian rhythms [35]. In addition, circadian gene knockout mice display disrupted rhythmicity in the expression of genes involved in mitochondrial dynamics, leading to perturbations in the rhythms of ATP synthesis and mitochondrial respiration. In this aspect, BMAL1 is involved in transcriptional regulation of several mitochondrial genes, including mitofusin 1 (MFN1), optic atrophy 1 (OPA1), mitochondrial fission 1 protein (Fis1), and PTEN induced kinase 1 (PINK1) [25, 36]. Mitochondrial dynamics through phosphorylation and activation of dynamin-related protein 1 (DRP1) are regulated in a circadian-dependent manner [35]. DRP1 also influences circadian rhythms and contributes to mitochondrial network retrograde signals to the molecular core clocks [35]. Moreover, mitochondrial lipids, proteins, and metabolites show circadian

oscillations [37-39]. The circadian clock-mediated biosynthesis of nicotinamide adenine dinucleotide (NAD<sup>+</sup>) facilitates sustained sirtuin (SIRT) activity, which impacts mitochondrial function and cellular metabolism [40]. Conversely, availability of NAD<sup>+</sup> and SIRTs determines the functionality of peripheral clock, enabling precise adjustments to the metabolic state in accordance with circadian rhythms [41, 42]. Although many studies have suggested that changes in mitochondrial morphology and function exhibit circadian rhythms, the underlying mechanisms by which the molecular clocks regulate these changes are largely unclear.

**Table 1. Metabolic phenotype of clock gene knock out mice**

Mouse model	Body weight	WAT weight	Plasma Glucose	Glucose tolerance	Plasma Insulin	Insulin sensitivity	Plasma lipid	Ref.
<i>Clock<sup>mut</sup></i>	Normal	Normal	Decreased			Increased		[22]
<i>Clock<sup>mut</sup></i>	Increased		Increased		Normal		Increased	[43]
<i>Clock<sup>mut</sup></i>	Decreased		Normal		Normal		Decreased	[44]
<i>Clock<sup>Δ19/Δ19</sup></i>	Normal		Normal	Decreased	Decreased	Increased	Decreased	[45]
<i>Clock<sup>Δ19/Δ19</sup></i>			Increased	Decreased	Decreased	Normal		[46]
<i>Clock<sup>Δ19/Δ19</sup></i>	Increased	Increased					Decreased	[47]
<i>Bmal<sup>-/-</sup></i>						Increased	Increased	[22]
<i>pancreas-specific Bmal1 knockout mice (pdxCre Bmal1<sup>fl/fl</sup>)</i>					Decreased			[46]
<i>Bmal<sup>-/-</sup></i>	Decreased	Increased	Normal	Normal	Decreased	Normal	Normal	[48]
<i>Hepatocyte-specific Bmal1 knockout mice (AlbCre Bmal1<sup>fl/fl</sup>)</i>		Normal	Decreased	Decreased	Normal	Normal		[23]
<i>Adipocyte specific Bmal1 knockout mice (AdnCre - mal1<sup>fl/fl</sup>)</i>	Increased	Increased	Increased		Normal	Normal	Increased	[49]
<i>Per2<sup>-/-</sup></i>	Decreased	Decreased					Decreased	[50]
<i>Per2<sup>Brdm1</sup></i>			Decreased					[51]
<i>Per2<sup>-/-</sup></i>				Increased	Increased	Increased		[52]
<i>Per2<sup>Brdm1</sup></i>	Normal		Decreased	Normal		Normal	Decreased	[53]
<i>Cry1/Cry2<sup>-/-</sup></i>			Increased	Decreased	Normal	Normal		[54]
<i>Cry1/Cry2<sup>-/-</sup></i>	Decreased		Normal		Normal			[55]
<i>Cry1<sup>-/-</sup></i>	Normal		Increased	Increased		Decreased		[56, 57]
<i>Rev-erba<sup>-/-</sup></i>			Increased				Decreased	[58]
<i>Rev-erba<sup>-/-</sup></i>	Normal	Increased	Increased	Normal		Normal	Decreased	[59]

### **3) Roles of Cryptochrome 1 (CRY1)**

Mammalian CRY proteins, CRY1 and CRY2, are core clock repressor that, along with PER, determines circadian periodicity and degradation of PER and CRY affects period length [60-62]. Compared to PER, CRY exhibit a higher binding capacity to genomic sites, and many of which are independent of CLOCK-BMAL1 and contain DNA-binding motifs for nuclear receptors [63]. In mammals, CRY1 and CRY2 (at least, one of these) are necessary for a circadian rhythm because loss of both results in arrhythmicity. CRY1 knockout mice exhibit short circadian periods whereas CRY2 knockout shows long periods [64]. In mouse liver ChIP-seq data, CRY2 occupancy peaks at circadian time (CT) 16, coinciding with PER-mediated repression, while CRY1 binding peaks at CT 0. In addition, there are subtle tissue-specific and target-specific effects on transcription. For example, CRY1 results in widespread transcriptional repression, while CRY2 has minimal effects in liver and more pronounced effects in the cerebellum [65]. Moreover, CRY1 exhibits a larger number of uniquely bound sites compared to CRY2 [63]. Although the N-terminal domain of CRY1 and CRY2 are well-conserved photolyase homology regions, which are similar to photolyases, the C-terminal tails of these are highly divergent [66-68], resulting in functional diversity and their distinct roles in transcriptional complexes.

While major function of CRY1 is associated with circadian clock, recent studies have suggested that there would be additional roles in

mammalian CRY1. For example, CRY1 is involved in diverse cellular processes including energy metabolism, cell proliferation, cell cycle progression, cancer cell metabolism, and inflammatory response [69, 70]. CRY1 binds and suppresses adenylyl cyclase, resulting in PKA-dependent NF- $\kappa$ B activation and increasing expression of inflammatory cytokines [71]. Furthermore, the autophagic degradation of CRY1, facilitated by two functional LIR motifs, enables its interaction with LC3 and allows it to be degraded by autophagy, which helps regulate glucose metabolism [72].

It is likely that CRY1 exerts a pivotal influence on maintaining energy homeostasis in metabolic organs, such as liver and pancreas. Hepatic CRY1 represses hepatic glucose production by the interaction with the glucocorticoid receptor and/or with G protein-coupled receptor signaling [73, 74]. In addition, insulin-mediated suppression of hepatic glucose production is dependent upon CRY1-mediated forkhead box O1 (FOXO1) degradation in liver [56]. In addition, mutant CRY1 transgenic mice show  $\beta$  cell dysfunction, resulting in hyperglycemia and impaired glucose tolerance [75].

## **2. Glucose metabolism in liver**

### **1) Liver as a regulator of glucose homeostasis**

Given that glucose is the primary energy source for most organs, the tight regulation of glucose homeostasis is crucial to meet the metabolic demands in numerous tissues. For example, liver has a major role in the

control of glucose homeostasis by controlling various pathways of glucose metabolism, including glucose uptake and storage through glycogenesis, glycogenolysis, glycolysis and gluconeogenesis [76]. In the postprandial state, glucose derived directly from the diet is stored in liver as glycogen and is processed into diverse metabolic byproducts. In contrast, during fasting, liver actively releases glucose through glycogenolysis and gluconeogenesis to maintain adequate blood glucose levels for systemic homeostasis [77].

## **2) Hepatic glucose production**

Hepatic glucose production is one of the key metabolic processes to maintain systemic glucose homeostasis. Under fasting periods, liver provides glucose as a primary fuel for other tissues through synthesizing and releasing it via glycogenolysis and gluconeogenesis. In humans, glycogenolysis occurs within 2~6 hours after a meal, and gluconeogenesis has greater importance for prolonged fasting [78]. Despite being an anabolic process, gluconeogenesis needs to occur during starvation in order to continuously supply glucose to brain and red blood cells. In addition, hepatic glucose production is tightly regulated for adequate blood glucose levels, and excessive hepatic glucose production is a causative factor of hyperglycemia in diabetes.

Hepatic gluconeogenesis is an important metabolic process that synthesizes glucose from lactate, amino acids, or glycerol, and the required

ATP is supplied through beta-oxidation. Hepatic gluconeogenesis is regulated by several key rate-limiting enzymes, including phosphoenolpyruvate carboxykinase 1 (PEPCK) and glucose-6-phosphatase (G6Pase) [79]. PEPCK generates phosphoenol pyruvate (PEP) through oxidization of malate to oxaloacetate. G6Pase catalyzes glucose 6-phosphate, which is the final step of gluconeogenesis. These enzymes have been considered as the potential to be therapeutic targets against type 2 diabetes by regulating hepatic glucose production.

### **3) Transcriptional regulation of hepatic glucose production**

The rate of gluconeogenesis is modulated principally by expression of gluconeogenic enzyme genes through major transcriptional factors including FOXO1, cAMP response element binding protein (CREB), and hepatic nuclear factor 4 (HNF4). These transcription factors are upregulated by glucagon and glucocorticoids upon fasting, exercise, and hypoglycemia [80]. In addition, peroxisome proliferator-activated receptor  $\gamma$  (PPAR $\gamma$ ) coactivator-1 $\alpha$  (PGC-1  $\alpha$ ) acts as an inducer of gluconeogenesis via enhancing gluconeogenic transcription factors under fasting conditions. On the contrary, insulin inhibits the activity of FOXO1, which is a major mechanism for suppressing gluconeogenesis by insulin action [81]. In response to insulin, FOXO1 activity is modulated by several post-translational modifications, including deacetylation by histone deacetylases (HDACs) and Akt-mediated phosphorylation and subsequent

polyubiquitination and degradation in response to insulin [82, 83] (Figure 3).

Type 2 diabetes is characterized by high fasting glucose level, which is primarily caused by increased rate of hepatic glucose production. In particular, suppressed insulin action in liver leads to dysregulation of gluconeogenesis, resulting in hyperglycemia [84-87]. In diabetic animals, hepatic FOXO1 is elevated, accompanied by increased gluconeogenic gene expression [88, 89]. However, the underlying mechanisms by which factors contribute to failure of insulin action to repress FOXO1-mediated hepatic gluconeogenesis have not been largely understood yet.

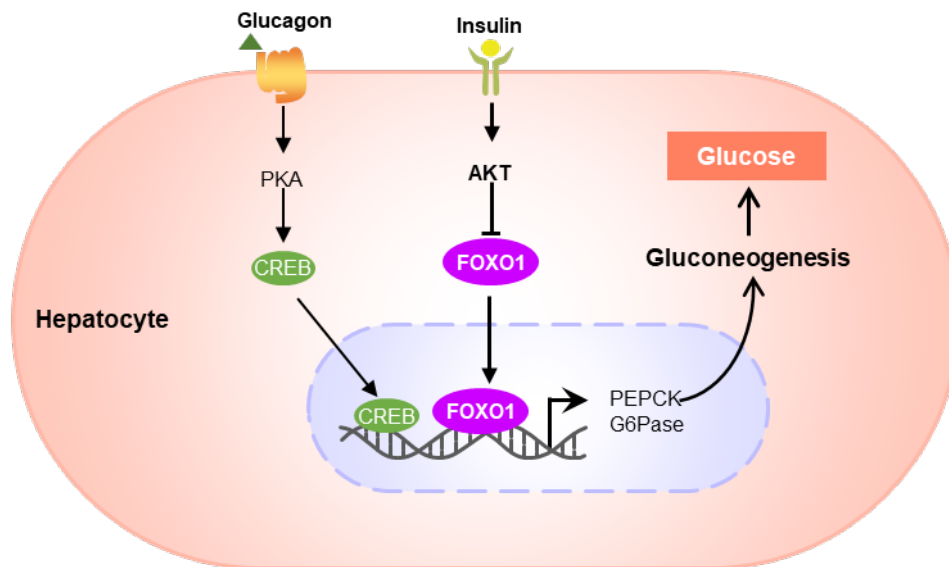


**Figure 3. Hormonal and transcriptional regulation of hepatic glucose production**

Upon fasting, hepatic glucose production is enhanced by upregulated transcriptional factors such as FOXO1 and CREB. In the postprandial state, insulin-Akt axis potently inhibits FOXO1 activity and promotes its degradation, resulting in the suppression of hepatic glucose production.

### **3. Brown adipose tissue (BAT)**

#### **1) BAT as a regulator of energy homeostasis**

Adipose tissue is the major organ for systemic energy homeostasis. WAT is responsible for storing excess energy in the form of triglycerides, while BAT is specialized in the dissipation of stored energy sources through heat production to keep body temperature and energy consumption [90-92]. In particular, heat production from BAT is important for small animals and neonates, which require more heat to survive due to their large surface-to-volume ratio and hibernation of animals. By combusting large amounts of lipids and glucose, activation of BAT is able to improve glucose homeostasis and insulin sensitivity and potentially decreases obesity in obese and diabetic animals [93, 94].

#### **2) Characteristics of mitochondria in BAT**

Mitochondria are a crucial intracellular organelle for energy production but also are closely associated with diverse cellular processes by regulating their abundance, morphology, and remodeling their organization and distribution [95-98]. Recent studies have shown that mitochondria are closely associated with adipocyte biology and their numerous functions including adipogenesis and lipid metabolism are responsible for thermogenesis in BAT [99]. Compared to mitochondria in white adipocytes, mitochondria in brown adipocytes are morphologically distinct and contain

densely packed cristae. High abundance of mitochondria in brown adipocyte gives them a brownish appearance due to high contents of an iron-containing heme cofactor in the mitochondrial enzyme cytochrome oxidase [100]. In addition, proteins for fatty acid metabolism, oxidative phosphorylation (OXPHOS), and tricarboxylic acid (TCA) cycle are more abundant in mitochondria of BAT compared to those of WAT [101]. Furthermore, brown adipocytes have unique mitochondrial proteins uncoupling protein-1 (UCP1). UCP1 is located in the inner membrane of the mitochondria and functions to facilitate a proton leak, thereby blocking ATP production and converting the electrochemical energy into heat [102]. Thus, diverse and distinct features of mitochondria confer thermogenic activity of BAT (Figure 4).

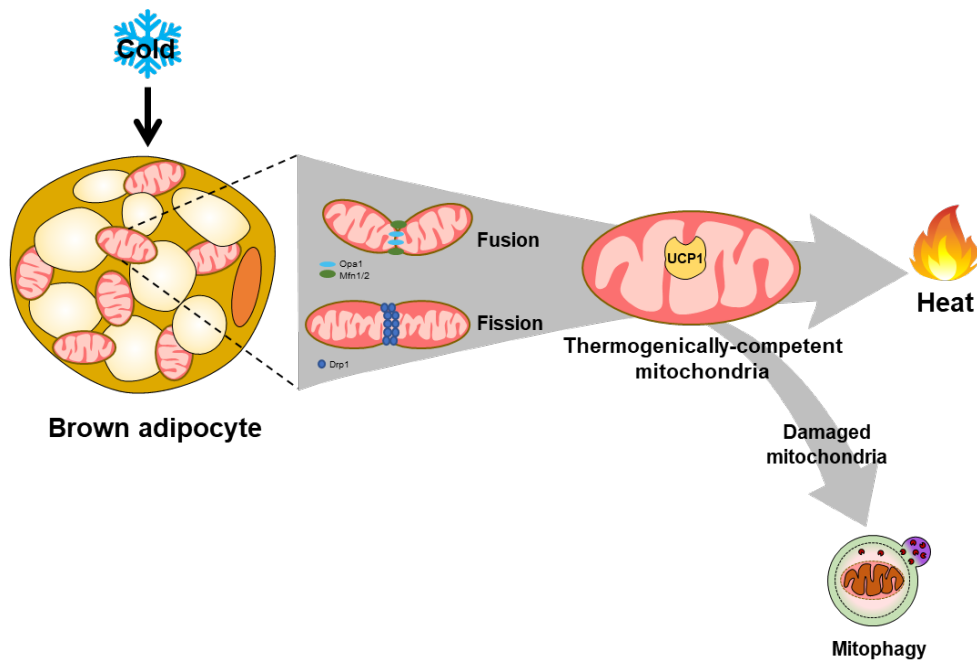


**Figure 4. Mitochondrial quality control in brown adipocyte**

Brown adipose tissue is characterized by a high abundance of mitochondria, which play a central role in regulating non-shivering thermogenesis through uncoupled respiration by UCP1. For preserving healthy and thermogenically competent mitochondria, mitochondrial quality control actively occurs during cold exposure. The consequential burst in mitochondrial ROS production causes oxidative damage to mitochondrial components, which are selectively removed through mitophagy to avoid thermogenic failure.

### **3) Mitochondrial quality control in thermogenesis**

Mitochondrial quality control through mitochondrial biogenesis, dynamics, and mitophagy is essential for preserving a healthy mitochondrial population [103]. It is involved in removal of defective mitochondria, timely replenishment of mitochondrial network and restoration of functionality of damaged mitochondria. Emerging evidence suggests that mitochondrial quality control in brown adipocytes is important for thermogenic activity during cold exposure [104, 105] (Figure 4). As thermogenesis is a complex process that heavily requires activation of mitochondria, which are exposed to metabolic and oxidative stress, mitochondrial function in thermogenesis imposes both metabolic flexibility and structural dynamics [106, 107]. Following thermogenesis, the prominent mitochondrial morphology in brown adipocytes is their fragmentations, which might potentiate uncoupling and increase energy expenditure. [108]. Even though BAT exhibits fragmented mitochondrial morphology for efficient thermogenesis through DRP1-mediated fission, it seems that precise coordination and regulation for both fission and fusion are required for appropriate thermogenic activity under cold exposure [108, 109]. For example, knockout mice lacking mitochondrial fusion related genes such as MFN2, OPA1, and OMA1 zinc metallopeptidase (OMA1) exhibit impaired cold-induced thermogenesis[110-113].

The role of mitophagy in thermogenesis would be dependent on the different phases of thermogenesis and/or the duration of cold exposure [104,

114, 115]. During acute cold exposure, mitophagy is necessary to rapid clearance of damaged and oxidized mitochondria. Deletion of key autophagy-related genes (Atg), such as Atg3, Atg5, Atg16L1, or Atg6, in mouse BAT results in impaired cold-induced thermogenesis with increased oxidative stress-mediated damages, disrupted mitochondrial network, and the accumulation of dysfunctional mitochondria [115-117]. In addition, PINK1 is induced following acute cold stimulation and its specific deletion in brown adipocytes leads to failure of the thermogenic program [114, 118]. However, it is likely that a sustained cold challenge could effectively induce an antioxidant response and protect mitochondria from oxidative stress. To maintain an adequate mitochondrial abundance for thermogenesis, it seems that mitophagy might be inhibited [118]. Therefore, it is likely that guarding mitochondrial health would play essential roles in regulation of the thermogenic roles in BAT.

#### **4. Purpose of this study**

CRY1 could act as a regulator of energy homeostasis as well as serving circadian clock and its dysregulation is associated with metabolic diseases. Although CRY1 has been implicated in systemic energy homeostasis, molecular mechanisms by which CRY1 could mediate and/or cause metabolic dysregulation have not been fully elucidated. In this thesis, I examined the roles of CRY1 and its regulating mechanisms in liver and BAT.

Although a decrease in hepatic CRY1 protein contributes to dysregulated glucose metabolism in diabetes, it is largely unknown the underlying mechanisms by which the reduction of CRY1 protein leads to hyperglycemia. In chapter one, I have elucidated the molecular mechanism by which dysregulation of hepatic CRY1 by GSK3 $\beta$  and FBXL3 provokes hyperglycemia through upregulation of hepatic glucose production. In chapter two, I aimed to elucidate the roles of CRY1 in mitochondrial quality control and thermogenesis. I found that CRY1-deficient MEF and BAT exhibited decreased mitochondrial bioenergetics and activated mitophagy. Moreover, CRY1 KO mice showed cold-intolerant phenotype with decreased mitochondrial contents. Thus, I hypothesized that CRY1 in BAT would be involved in thermogenesis by mitochondrial quality control.

Collectively, I suggest that CRY1 contributes to the maintenance of energy homeostasis in liver and brown adipose tissue.

## **CHAPTER ONE:**

# **Hepatic GSK3 $\beta$ -dependent CRY1 degradation contributes to diabetic hyperglycemia**

## 1. Abstract

Excessive hepatic glucose production (HGP) is a key factor promoting hyperglycemia in diabetes. Hepatic cryptochrome 1 (CRY1) plays an important role in maintaining glucose homeostasis by suppressing forkhead box protein O1 (FOXO1)-mediated HGP. Although downregulation of hepatic CRY1 appears to be associated with increased HGP, the mechanism(s) by which hepatic CRY1 dysregulation confers hyperglycemia in diabetic subjects is largely unknown. In this study, I demonstrate that a reduction in hepatic CRY1 protein is stimulated by elevated E3 ligase F-box and leucine-rich repeat protein 3 (FBXL3)-dependent proteasomal degradation in diabetic mice. In addition, I found that GSK3 $\beta$ -induced CRY1 phosphorylation potentiates FBXL3-dependent CRY1 degradation in the liver. Accordingly, in diabetic mice, GSK3 $\beta$  inhibitors effectively decreased HGP by facilitating the effect of CRY1-mediated FOXO1 degradation on glucose metabolism. Collectively, these data suggest that tight regulation of hepatic CRY1 protein stability is crucial for maintaining systemic glucose homeostasis.

## 2.Introduction

Liver plays important roles in glucose homeostasis by balancing glucose production and storage in the form of glycogen [119]. During fasting, liver maintains adequate levels of blood glucose by promoting hepatic glucose production (HGP) and glycogenolysis to meet metabolic demands in the peripheral tissues. In contrast, during the postprandial state, liver suppresses HGP and converts excess glucose into glycogen [120]. In type 2 diabetes, aberrant HGP regulation is one of the key contributors to hyperglycemia [85, 119], which results from hepatic insulin resistance, which is characterized by the inability of insulin to suppress HGP [121].

HGP is regulated by several key enzymes, including phosphoenolpyruvate carboxykinase 1 (PEPCK) and glucose-6-phosphatase (G6Pase), which convert pyruvate to glucose [79]. Several transcription factors and coactivators modulate the expression of gluconeogenic enzymes in response to hormones such as glucagon and insulin [119]. Forkhead box protein O1 (FOXO1), a pivotal transcription factor for gluconeogenic gene expression, mediates the effect of glucagon on HGP during fasting. In contrast, in response to insulin, Akt-dependent phosphorylated FOXO1 is ubiquitinated and degraded via proteasomal degradation pathways during postprandial periods [84]. In animal models of diabetes, the level of hepatic FOXO1 is elevated, accompanied by increased gluconeogenic gene expression [88]. As the suppression of FOXO1 is a major route of insulin to inhibit HGP, it is likely that elevated FOXO1 leads to surplus HGP [122].

Cryptochrome 1 (CRY1) is an essential molecular clock component for the generation of circadian rhythms [60]. Mammalian circadian clocks are tightly regulated by negative feedback loops [62]. In addition to transcriptional regulation, post-translational modifications of circadian clock proteins accompanied by altered levels of clock proteins affect circadian clock activities [15]. Besides serving as circadian regulators, peripheral circadian clocks are highly associated with glucose metabolism for systemic energy homeostasis [123]. Recent studies have shown that dysregulated levels of clock proteins are associated with type 2 diabetes [124]. It has been reported that CRY1 represses HGP by inhibiting glucagon receptor and/or glucocorticoid receptor signaling pathways [73, 74], indicating that CRY1 plays certain roles in glucose metabolism [125]. In addition, hepatic CRY1 protein downregulates HGP by promoting MDM2-mediated nuclear FOXO1 degradation upon feeding or insulin [56, 126]. Although decreased hepatic CRY1 protein is closely linked to hyperglycemia in diabetic animals [56, 72], how hepatic CRY1 dysregulation induces excessive HGP in diabetes remains largely unknown.

In this study, I aimed to elucidate the mechanism(s) underlying hepatic CRY1 protein reduction in diabetic animals. I performed proteomic analysis to identify regulatory factor(s) for hepatic CRY1 protein degradation in diabetic animals. Using mass spectrometry and CRY1 mutagenesis, I investigated the signaling pathway(s) involved in hepatic CRY1 protein degradation. Moreover, the effect of enhanced CRY1 on HGP

was investigated in a diabetic animal model established through high-fat, high-cholesterol, and high-fructose diet (HFCHF) feeding. Collectively, current data suggest that enhanced GSK3 $\beta$ -dependent hepatic CRY1 degradation is crucial for promoting HGP in diabetic animals.

### 3. Materials and methods

#### Animal Experiments

Male *db/+* and *db/db* mice were obtained from Dae Han Bio Link (Seoul, Korea). CRY1 knockout (KO) mice are gratefully provided by Dr. Sancar Aziz from the University of North Carolina. All animals were maintained under a 12-h/12-h light/dark cycle in a pathogen-free animal facility. To establish a mouse model of diabetes, 8-week-old mice were fed the HFHF diet consisting of 40 kcal% fat, 2% cholesterol, and 20 kcal% fructose (D09100310; Research Diets, New Brunswick, NJ, USA) for next 12~16 weeks. For intraperitoneal glucose tolerance test (GTT), mice were fasted for 16 hours, and glucose was administered (1 g/kg body weight). For pyruvate tolerance test (PTT), normal chow (NC)- or HFHF-fed mice were fasted for 18 hours and then injected intraperitoneally with pyruvate (1 g/kg body weight). GSK3 $\beta$  inhibitors were treated for 2 hours before performing PTT. HFHF fed wild type (WT) and CRY1 KO mice were intraperitoneally injected with vehicle (3% DMSO in PBS or PBS). Dissected tissue specimens were immediately stored at  $-80^{\circ}\text{C}$  until analysis. For *in vivo* FBXL3 and GSK3 $\beta$  knockdown, vehicle (PBS) or siRNA complex was intravenously injected (2.0 mg/kg) using invivolectamine<sup>®</sup> 3.0 (Invitrogen, IVF 3001) according to the manufacturer's protocol. After 3 days, mice were subjected to the PTT and analyzed. All animal experiments were approved by the Seoul National University Institutional Animal Care and Use Committee.

## **Liquid Chromatography-Tandem Mass Spectrometry (LC-MS/MS)**

### **Analysis**

Protein sampling and proteomics analyses were performed as previously reported [127]. Briefly, CRY1 peptides were generated by in-gel or in-solution digestion. For in-gel digestion, gel slices were destained in 50% acetonitrile solution, followed by in-gel alkylation of cysteine residues with dithiothreitol and iodoacetamide. Then, the samples were digested with sequencing-grade trypsin at a ratio of 1:50 (w/w) at 37°C overnight. For in-solution digestion, purified CRY1 samples were denatured in 8 M urea and subjected to reduction and alkylation, followed by trypsinization after dilution to obtain 1 M urea. LC-MS/MS was performed using a Q-Exactive mass spectrometer (Thermo) coupled with a nanoACQUITY UPLC instrument (Waters) equipped with an in-house packed capillary trap column (150- $\mu\text{m}$  i.d., 3 cm) and analytical column (75- $\mu\text{m}$  i.d., 100 cm) with 3- $\mu\text{m}$  Jupiter C18 particles (Phenomenex) at a flow rate of 300 nL/min. A linear gradient (100 min) was applied to each biological replicate. The data were analyzed in MaxQuant (v. 1.5.3.30) with the Andromeda search engine at 10 ppm precursor ion mass tolerance against the *M. musculus* proteome database at a protein false discovery rate of <1%. Extracted ion chromatograms were plotted using Qual Browser in the Xcalibur software (Thermo Scientific).

### **RNA-sequencing analysis**

Raw sequence reads were trimmed and quality-controlled using Trim Galore! (version 0.6.7) [128]. Trimmed reads were mapped to the mouse reference genome GRCm39/mm39 using HISAT2 (version 2.2.1) [129]. Mapped reads were assembled and quantified using StringTie (version 2.1.7) [130]. Differential expression analysis was conducted using Limma (version 3.42.2) [131]. Significance threshold was *Adjusted P-value* < 0.05 for CRY1 KO samples versus WT samples. Identified 198 DEGs consisted of 135 upregulated genes and 63 down-regulated genes. Gene ontology and pathway enrichment analysis of the upregulated DEGs in CRY1 KO samples was conducted using EnrichR [132].

### **Network Propagation**

Whole transcription-factor target gene (TFTG) network was downloaded from TRRUST version 2 database [133]. After filtering and preprocessing, the network contained 1,729 genes and 4,262 interactions. 198 DEGs are mapped on the TFTG network and network propagation (NP) was conducted using a random walk with restart algorithm to interpret individual gene-level perturbations at the network-level associations [134]. NP is a graph-based analysis method that propagates information of a node to nearby nodes through the edges at each iteration for a fixed number of steps or until convergence, allowing estimation of gene interactions. I denoted the value of each node after NP as the NP score.

### **Antibodies, Chemicals and Plasmids**

MG132 was purchased from Calbiochem (San Diego, CA, USA). SB-

415286 was purchased from Enzo Life Sciences (Farmingdale, NY, USA). Antibodies against MYC (Cell Signaling, 2276, 1:1000 dilution), HA (Cell Signaling, 3724, 1:1000 dilution), V5 (Millipore, 3792, 1:1000 dilution), phosphor-serine (Abcam, 9332, 1:500 dilution), FOXO1 (Cell Signaling, 2880, 1:1000 dilution), AKT (Cell Signaling, 9272, 1:1000 dilution), phosphor-AKT-S473 (Cell Signaling, 9271, 1:1000 dilution), GSK3 $\beta$  (BD, 610201, 1:1000 dilution), phosphor-GSK3 $\beta$ -S9 (Cell signaling, 9336, 1:1000), FLAG (Sigma-Aldrich, F3165, 1:1000 dilution), actin (Sigma-Aldrich, A5316, 1:2000 dilution), GAPDH (LabFrontier Co., LF-PA0018, 1:1000 dilution), PEPCCK (Santa Cruz Biotechnology, sc-32879, 1:500 dilution), FBXL3 (Abcam, 123116, 1:500 dilution) and CRY1 (Abcam, 104736, 1:1000 dilution; lab made antibody obtained from Dr. Aziz Sancar [135], 1:500 dilution) are used. MYC-CRY1, V5-GSK3 $\beta$ , 2SA CRY1-MYC, 2SD CRY1-MYC, and V5-CA-GSK3 $\beta$  cDNAs were cloned into the pcDNA3.1 vector, and Flag-FBXL3 cDNA was cloned into pCMV-3 Flag.

#### **Cell-based Ubiquitination Assays**

COS1 cells (ATCC, CRL1650) were transfected with plasmids encoding CRY1-MYC, FBXL3-Flag and ubiquitin-HA in the presence of 20  $\mu$ M MG132 for 6 h. Total cell lysates were prepared using TGN (Tris-Glycine Novel) buffer (50 mM Tris-HCl, pH 7.5, 150 mM NaCl, 1% Tien-20 and 0.3% NP-40). CRY1-MYC was immunoprecipitated with an anti-MYC antibody (Cell Signaling Technology, USA), and after washing in TGN

buffer, the proteins were separated by sodium dodecyl sulfate polyacrylamide gel electrophoresis followed by western blotting with an anti-HA antibody.

### **Mouse Primary Hepatocytes Culture**

Mouse primary hepatocytes were isolated from 10-week-old mice using the collagenase perfusion method [56] and seeded in medium 199 (M199) supplemented with 10% fetal bovine serum. After 6 hours of attachment, cells were transfected with siRNA or vectors in serum-free medium.

### **Cell Lysis and Immunoprecipitation**

After washing in cold PBS, cells were treated with the TGN buffer supplemented with 0.1% protease inhibitor cocktail (P3100; GenDEPOT, Katy, TX). The lysates were incubated with primary antibodies at 4°C for 16 h, and then in a 50% slurry of protein A sepharose pre-saturated with lysis buffer for 1 h. After three washes with lysis buffer, the immunoprecipitated proteins were recovered from the beads and analyzed by sodium dodecyl sulfate polyacrylamide gel electrophoresis and immunoblotting.

### **RNA Isolation and Quantitative Reverse Transcription (qRT)-PCR**

#### **Analysis**

RNA isolation and qRT-PCR analysis were performed as previously described [136]. Total RNA was isolated using TRIzol reagent (Invitrogen). cDNA was synthesized using a reverse transcriptase kit (Toyobo, Osaka, Japan) according to the manufacturer's instructions. The primers were generated at Bioneer (Daejeon, South Korea) and were listed in Table 2.

Relative mRNA levels were measured using a CFX-real-time quantitative PCR detection system (Bio-Rad Laboratories).

**Table 2. Primers used for qRT-PCR**

<b>Gene</b>	<b>Forward</b>	<b>Reverse</b>
Mouse Cry1	GTGGATCAGCTGGGAAGAAG	CACAGGGCAGTAGCAGTGAA
Mouse Fbx13	CAGGACTCTGCTGAGGAAGG	CAGCTGATTCTTTGCTGCTG
Mouse Pck1	ATCTTTGGTGGCCGTAGACCT	CCGAAGTTGTAGCCGAAGAA
Mouse G6pc	AGGAAGGATGGAGGAAGGAA	TGGAACCAGATGGGAAAGAG
Mouse Dtx3l	GAATGCAGCCTTACCTGCTC	TGGCTTGCTGATACACGAG
Mouse Tbp	GGGAGAATCATGGACCAGAA	CCGTAAGGCATCATTGGACT

### **siRNA Transfection**

siRNA duplexes for FBXL3 and GSK3 $\beta$  are purchased from Bioneer (Daejeon, South Korea). Primary hepatocytes are transiently transfected using Lipofectamine 3000 reagent (Invitrogen, Carlsbad, CA, USA) according to the manufacturer's protocol.

### **Glucose Production Assays**

Glucose production by mouse primary hepatocytes was measured using a glucose oxidase assay (Sigma-Aldrich, St. Louis, MO, USA) according to the manufacturer's protocol. Briefly, cells are treated with forskolin (10  $\mu$ M) and incubated in Krebs-Ringer buffer (115 mM NaCl, 5.9 mM KCl, 1.2 mM MgCl<sub>2</sub>, 1.2 mM NaH<sub>2</sub>PO<sub>4</sub>, 2.5 mM CaCl<sub>2</sub>, 25 mM NaHCO<sub>3</sub>, 10 mM lactate and 2 mM pyruvate, pH 7.4) equilibrated with 5% CO<sub>2</sub> at 37°C for 6 h. The assays are performed at least in duplicate.

### **Statistical Analysis**

Data are presented as the mean  $\pm$  SD or SEM. All *n* values indicated in the figures refer to biological replicates. Two-tailed Student *t*-tests are used to compare the means of two groups. One-way ANOVA followed by Tukey post-hoc tests was used to compare means of more than two groups. Two-way ANOVA followed by Sidak multiple comparisons tests was used to compare two independent variables. Statistical analyses are performed using GraphPad Prism 7 software (GraphPad Software, La Jolla, CA, USA).

### **Data availability**

The datasets generated during and/or analyzed during the current study are

available in the accession number GSE197839

## 4. Results

### Elevated hepatic FBXL3 promotes CRY1 degradation in diabetic mice

While hepatic CRY1 protein was downregulated in genetically diabetic *db/db* mice [56], it is unclear whether hepatic CRY1 expression is altered in diet-induced diabetic animal models. To generate a diet-induced diabetic mouse model with elevated HGP, C57BL/6J mice are fed a HFCF diet (Fig. 5A–E; [137]). Similar to *db/db* mice (Fig. 6A, B), the level of hepatic CRY1 protein, but not mRNA, was decreased in HFCF-fed mice compared to NC-fed mice (Fig. 6C, D), implying that hepatic CRY1 protein would be modulated at the post-transcriptional level. It is well established that various post-translational modifications modulate CRY1 protein stability, and proteasomal degradation is a key determinant of CRY1 protein levels [15, 60]. Consistently, the proteasomal degradation blocker MG132 attenuated the degradation of CRY1 protein in hepatocytes (Fig. 7A). To investigate which factor(s) are responsible for hepatic CRY1 protein degradation, I overexpressed myc-tagged CRY1 in the livers of *db/db* mice, pulled-down CRY1-binding proteins, and performed LC-MS/MS (Fig. 7B). The results indicated that FBXL3 and Deltex E3 ubiquitin ligase 3 L (DTX3L), which are E3 ligases, interacted with CRY1 (Fig. 7C; Table 3).

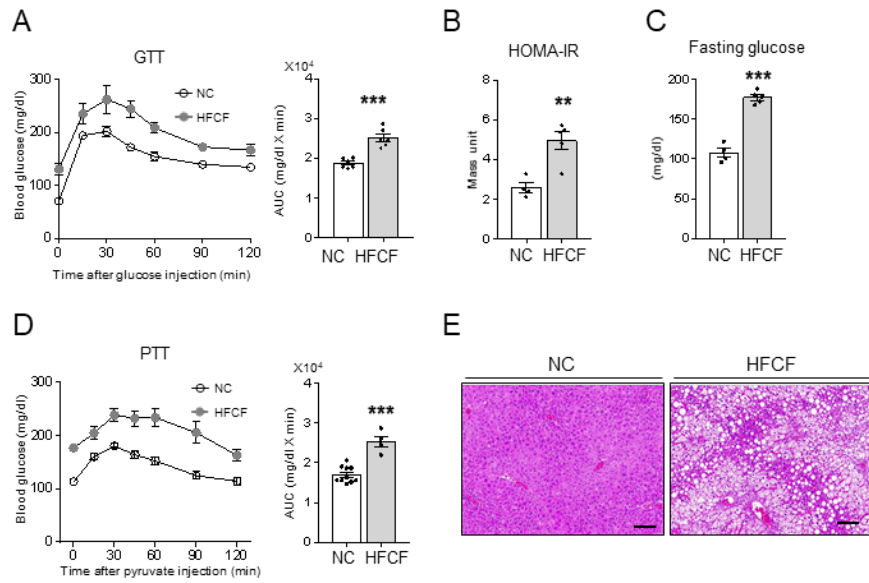


**Figure 5. The phenotype of NC-fed and HFCF-fed mice and strategy of CRY1 binding proteins in liver**

A: Intra-peritoneal GTT and AUC analysis of NC- or HFCF-fed WT mice.  $***P < 0.001$  vs. NC-fed WT mice by Student's *t*-test. B and C: Measurement of HOMA-IR (B) and fasting blood glucose levels (C) of NC- or HFCF-fed WT mice.  $**P < 0.01$ ,  $***P < 0.001$  vs. NC-fed WT mice by Student's *t*-test. D: Intra-peritoneal PTT and AUC analysis of NC- or HFCF-fed WT mice.  $***P < 0.001$  vs. NC-fed WT mice by Student's *t*-test. E: Representative images of hematoxylin and eosin-stained sections of livers of NC- or HFCF-fed WT mice. Data are mean  $\pm$  SEM. n.s. not significant.

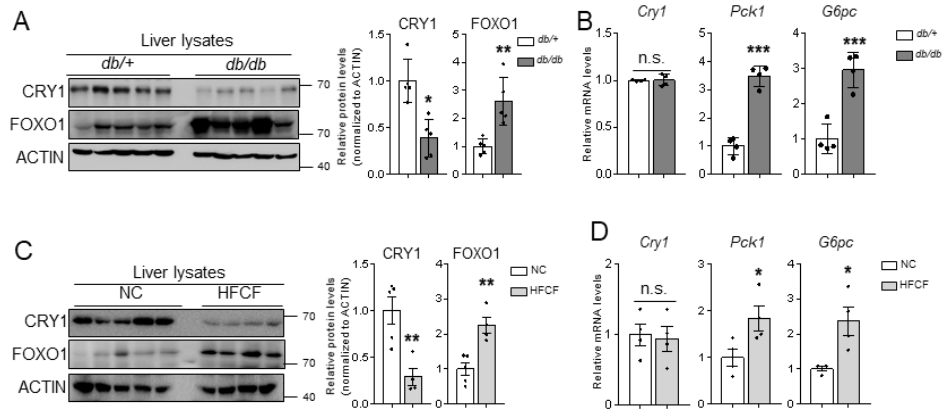


**Figure 6. Hepatic CRY1 protein is downregulated in mouse models of diabetes**

A and B: Western blot analysis (A) qRT-PCR analysis (B) in liver lysates from *db/+* and *db/db* mice. C and D: Western blot analysis (A) qRT-PCR analyses (B) in liver lysates from NC- and HFCF-fed mice (G). \* $P < 0.05$ , \*\* $P < 0.01$ , \*\*\* $P < 0.001$  vs. each control group by Student's *t*-test.

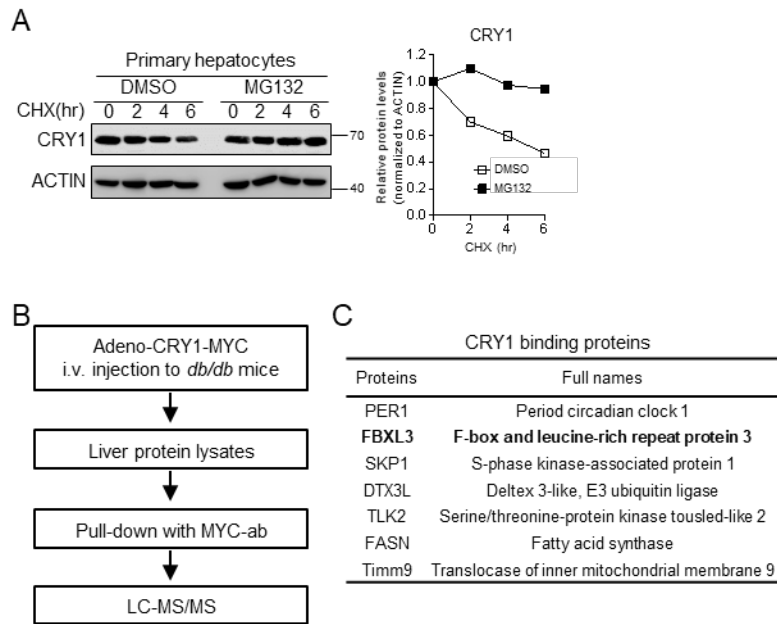


**Figure 7. Proteasomal degradation is a determinant of CRY1 protein**

A: CRY1 protein stability in primary hepatocytes treated with CHX (30  $\mu\text{mol/L}$ ) for the indicated periods with or without MG132 (20  $\mu\text{mol/L}$ ) treatment. B: Experimental strategy of the LC-MS/MS analysis to identify CRY1 binding proteins in the liver. C: List of potential CRY1-interacting proteins based on mass spectrometry analysis. Mean of the band intensities was calculated from independent experiments using Image J. Data are mean. n.s., CHX, cycloheximide.

**Table 3. List of the putative binding proteins of CRY1**

<b>Proteins</b>	<b>Full names</b>
PER1	Period circadian clock 1
FBXL3	F-box and leucine-rich repeat protein 3
SKP1	S-phase kinase-associated protein 1
DTX3L	Deltex 3-like, E3 ubiquitin ligase
TLK2	Serine/threonine-protein kinase tousled-like 2
FASN	Fatty acid synthase
Timm9	Translocase of inner mitochondrial membrane 9
PYC	Pyruvate carboxylase, mitochondrial
RL40	Ubiquitin-60S ribosomal protein L40
THIKB	3-ketoacyl-CoA thiolase B, peroxisomal
APOE	Apolipoprotein E
ECHM	Enoyl-CoA hydratase, mitochondrial
AATM	Aspartate aminotransferase, mitochondrial
GPX1	Glutathione peroxidase 1
PLIN4	Perilipin-4
ACADV	Very long-chain specific acyl-CoA dehydrogenase, mitochondrial
CX6B1	Cytochrome c oxidase subunit 6B1
THIM	3-ketoacyl-CoA thiolase, mitochondrial
AL1L1	Cytosolic 10-formyltetrahydrofolate dehydrogenase
ODPB	Pyruvate dehydrogenase E1 component subunit beta, mitochondrial
APOA1	Apolipoprotein A-I
NDUA7	NADH dehydrogenase [ubiquinone] 1 alpha subcomplex subunit 7
ACLY	ATP-citrate synthase

Although FBXL3 reportedly is involved in CRY1 degradation [138], it has not been studied whether it could affect hepatic CRY1 protein stability. As shown in Fig. 8A, FBXL3 potently increased the extent of CRY1 polyubiquitination, whereas DTX3L was less active in inducing CRY1 protein polyubiquitination. To affirm the physical interaction between FBXL3 and CRY1, a coimmunoprecipitation assay was performed with liver extract. Endogenous FBXL3 formed a protein complex with CRY1 (Fig. 8B), and hepatic CRY1 associated with endogenous SCF complex (SKP1-CUL1-FBXL3) (Fig. 8C). When I evaluated FBXL3 expression in the liver, both protein and mRNA levels of FBXL3 are increased in *db/db* mice (Fig. 9A, B) and HFCF-fed mice (Fig. 9C, D). To further examine the effect of FBXL3 on hepatic CRY1 protein stability, a cycloheximide-chase experiment was performed in mouse primary hepatocytes. FBXL3 suppression via siRNA mitigated CRY1 protein degradation (Fig. 10A) and attenuated polyubiquitination of CRY1 protein in hepatocytes (Fig. 10B). In contrast, FBXL3 overexpression stimulated polyubiquitination and degradation of CRY1 protein (Fig. 10C, D). These data propose that elevated FBXL3 expression promotes hepatic CRY1 protein degradation in diabetic animals.

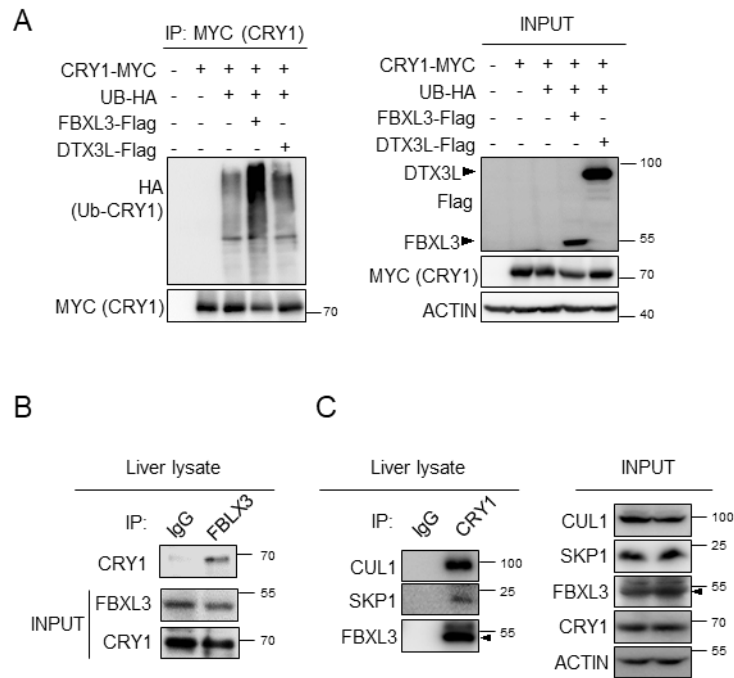


**Figure 8. Hepatic FBXL3 interacts with CRY1**

A: Cell-based ubiquitination assay. COS1 cells were cotransfected with plasmids encoding CRY1-MYC, ubiquitin-HA, FBXL3-Flag, or DTX3L-Flag. B: Endogenous coimmunoprecipitation using FBXL3 antibody with liver lysates. C: Endogenous coimmunoprecipitation using CRY1 antibody with liver lysates. IP, immunoprecipitation; UB, ubiquitin.

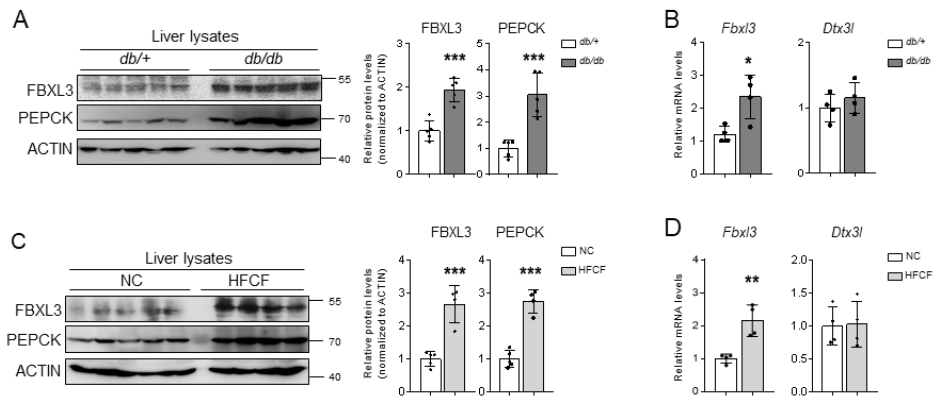


**Figure 9. FBXL3 expression is increased in mouse model of diabetes**

A and B: Western blot analysis of FBXL3 and PEPCK protein levels (A) and qRT-PCR analysis of *Fbxl3* and *Dtx3l* mRNA levels (B) in livers of *db/+* and *db/db* mice.  $*P < 0.05$ ,  $***P < 0.001$  vs. *db/+* group by Student *t* test. C and D: Western blot analysis of FBXL3 and PEPCK protein levels (C) and qRT-PCR analysis of *Fbxl3* and *Dtx3l* mRNA levels (D) in livers of NC- or HFCE-fed mice.  $**P < 0.01$ ,  $***P < 0.001$  vs. NC-fed group by Student *t* test. Mean and SD of the band intensities were calculated from independent experiments with ImageJ.

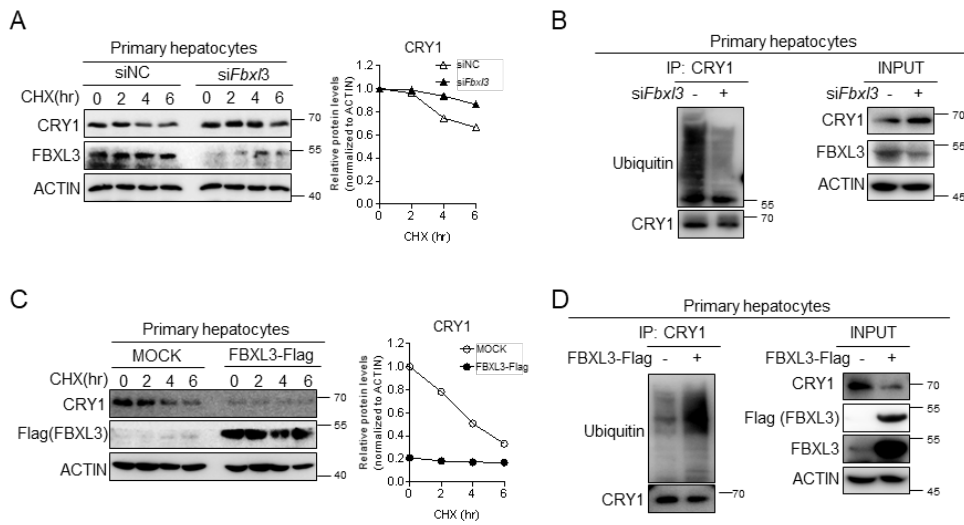


**Figure 10. Hepatic FBXL3 promotes polyubiquitination and degradation of CRY1 protein**

A: CRY1 protein stability. Primary hepatocytes were transfected with siNC or siFbxl3 in the absence or presence of cycloheximide (CHX) (30  $\mu$ mol/L). B: Cell-based ubiquitination assay in primary hepatocytes. Cells were transfected with siNC or siFbxl3 without MG132 treatment. C: CRY1 protein stability. Primary hepatocytes were transfected with MOCK or FBXL3 expression vectors and were harvested at the indicated time points after CHX (30  $\mu$ mol/L) treatment. D: Cell-based ubiquitination assay in primary hepatocytes. Cells were transfected with MOCK or FBXL3 expression vectors without MG132 treatment. Mean of the band intensities was calculated from independent experiments using Image J. Data are mean  $\pm$ SD. hr, hour; IP, immunoprecipitation; UB, ubiquitin.

### **FBXL3-CRY1 axis in hepatocytes regulates FOXO1-mediated HGP**

CRY1 acts as a negative regulator of HGP, whose dysregulation leads to excessive HGP [56, 126]. To identify key factor(s) involved in CRY1-mediated HGP regulation, I conducted unbiased bioinformatics analyses using bulk RNA-sequencing (RNA-seq) data of liver from WT and CRY1 KO mice. As shown in Fig. 11 and Table 4, *in silico* analysis revealed that FOXO1 was one of key transcription factors that could affect gene expression profile in liver of CRY1 KO mice.

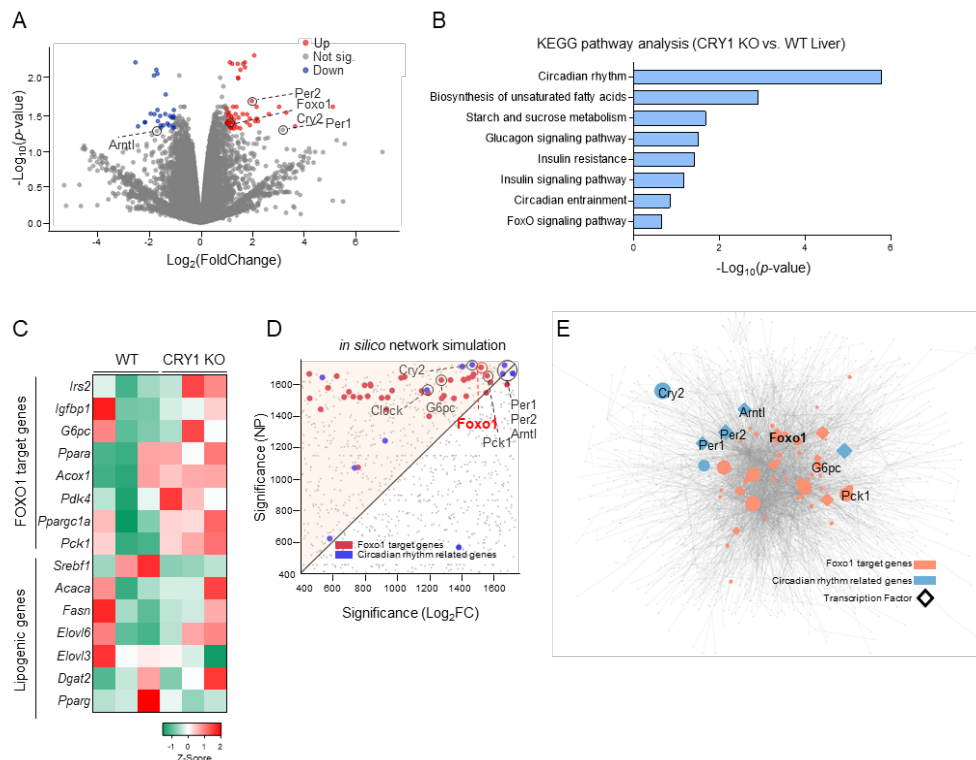


**Figure 11. FOXO1 target genes are highly expressed in liver of CRY1 KO mice**

**A:** Volcano plot of differentially expressed genes (DEG) identified with  $0.05 > \text{adjusted } p\text{-value}$  threshold. Red dots represent upregulated genes and blue dots represent downregulated genes of the plot. **B:** KEGG pathway enrichment of upregulated genes in liver from CRY1 KO. **C:** Heatmap showing the expression levels of FOXO1 target genes and lipogenic genes in liver from CRY1 KO and WT mice. **D:** Scatter plot representing gene significance of network propagation (NP) scores and fold change (FC). Red dots represent genes that are FOXO1 target genes and blue dots represent circadian rhythm-related genes. **E:** The whole transcription-factor target gene (TFTG) network containing genes in the FOXO1 target genes and circadian rhythm-related genes, respectively. Node size corresponds to NP score. The higher the NP score, the bigger the node size.

**Table 4. NP score of candidate genes in liver of CRY1 KO mice compared to WT**

Proteins	NP_score	Log2FC	NP_score_rank	Log2FC_rank	NP_rank_ratio
Cyp3a11	0.2188	1.6401	1	97	0.0578
Bik	0.2147	0.4220	2	619	0.1157
Cpt1a	0.2142	0.7082	3	349	0.1735
Nfe2l2	0.2114	0.6373	4	390	0.2313
Bhlhe40	0.2103	1.8925	5	74	0.2892
Cry2	0.2056	0.8738	6	264	0.3470
Per2	0.2055	1.9774	7	65	0.4049
Pklr	0.2054	0.7348	8	328	0.4627
Dbp	0.2050	2.2127	9	53	0.5205
Skil	0.2037	-0.7206	10	335	0.5784
Txnip	0.2037	2.1550	11	57	0.6362
Scd1	0.2015	1.2493	12	157	0.6940
Elovl5	0.2015	0.9301	13	240	0.7519
Zbtb16	0.2009	3.3035	14	13	0.8097
Gys2	0.2009	0.8967	15	257	0.8676
Hnf4a	0.2007	0.7358	16	326	0.9254
Tfb2m	0.2006	0.4572	17	563	0.9832
Il6ra	0.2005	2.1051	18	60	1.0411
Pex11a	0.2004	0.7733	19	307	1.0989
Lgals4	0.2004	1.4320	19	131	1.0989
Tert	0.2004	-0.9635	21	232	1.2146
Foxo1	0.2002	1.0077	22	212	1.2724
Itga7	0.2002	-0.7295	23	332	1.3302
Bnip3	0.2002	0.7803	24	302	1.3881
Wee1	0.2001	3.0286	25	21	1.4459
Krt18	0.2001	-0.7112	25	346	1.4459
Mmp15	0.2001	0.5431	27	464	1.5616
Glrx	0.2000	-0.9197	28	247	1.6194
Rorc	0.2000	1.4534	29	128	1.6773

Hinfp	0.2000	1.1789	30	167	1.7351
Slc20a1	0.2000	1.3023	31	147	1.7929
Zbtb20	0.2000	1.0042	32	214	1.8508
Tgml	0.2000	-1.5686	33	111	1.9086
Pdk1	0.2000	1.0045	34	213	1.9665
St3gal5	0.2000	1.8960	35	72	2.0243
Nfyb	0.2000	-0.7379	36	325	2.0821
Rgs16	0.2000	5.1011	37	3	2.1400
Sh3bp2	0.2000	-0.5651	38	451	2.1978
Stard5	0.2000	0.5030	39	512	2.2556
Herpud1	0.2000	1.7795	39	84	2.2556
Klf10	0.2000	2.6314	41	33	2.3713
Nr1i3	0.2000	1.3975	41	134	2.3713
Klf13	0.2000	1.2988	41	149	2.3713
Hlf	0.2000	1.1858	41	166	2.3713
Tef	0.2000	1.5343	41	115	2.3713
Nr1d2	0.2000	0.8665	41	268	2.3713
Atf4	0.2000	-0.5334	41	479	2.3713
Sall1	0.2000	0.9648	41	230	2.3713
Trim24	0.2000	0.7176	41	337	2.3713
Il2ra	0.1698	-0.3575	50	704	2.8918
Gja1	0.1616	0.6764	51	363	2.9497
Sox9	0.1605	0.8760	52	263	3.0075
Ccl5	0.1604	-0.5540	53	459	3.0654
Stat1	0.1600	-0.5304	54	482	3.1232
Abcb1a	0.1600	0.3311	55	755	3.1810
Kif26b	0.1600	0.2025	56	1033	3.2389
Cdkn1a	0.1196	0.1022	57	1373	3.2967
Ddit4	0.0806	1.0766	58	191	3.3545
Ctnnb1	0.0697	0.0322	59	1627	3.4124
Per1	0.0597	3.1719	60	15	3.4702

To test whether FBXL3 modulates HGP through CRY1 degradation, FBXL3 was ectopically expressed in primary hepatocytes. In WT hepatocytes, FBXL3 overexpression boosted HGP (Fig. 12A). In addition, ectopic expression of FBXL3 markedly increased FOXO1 protein levels and gluconeogenic gene expression, concomitant with decreased CRY1 protein levels (Fig. 12B, C). On the contrary, in CRY1 KO hepatocytes, FBXL3 overexpression did not affect HGP and gluconeogenic gene expression (Fig. 12A–C). Further, I studied whether FBXL3 suppression would downregulate HGP via an increase in CRY1. When FBXL3 was suppressed via siRNA, knockdown of FBXL3 repressed HGP and gluconeogenic gene expression in WT hepatocytes (Fig. 13A–C). Simultaneously, the level of FOXO1 protein decreased (Fig. 13D). However, these effects of FBXL3 suppression are nullified in CRY1 KO hepatocytes (Fig. 13A–D). These findings led us to investigate the *in vivo* effect of FBXL3 on HGP. To address this, FBXL3 was suppressed via siRNA in liver of WT mice through tail-vein injection. *siFbxl3* treatment did not affect body weight and expression of FBXL3 mRNA in other tissues except liver (Fig. 14A, B). Consistent with above data, PTT showed that *in vivo* FBXL3 suppression significantly decreased the level of blood glucose following pyruvate challenge (Fig. 14C). Moreover, hepatic FBXL3 suppression upregulated the level of CRY1 protein, resulting in suppression of FOXO1 protein and gluconeogenic genes in liver (Fig. 15A–C). To further investigate the role(s) of FBXL3-CRY1 axis in diabetic animals, I explored the effect of FBXL3

suppression on HGP in *db/db* mice. As shown in Fig. 16A, hepatic FBXL3 suppression decreased blood glucose level during PTT in *db/db* mice. Additionally, hepatic FBXL3 suppression increased the level of CRY1 protein in diabetic animals (Fig. 16B). Together, these data suggest that hepatic FBXL3 suppression would ameliorate hyperglycemia by promoting CRY1-mediated FOXO1 degradation in diabetic animals.

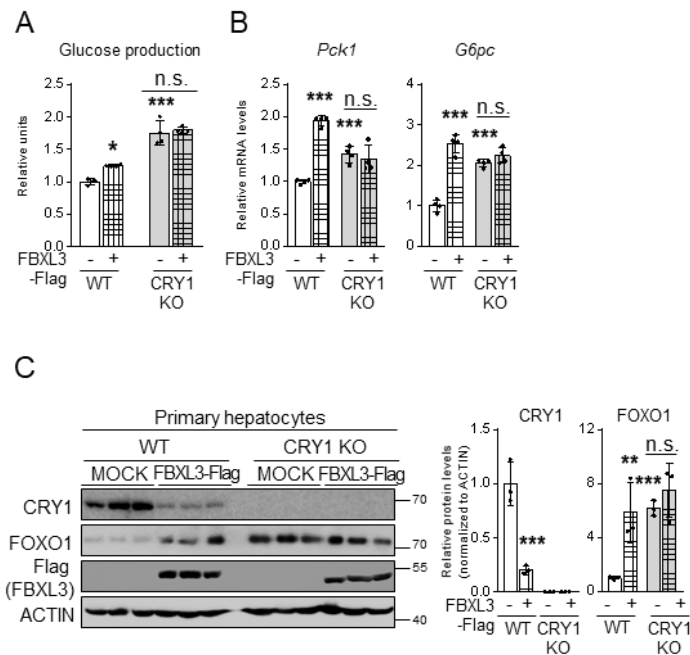


**Figure 12. FBXL3 overexpression boosts hepatic glucose production with decreased CRY1 protein**

A–C: Primary hepatocytes were isolated from WT or CRY1 KO mice. Cells were transfected with MOCK (empty vector control) or FBXL3-Flag expression vectors. Glucose production assay (A), qRT-PCR analysis of gluconeogenic gene expression (B), and Western blot analysis of CRY1 and FOXO1 protein levels (C) are shown. \* $P < 0.05$ , \*\* $P < 0.01$ , \*\*\* $P < 0.001$  vs. WT, empty vector control (MOCK) group by two-way ANOVA followed by Sidak post hoc test. Mean and SD of the band intensities were calculated from independent experiments using ImageJ. Data are means  $\pm$  SD. n.s., not significant.

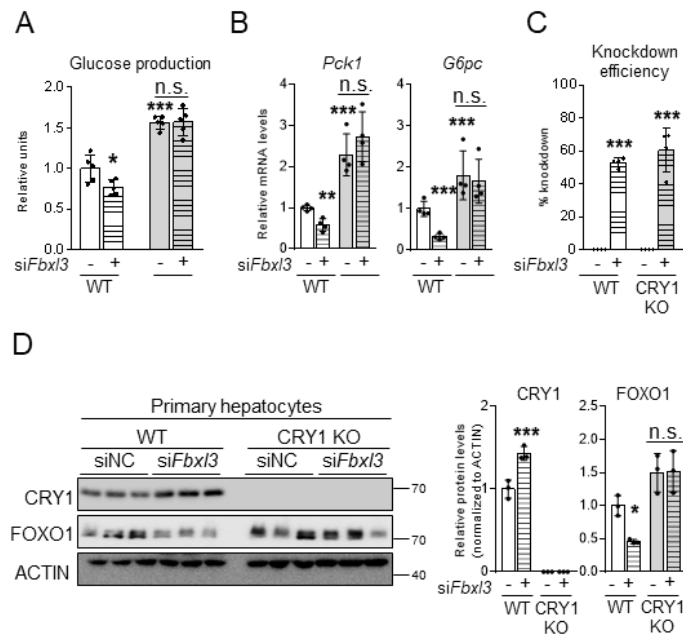


**Figure 13. Suppression of FBXL3 represses hepatic glucose production via an increase in CRY1 protein**

A–D: Primary hepatocytes were isolated from WT or CRY1 KO mice. Cells were transfected with siRNA negative control (siNC) or *siFbxl3*. Glucose production assay (A), qRT-PCR analysis of gluconeogenic gene expression (B), knockdown efficiency of *Fbxl3* gene expression (C) and Western blot analysis of CRY1 and FOXO1 protein levels (D) are shown. \* $P < 0.05$ , \*\* $P < 0.01$ , \*\*\* $P < 0.001$  vs. WT, siNC group by two-way ANOVA followed by Sidak post hoc test. Mean and SD of the band intensities were calculated from independent experiments using ImageJ. Data are means  $\pm$  SD. n.s., not significant.

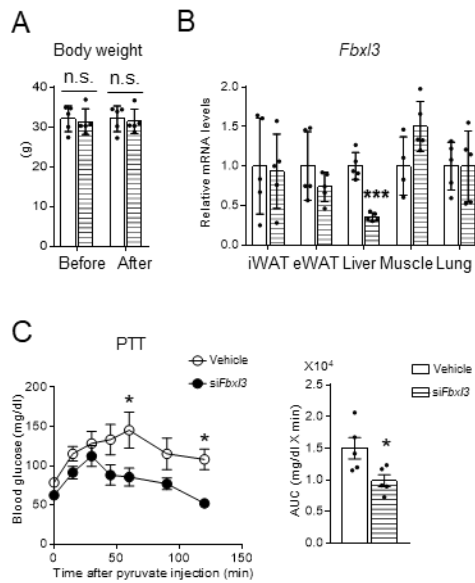


**Figure 14. *in vivo* FBXL3 suppression decreases hepatic glucose production**

A–C: *siFbxl3* was intravenously injected into WT (12-week-old) mice. A: Body weights of vehicle-treated and *siFbxl3*-treated mice before and after treatment. B: qRT-PCR analysis of *Fbxl3* in inguinal white adipose tissue (iWAT), epididymal white adipose tissue (eWAT), liver, skeletal muscle, and lung of vehicle-treated and *siFbxl3*-treated mice. C: Intraperitoneal PTT and area under the curve (AUC) analysis. \* $P < 0.05$ , \*\*\* $P < 0.001$  vs. vehicle-treated WT mice by two-way ANOVA followed by Sidak post hoc test. Data are means  $\pm$  SD. n.s., not significant.

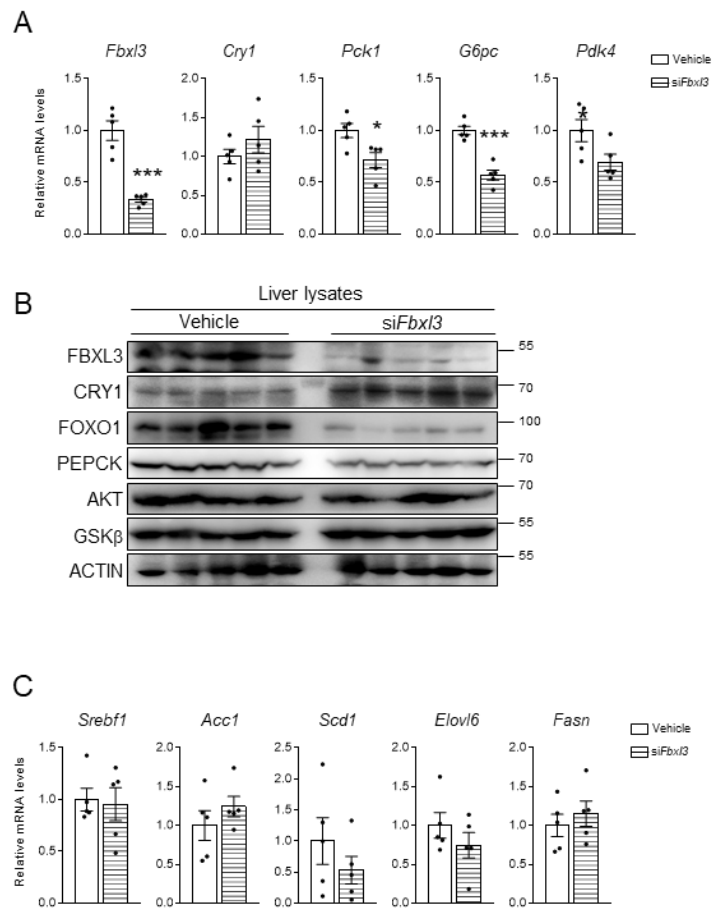


**Figure 15. *in vivo* FBXL3 knockdown downregulates hepatic glucose production**

A–C: *siFbxl3* was intravenously injected into WT (12-week-old) mice. qRT-PCR analysis of gluconeogenic gene expression in liver (A), Western blot analysis of liver lysates (B), and qRT-PCR analysis of lipogenic gene expression (C) from vehicle or *siFbxl3*-treated mice are shown. \* $P < 0.05$ , \*\*\* $P < 0.001$  vs. vehicle-treated WT mice by two-way ANOVA followed by Sidak post hoc test.

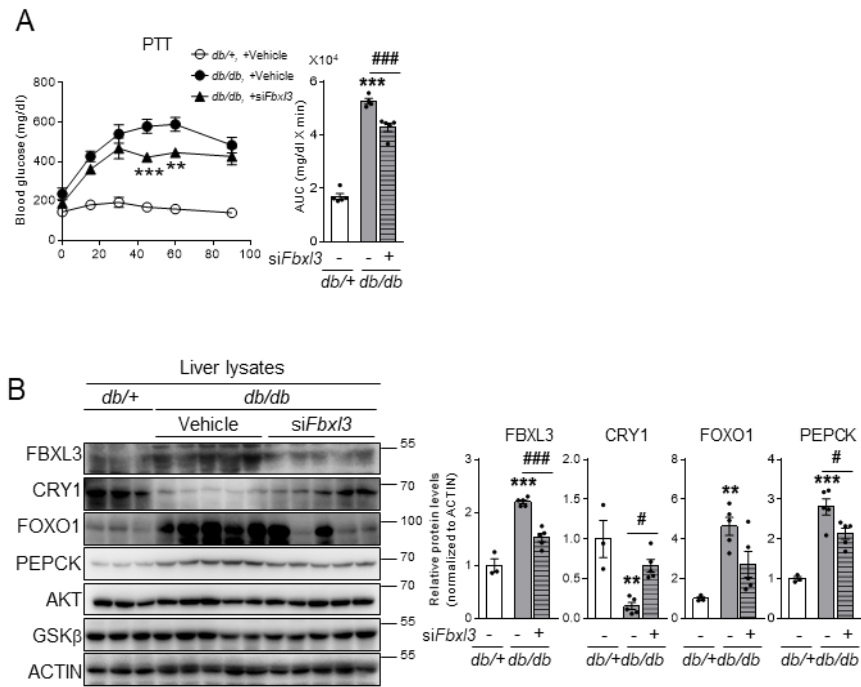


**Figure 16. *in vivo* FBXL3 suppression ameliorates hyperglycemia in diabetic animals**

A–B: *siFbxl3* was intravenously injected into *db/db* mice. Intraperitoneal PTT and AUC analysis (A) and Western blot analysis of liver lysates (B) from vehicle-treated *db/+* mice and vehicle or *siFbxl3*-treated *db/db* mice are shown. \*\* $P < 0.01$ , \*\*\* $P < 0.001$  vs. vehicle-treated *db/+* group; # $P < 0.05$ , ### $P < 0.001$  vs. vehicle-treated *db/db* mice by two-way ANOVA followed by Sidak post hoc test. Mean and SD of the band intensities were calculated from independent experiments using ImageJ. Data are means  $\pm$  SD. n.s., not significant.

## **Hepatic GSK3 $\beta$ promotes FBXL3-dependent CRY1 degradation in diabetic mice**

Given that FBXL3 promotes the degradation of its substrates in a phosphorylation-dependent manner [139], I questioned whether FBXL3-dependent CRY1 degradation might be linked to its phosphorylation. To answer this question, the level of hepatic CRY1 phosphorylation was examined in *db/db* mice. As indicated in Fig. 17, the level of CRY1 phosphorylation was enhanced in the livers of *db/db* mice. To determine which kinase(s) are responsible for hepatic CRY1 phosphorylation, I performed *in silico* analyses [140, 141] and found that there are, at least, five potential kinases including AMPK, MAPK, GSK3 $\beta$ , DNA-PK, and CK-1 (Fig. 18A). To elucidate the key kinase(s) responsible for modulating CRY1 protein stability, primary hepatocytes are treated with an inhibitor of each kinase (i.e., SB415286, GSK3 $\beta$ ; NU-7441, DNA-PK; IC261, CK-1; SB203580, p38 MAPK). As shown in Fig. 18B and C, the level of hepatic CRY1 protein was increased by the GSK3 $\beta$  inhibitor SB415286, but not by the other kinase inhibitors. Consistent with the previous findings that the enzymatic activity of GSK3 $\beta$  is augmented in diabetic animals [142, 143]), the level of S9 phosphorylation of GSK3 $\beta$ , a marker of inhibitory GSK3 $\beta$  activity, was decreased in *db/db* and HFCF-fed mice (Fig. 19A, B). To evaluate whether GSK3 $\beta$  might be involved in CRY1 phosphorylation, I examined the level of CRY1 phosphorylation using GSK3 $\beta$  inhibitors. The

GSK3 $\beta$  inhibitors LiCl and SB415286 decreased CRY1 phosphorylation (Fig. 20A, B). Accordingly, the level of CRY1 phosphorylation was increased upon GSK3 $\beta$  overexpression, whereas these effects are diminished after GSK3 $\beta$  inhibitor treatment (Fig. 20C). To investigate whether GSK3 $\beta$  might promote CRY1 protein degradation, a cycloheximide-chase assay was performed. In hepatocytes, CRY protein degradation was suppressed by GSK3 $\beta$  inhibitors (Fig. 21A, B). In order to study whether CRY1 phosphorylation by GSK3 $\beta$  might facilitate FBXL3-mediated ubiquitination, I performed ubiquitination assays using GSK3 $\beta$  inhibitors. As shown in Fig. 22A, B, FBXL3 accelerated CRY1 polyubiquitination, whereas GSK3 $\beta$  inhibitors abolished such effect. Therefore, these data suggest that GSK3 $\beta$  would phosphorylate hepatic CRY1 protein and promote its FBXL3-dependent degradation in diabetic animals.

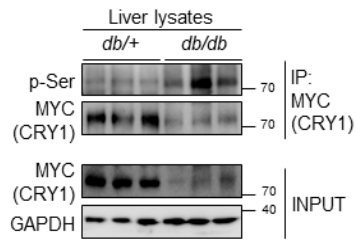


**Figure 17. CRY1 phosphorylation level is enhanced in the livers of *db/db* mice**

Immunoprecipitation–Western blot analysis to monitor the level of CRY1 protein phosphorylation in livers of *db/+* or *db/db* mice infected with adenovirus encoding CRY1-MYC. IP, immunoprecipitation; p-, phosphorylated.

A

Phosphorylation site	Sequence	Predicted kinase
CRY1 S71	NLRKLN <sub>s</sub> RRLFVIR	AMPK
CRY1 S247	ANSLLA <sub>s</sub> PTGLSP	MAPK
CRY1 S281	KVKKNS <sub>s</sub> PPLSLY	GSK3 $\beta$
CRY1 S588	SSGKRP <sub>s</sub> QEEDAQ	DNA-PK
CRY1 S595	QEEDAQ <sub>s</sub> VGPKVR	CK-1

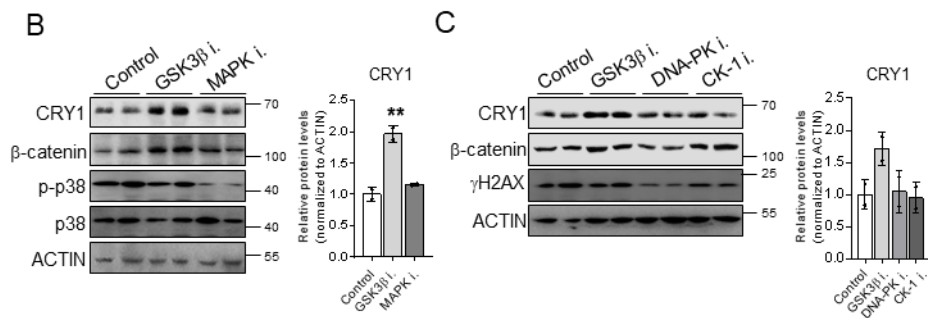


**Figure 18. The level of hepatic CRY1 protein is increased by the GSK3 $\beta$  inhibitor**

A: Scansite 4.0 and phosphoSitePlus predictions of mouse CRY1 phosphorylation sites [144, 145]. B: Western blot analysis of CRY1 protein in primary hepatocytes without or with the GSK3 $\beta$  inhibitor SB415286 (20  $\mu$ mol/L) and MAPK inhibitor SB203580 (20  $\mu$ mol/L) for 6 h. **\*\* $P$  < 0.01** vs. each control group by one-way ANOVA followed by Tukey post hoc tests. C: Western blot analysis of CRY1 protein in primary hepatocytes without or with SB415286 (20  $\mu$ mol/L), DNA-PK inhibitor NU-7441 (1  $\mu$ mol/L), and CK-1 inhibitor IC261 (1  $\mu$ mol/L) for 6 h. **\*\* $P$  < 0.01** vs. each control group by one-way ANOVA followed by Tukey post hoc tests. Mean and SD of the band intensities were calculated from independent experiments with ImageJ. Data are means  $\pm$  SD.

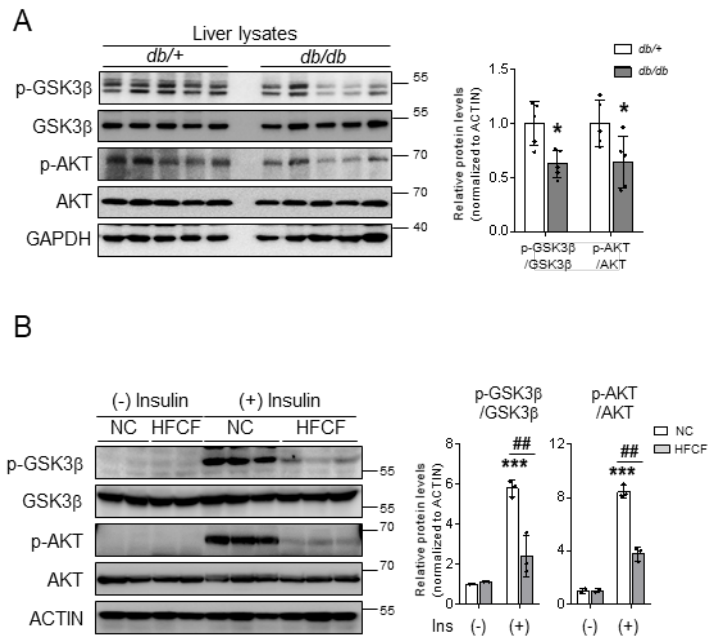


**Figure 19. Enzymatic activity of GSK3 $\beta$  is augmented in diabetic animals**

A: Western blot analysis of phospho-S9 GSK3 $\beta$ , GSK3 $\beta$ , phospho-S473 AKT, and AKT levels in livers of *db/+* and *db/db* mice under basal, not insulin-stimulated, conditions.  $*P < 0.05$  vs. each *db/+* group by two-way ANOVA followed by Sidak post hoc test. B: Western blot analysis of insulin signaling cascade in liver lysates from NC- or HFCF-fed mice.  $***P < 0.001$  vs. vehicle-treated NC-fed WT mice;  $###P < 0.01$  vs. vehicle-treated HFCF-fed WT mice by two-way ANOVA followed by Sidak's post-hoc test. Mean and SD of the band intensities were calculated from independent experiments with ImageJ. Data are means  $\pm$  SD.

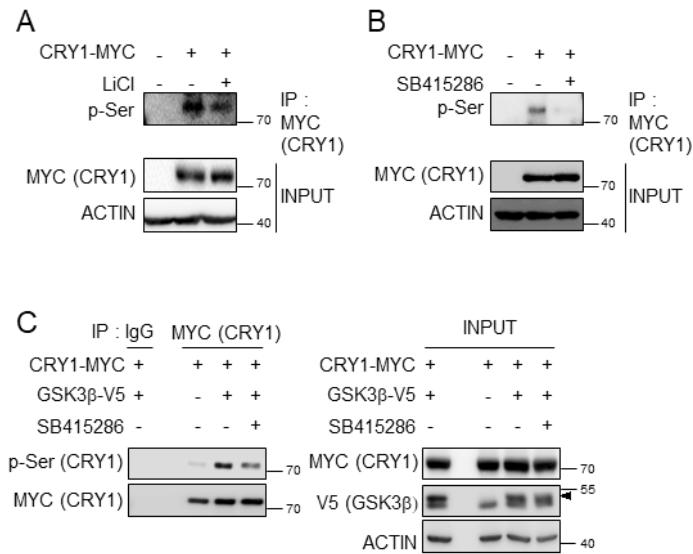


**Figure 20. GSK3β involves in CRY1 phosphorylation**

A and B: Immunoprecipitation-western blot analysis of the level of CRY1 protein phosphorylation in HEK293T cells treated without or with GSK3β inhibitor LiCl (20 mmol/L) (A) or SB415286 (20 μmol/L) (B) for 2 h. C: Coimmunoprecipitation assay with an anti-MYC antibody and Western blot analysis with the indicated antibodies. Human embryonic kidney (HEK)293T cells were cotransfected with CRY1-MYC and/or GSK3β-V5 expression vector without or with SB415286 (20 μmol/L) for 2 h. Mean and SD of the band intensities were calculated from independent experiments with ImageJ. Data are means ± SD. hr, hour; IP, immunoprecipitation; p-, phosphorylated.

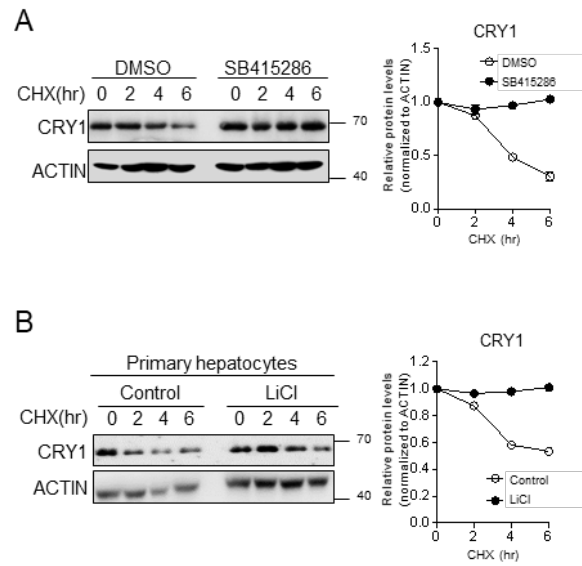


**Figure 21. CRY1 protein degradation is suppressed by GSK3 $\beta$  inhibitors**

A: CRY1 protein stability in primary hepatocytes treated with cycloheximide (CHX) (30  $\mu$ mol/L) for the indicated periods and with or without SB415286 (20  $\mu$ mol/L). B: CRY1 protein stability in primary hepatocytes treated with CHX (30  $\mu$ mol/L) for the indicated periods with or without GSK3 $\beta$  inhibitor LiCl (20 mmol/L). Mean and SD of the band intensities were calculated from independent experiments with ImageJ. Data are means  $\pm$  SD. hr, hour.

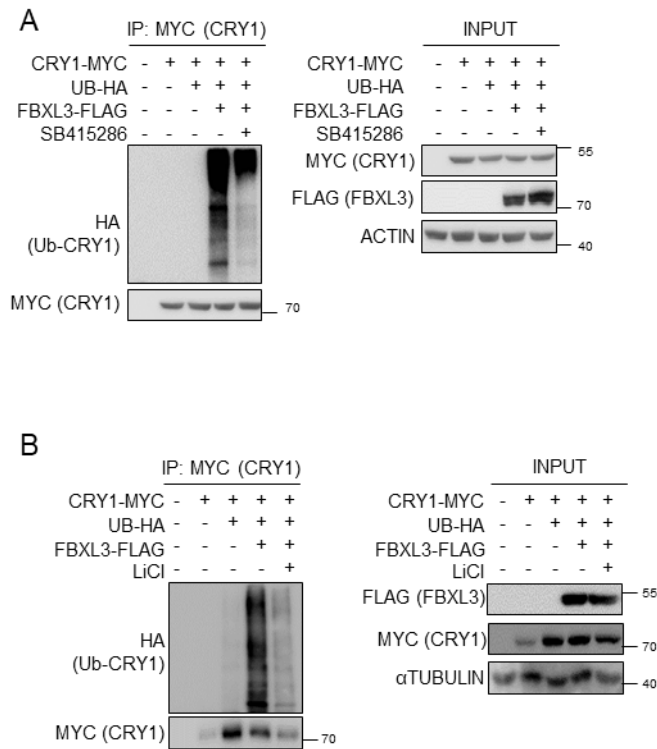


**Figure 22. CRY1 phosphorylation by GSK3 $\beta$  facilitates FBXL3-mediated ubiquitination**

A: Cell-based ubiquitination assay. COS1 cells were cotransfected without or with plasmids encoding CRY1-MYC, ubiquitin-HA, and FBXL3-Flag. Cells were incubated without or with LiCl (20 mmol/L) prior to MG132 (20  $\mu$ mol/L) treatment for 6 h. B: Cell-based ubiquitination assay. COS1 cells were cotransfected without or with plasmids encoding CRY1-MYC, ubiquitin-HA, and FBXL3-Flag. Cells were incubated without or with LiCl (20 mmol/L) prior to MG132 (20  $\mu$ mol/L) treatment for 6 h. UB, ubiquitin; CHX, cycloheximide; IP, immunoprecipitation.

## **GSK3 $\beta$ -induced CRY1 phosphorylation is crucial for FBXL3-dependent CRY1 degradation**

To identify potential phosphorylation residue(s) in the CRY1 protein by GSK3 $\beta$ , I performed mass spectrometry (Fig. 23A). Compared with control (Fig. 23B), overexpression of constitutively active-GSK3 $\beta$  (CA-GSK3 $\beta$ ; serine 9 to alanine mutation) induced CRY1 phosphorylation at S280 (Fig. 23C). *In silico* analysis revealed that the S281 in CRY1 might be another potential phosphorylation residue corresponding to the GSK3 $\beta$  consensus phosphorylation site (S-XXX-S) (Fig. 24A; [146]). As both S280 and S281 CRY1 are well conserved in various species (Fig. 24B), I examined whether these residues might be important for CRY1 degradation by FBXL3. To address this, I mutated both S280 and S281 to alanine (phospho-dead mutation; 2SA mutant CRY1) or aspartate (phospho-mimicking mutation; 2SD mutant CRY1) and examined CRY1 protein stability. The degradation rate of the 2SA mutant CRY1 protein was significantly decreased compared to that of WT CRY1 protein (Fig. 25A), whereas that of the 2SD mutant CRY1 protein was increased (Fig. 25B). To further affirm that these serine residues are crucial for FBXL3-dependent polyubiquitination, a cell-based ubiquitination assay was performed. As shown in Fig. 26A, FBXL3-dependent CRY1 polyubiquitination was downregulated in 2SA CRY1, whereas it was promoted in 2SD CRY1 (Fig. 26B). Collectively, these data suggest that CRY1 phosphorylation at

S280/S281 would be mediated by GSK3 $\beta$ , leading to FBXL3-dependent polyubiquitination and proteasomal degradation of hepatic CRY1 protein.

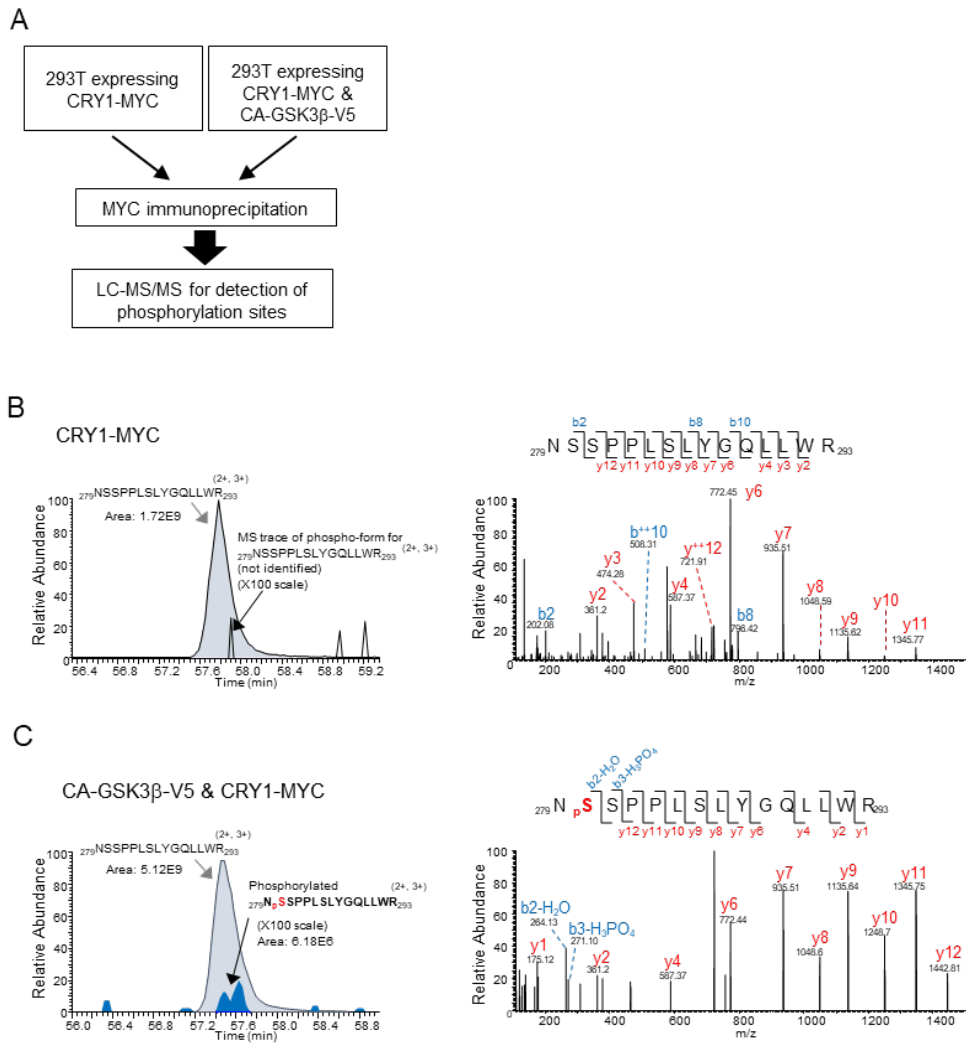


**Figure 23. GSK3β phosphorylates CRY1 protein at S280**

A: Scheme of MS analysis to identify CRY1 phosphorylation sites using liver lysates of *db/db* mice. B and C: Mass spectrometry (MS)-based extracted ion chromatogram of phosphorylated S280 of CRY1 peptide with 905.95 m/z and non-phospho-S280 of CRY1 peptide with 577.65 m/z (upper panel). Identified tandem mass spectrometry spectra of peptides containing non-phospho-S280 (B) and phospho-S280 (C) of CRY1 (bottom panel).

A		B	
GSK3β consensus sequence (S/T)-X-X-X-(S/T)		GSK3β consensus sequence	(S/T)-X-X-X-(S/T)
T180	GFD <u>I</u> DGLSSAV	281	<b>S</b> -P-P-L- <b>S</b> <sub>285</sub>
S243	NAN <u>S</u> LLASPTG		<b>S</b> <sub>280</sub> <b>S</b> <sub>281</sub>
S247	LLA <u>S</u> PTGLSPYL	M.musculus	KKN <u>S</u> SPPLSLYGQ
S281	KNS <u>S</u> PPLSLYG	H.sapiens	KKN <u>S</u> SPPLSLYGQ
T579	SAG <u>I</u> GLSSGKR	R.norvegicus	KKN <u>S</u> SPPLSLYGQ
		X.tropicalis	KKN <u>S</u> SPPLSLYGQ

**Figure 24. GSK3β induces CRY1 phosphorylation at S280/S281 residues**

A: Identification of GSK3β phosphorylation sites in CRY1 (data from GPS 5.0 software (<http://gps.biocuckoo.cn>) [144]). B: Alignment of CRY1 amino acid sequences from several species with potential CRY1 phosphorylation sites.

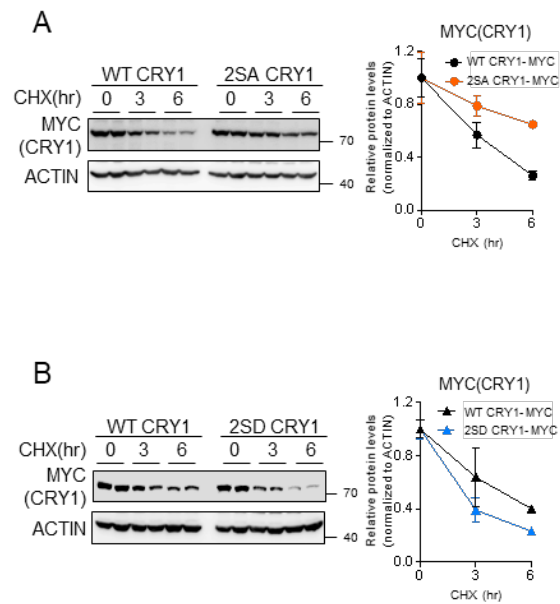


**Figure 25. GSK3 $\beta$ -induced CRY1 phosphorylation potentiates protein degradation**

A and B: CRY1 protein stability analyzed in HEK293T cells transfected without or with plasmids encoding WT-CRY1-MYC and 2SA-CRY1-MYC (A) and 2SD-CRY1-MYC (B). Cells were harvested at the indicated time points and treated with cycloheximide (CHX) (30  $\mu$ mol/L). Mean and SD of the band intensities were calculated from independent experiments with ImageJ. Data are mean  $\pm$  SD. hr, hour.

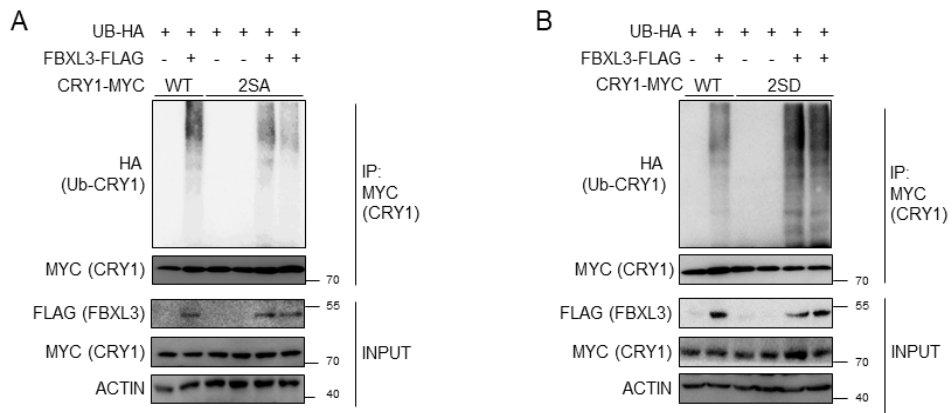


**Figure 26. GSK3 $\beta$ -induced CRY1 phosphorylation promotes FBXL3-dependent polyubiquitination**

A and B: Cell-based ubiquitination assay. COS1 cells were cotransfected without or with plasmids encoding ubiquitin-HA, FBXL3-Flag, WT-CRY1-MYC, and 2SA-CRY1-MYC (A) and 2SD-CRY1-MYC (B). Cells were incubated without or with MG132 (20  $\mu$ mol/L) for 6 h. hr, hour; IP, immunoprecipitation; UB, ubiquitin.

### **GSK3 $\beta$ regulates CRY1-mediated gluconeogenesis in hepatocytes**

To investigate whether GSK3 $\beta$ -induced CRY1 phosphorylation and degradation might modulate HGP, the effects of GSK3 $\beta$  suppression on HGP are examined using RNA interference (RNAi) and LiCl. In WT hepatocytes, GSK3 $\beta$  suppression downregulated glucose production (Fig. 27A; 28A). In accordance with this, the levels of *Pck1* and *G6pc* mRNA and FOXO1 protein are decreased by GSK3 $\beta$  suppression and LiCl treatment, accompanied by increased CRY1 protein (Fig. 27B–C; 28B–C). In contrast, in CRY1 KO hepatocytes, GSK3 $\beta$  suppression had little effects on glucose production and gluconeogenic gene expression (Fig. 27A–C; Fig. 28A–C), indicating that hepatic CRY1 would be one of key factors mediating the effect of GSK3 $\beta$  on HGP.

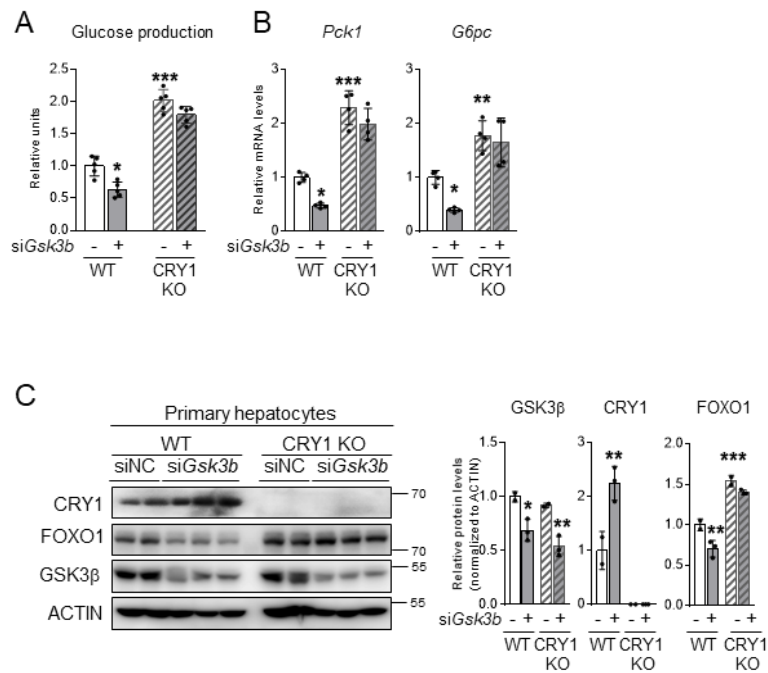


**Figure 27. GSK3 $\beta$  suppression downregulates hepatic glucose production with increased CRY1**

A–C: Primary hepatocytes isolated from WT and CRY1 KO mice were transfected without or with siGsk3b. Glucose production assay (A), qRT-PCR analysis of gluconeogenic gene expression (B), and Western blot analysis of CRY1 and FOXO1 protein levels (C) are shown. \* $P < 0.05$ , \*\* $P < 0.01$ , \*\*\* $P < 0.001$  vs. siNC group by two-way ANOVA followed by Sidak post hoc test. Mean and SD of the band intensities were calculated from independent experiments using Image J. Data are mean  $\pm$ SD.

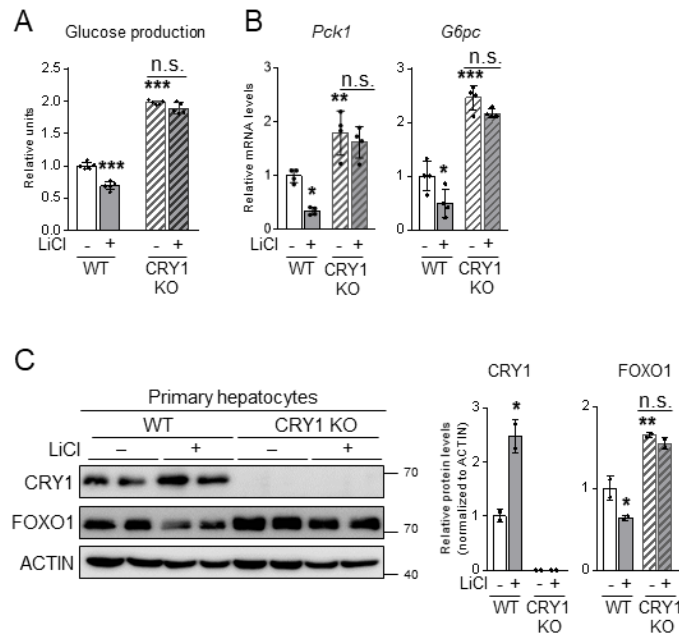


**Figure 28. Inhibition of GSK3 $\beta$  downregulates CRY1-mediated gluconeogenesis**

A–C: Primary hepatocytes isolated from WT and CRY1 KO mice were incubated without or with LiCl (20 mmol/L) for 8 h. Glucose production assay (A), qRT-PCR analysis of gluconeogenic gene expression (B), and western blot analysis of CRY1 and FOXO1 protein (C) are shown. \* $P < 0.05$ , \*\* $P < 0.01$ , \*\*\* $P < 0.001$  vs. WT, PBS group by two-way ANOVA followed by Sidak's post-hoc test. Mean and SD of the band intensities were calculated from independent experiments using Image J. Data are mean  $\pm$ SD.

Next, I decided to study whether decreased HGP through GSK3 $\beta$  inhibition might be associated with degradation of phosphorylated CRY1 protein. In CRY1 KO hepatocytes, ectopic expression of CRY1 WT attenuated glucose production and gluconeogenic gene expression while that of 2SA CRY1 mutant further potently repressed them (Fig. 29A, B). Moreover, GSK3 $\beta$  inhibition failed to repress glucose production and gluconeogenic gene expression induced by 2SA CRY1 overexpression (Fig. 29A, B). Additionally, the FOXO1 protein level was lowered by WT CRY1 and appeared to be further downregulated by 2SA CRY1 (Fig. 29C). In WT CRY1 -overexpressing hepatocytes, there was a clear difference in the levels of FOXO1 and CRY1 proteins after GSK3 $\beta$  inhibition (Fig. 29C). However, these differences are abolished in 2SA CRY1-overexpressing hepatocytes (Fig. 29C). To confirm that GSK3 $\beta$  modulates HGP through FBXL3-dependent CRY1 degradation, FBXL3 was ectopically expressed in primary hepatocytes with or without GSK3 $\beta$  inhibitors. As shown in Fig. 30A, FBXL3 overexpression elevated glucose production while FBXL3 did not promote glucose production in the presence of a GSK3 $\beta$  inhibitor. In primary hepatocytes, FBXL3 overexpression increased the levels of FOXO1 protein and gluconeogenic gene expression, which are abrogated by GSK3 $\beta$  inhibition (Fig. 30B, C). Furthermore, FBXL3 overexpression did not decrease CRY1 protein expression in the presence of LiCl (Fig. 30C). Together, these findings propose that GSK3 $\beta$ -induced CRY1

phosphorylation could elevate HGP through FBXL3-dependent CRY1 degradation in the liver.

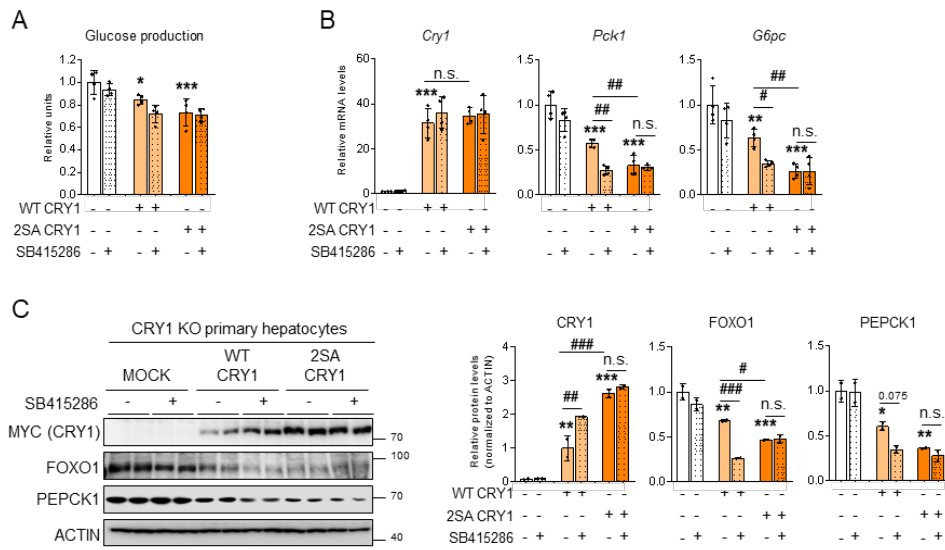


**Figure 29. GSK3 $\beta$ -induced CRY1 phosphorylation elevates hepatic glucose production**

A–C: Primary hepatocytes isolated from CRY1 KO mice were transfected without or with plasmids encoding MOCK (empty vector control) group, WT CRY1-MYC, and 2SA CRY1-MYC. Cells were incubated without or with SB415286 (20  $\mu$ mol/L) for 8 h. Glucose production assay (D), qRT-PCR analysis of gluconeogenic gene expression (E), and Western blot analysis of CRY1 and FOXO1 protein levels (F) are shown. \* $P < 0.05$ , \*\* $P < 0.01$ , \*\*\* $P < 0.001$  vs. MOCK, PBS group; # $P < 0.05$ , ## $P < 0.01$ , ### $P < 0.001$  vs. WT CRY1-MYC, PBS group by two-way ANOVA followed by Sidak post hoc test. Mean and SD of the band intensities were calculated from independent experiments using Image J. Data are mean  $\pm$ SD.

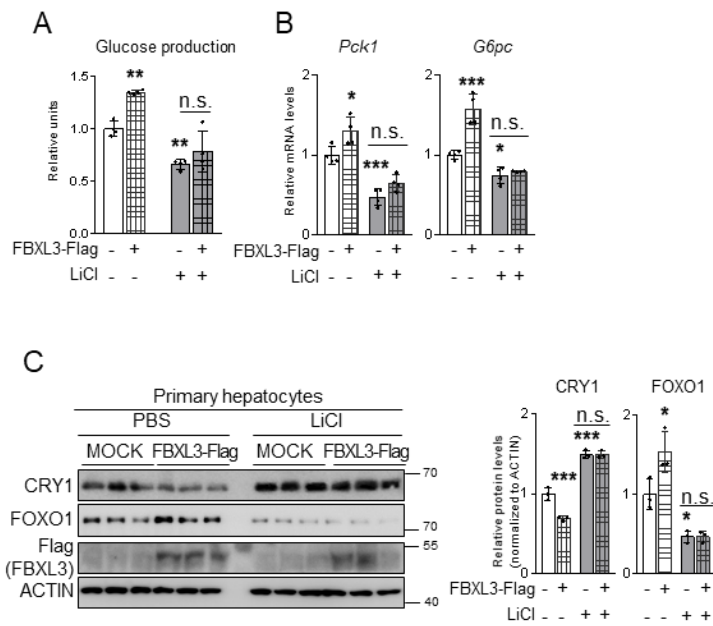


**Figure 30. GSK3 $\beta$  modulates hepatic glucose production through FBXL3-dependent CRY1 degradation**

A–C: Primary hepatocytes isolated from WT mice were transfected with FBXL3-Flag expression vectors. After transfection, cells were incubated without or with LiCl (20 mmol/L) for 8 h. Glucose production assay (A), qRT-PCR analysis of gluconeogenic gene expression (B), and Western blot analysis of CRY1 and FOXO1 protein levels (C) are shown. \* $P < 0.05$ , \*\* $P < 0.01$ , \*\*\* $P < 0.001$  vs. MOCK, PBS group by two-way ANOVA followed by Sidak post hoc test. Mean and SD of the band intensities were calculated from independent experiments using ImageJ. Data are means  $\pm$  SD. n.s., not significant.

## **Restoration of CRY1 protein with GSK3 $\beta$ inhibitor mitigates hyperglycemia in diabetic mice**

As CRY1 KO mice exhibit impaired HGP [56], I explored whether CRY1 reduction by activated GSK3 $\beta$  might be attributable to HFCF-mediated hyperglycemia. Compared with WT mice, CRY1 KO mice exhibited higher levels of fasting glucose and homeostatic model assessment for insulin resistance (HOMA-IR) (Fig. 31A, B). Interestingly, upon HFCF, CRY1 KO mice became glucose intolerant (Fig. 31C). In HFCF-fed CRY1 KO mice, the levels of pyruvate-induced blood glucose production and gluconeogenic gene expression are significantly increased (Fig. 32A, B). Together, these results suggest that CRY1 deficiency would lead to more glucose-intolerant and elevated hepatic gluconeogenesis in diabetic animals.

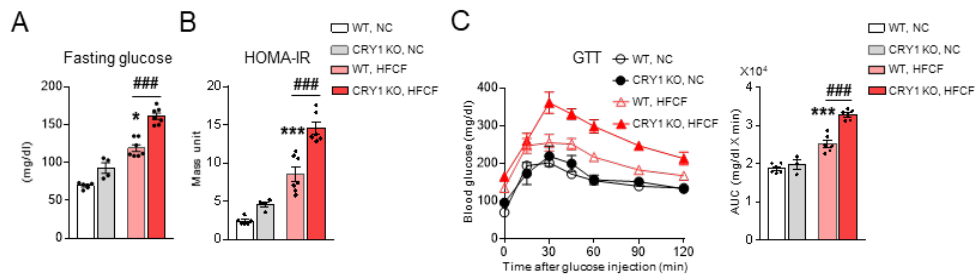


**Figure 31. CRY1 deficiency leads to glucose intolerance**

A and B: Fasting blood glucose levels (A) and measurement of HOMA of insulin resistance (HOMA-IR) (B) of NC- or HFCF-fed WT and CRY1 KO mice.  $*P < 0.05$ ,  $***P < 0.001$  vs. NC fed WT mice;  $###P < 0.001$  vs. HFCF-fed WT mice by two-way ANOVA followed by Sidak post hoc test. C: Intraperitoneal glucose tolerance test (GTT) and area under the curve (AUC) analysis of NC- or HFCF-fed WT and CRY1 KO mice.  $***P < 0.001$  vs. NC-fed WT mice;  $###P < 0.01$  vs. HFCF-fed WT mice by two-way ANOVA followed by Sidak post hoc test.

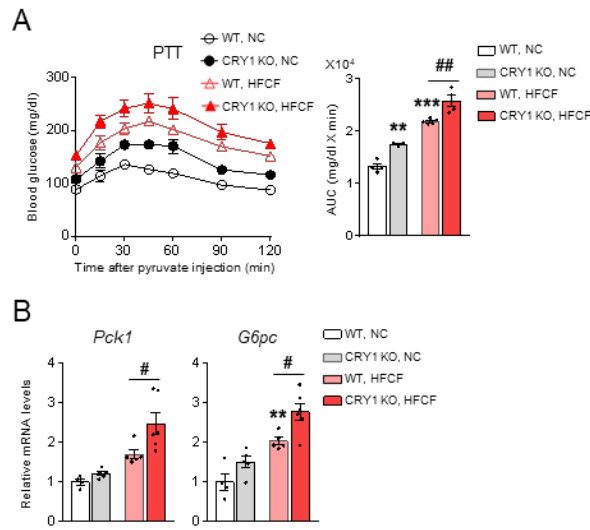


**Figure 32. CRY1 knockout mice exhibit elevated hepatic glucose production**

A: Intraperitoneal PTT and AUC analysis of NC- or HFCF-fed WT and CRY1 KO mice.  $**P < 0.01$ ,  $***P < 0.001$  vs. NC-fed WT mice;  $##P < 0.01$  vs. HFCF-fed WT mice by two-way ANOVA followed by Sidak post hoc test. B: qRT-PCR analysis of gluconeogenic gene expression in livers of WT and CRY1 KO mice.  $**P < 0.01$  vs. NC-fed WT mice.  $#P < 0.05$  vs. HFCF-fed WT mice.

To examine whether GSK3 $\beta$ -induced CRY1 degradation is involved in hyperglycemia with enhanced HGP in diabetic animals, the *in vivo* effects of a GSK3 $\beta$  inhibitor on HGP are evaluated. GSK3 $\beta$  inhibitors did not largely affect body weights in either WT or CRY1 KO mice (Fig. 33A, C). Also, there are little histological differences in liver with or without GSK3 $\beta$  inhibitors (Fig. 33B, D). In WT mice, the level of blood glucose was mitigated by GSK3 $\beta$  inhibition during PTT, while GSK3 $\beta$  inhibitors did not significantly affect the level of blood glucose upon pyruvate challenge in CRY1 KO mice (Fig. 34A; 35A). In accordance with these, the expression of *Pck1* and *G6pc* was downregulated by GSK3 $\beta$  inhibitors in WT mice, whereas it was not affected in CRY1 KO mice (Fig. 34B; Fig. 35B). Furthermore, in the presence of a GSK3 $\beta$  inhibitor, the level of hepatic FOXO1 protein was downregulated, which was not observed in CRY1 KO mice (Fig. 34C; Fig. 35C). Moreover, hepatic glucose production was examined with *in vivo* GSK3 $\beta$  suppression in animal models. Similar to pharmacological intervention of GSK3 $\beta$ , si*Gsk3b*-treated WT mice decreased HGP during PTT and reduced hepatic FOXO1 protein, which was not observed in CRY1 KO mice (Fig. 36A-C). Together, these data evidently suggest that maintaining CRY1 protein stability would be crucial to attenuate hyperglycemia by repressing HGP in diabetic mice.

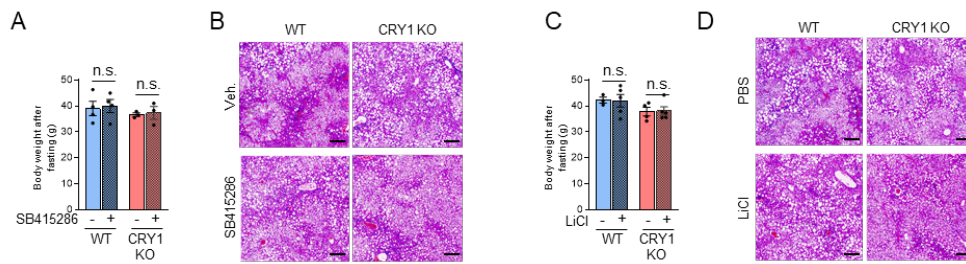


**Figure 33. GSK3 $\beta$  inhibitors do not largely affect body weights**

A–B: SB415286 (5 mg/kg) was intraperitoneally injected into HFHF-fed WT or CRY1 KO mice. Body weights (A), representative images of hematoxylin and eosin-stained liver sections (B) of vehicle or SB415286-treated mice. C–D: LiCl (3 mM/kg) was intraperitoneally injected into HFHF-fed WT or CRY1 KO mice. Body weights (C), representative images of hematoxylin and eosin-stained liver sections (D). n.s. not significant

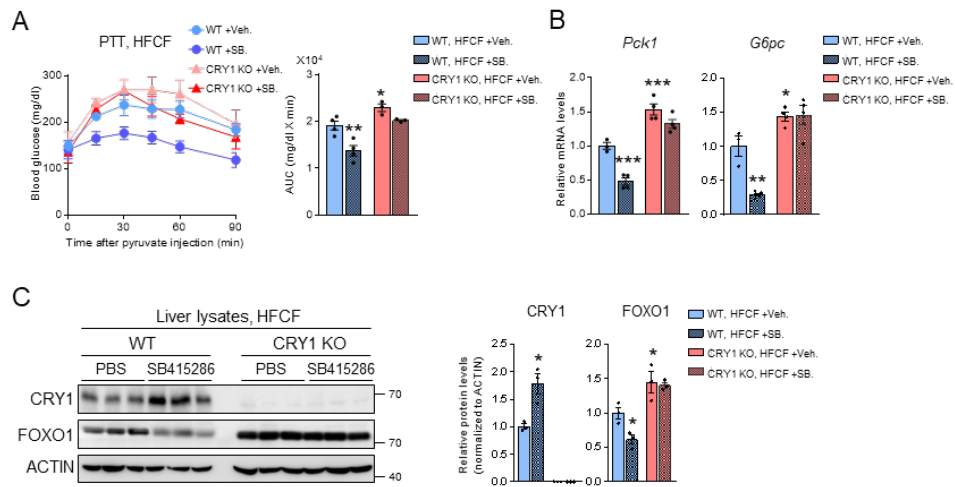


**Figure 34. Increase in CRY1 protein by GSK3 $\beta$  inhibitors mitigates hyperglycemia in diabetic mice.**

A–C: SB415286 (5 mg/kg i.p.) was injected into HFCF-fed WT or CRY1 KO mice. Intraperitoneal PTT and area under the curve analysis (A), qRT-PCR analysis of gluconeogenic gene expression in liver (B), and Western blot analysis of liver lysates (C) from HFCF-fed WT and KO mice are shown. \* $P < 0.05$ , \*\* $P < 0.01$ , \*\*\* $P < 0.001$  vs. vehicle-treated HFCF-fed WT mice by two-way ANOVA followed by Sidak post hoc test. Mean and SEM of the band intensities were calculated from independent experiments using ImageJ. Data are means  $\pm$  SEM. SB., SB415286; Veh., vehicle.

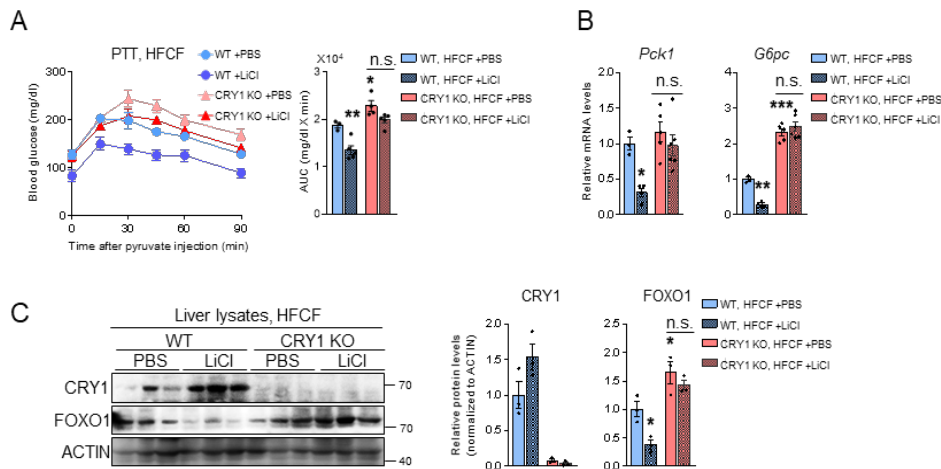


**Figure 35. GSK3 $\beta$  inhibitor mitigates hyperglycemia in diabetic animals**

A–C: LiCl (3 mM/kg) was intraperitoneally injected into HFCF-fed WT or CRY1 KO mice. Intraperitoneal PTT and AUC analysis (A) of vehicle or LiCl-treated mice. qRT-PCR analysis of gluconeogenic gene expression (B) and western blot analysis (C) in the livers of vehicle or LiCl-treated mice. \* $P < 0.05$ , \*\* $P < 0.01$ , \*\*\* $P < 0.001$  vs. vehicle-treated HFCF-fed WT mice by two-way ANOVA followed by Sidak's post-hoc test. Mean and SEM of the band intensities were calculated from independent experiments using ImageJ. Data are means  $\pm$  SEM.

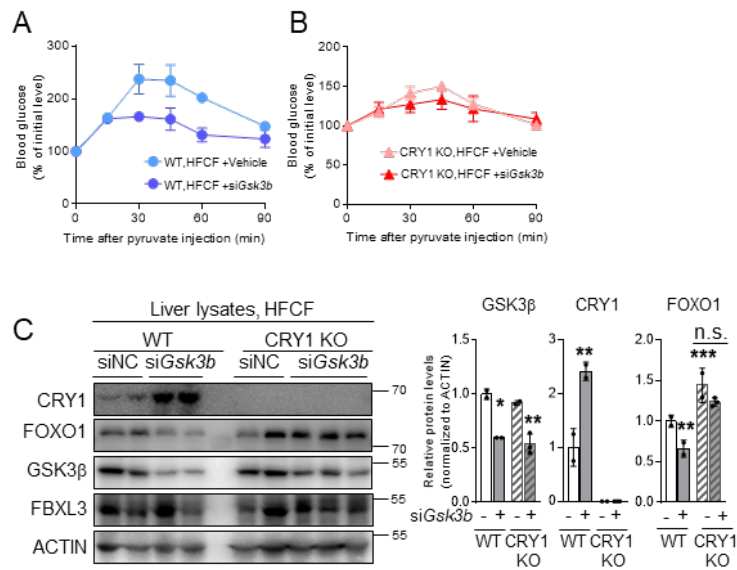


**Figure 36. *in vivo* GSK3 $\beta$  suppression reduces hepatic glucose production in diabetic mice**

A–C: *siGsk3b* was intravenously injected into HFCF-fed WT or CRY1 KO mice. Intraperitoneal PTT analysis of HFCF-fed WT mice (A), Intraperitoneal PTT analysis of HFCF-fed CRY1 KO mice (B). Western blot analysis of livers of HFCF-fed WT and KO mice (C). Mean and SEM of the band intensities were calculated from independent experiments using Image J. Data are mean  $\pm$  SEM. n.s., not significant. \* $P < 0.05$ , \*\* $P < 0.01$ , \*\*\* $P < 0.001$  vs. siNC-treated HFCF-fed WT mice by two-way ANOVA followed by Sidak's post-hoc test

## 5. Discussion

Emerging evidence suggests that a decrease in hepatic CRY1 protein is responsible for dysregulated glucose metabolism in diabetes [56, 72]. Also, several studies have shown that single-nucleotide polymorphisms (SNPs) of CRY1 genes are associated with hyperglycemia, insulin resistance, and diabetes risk [147, 148]. However, it is largely unknown the underlying mechanism(s) by which CRY1 protein would be reduced to confer hyperglycemia. In this study, I demonstrated that elevated GSK3 $\beta$ -dependent hepatic CRY1 degradation is attributable to hyperglycemia due to upregulated HGP. Hepatic FBXL3 expression was elevated, promoting CRY1 degradation in diabetes. Mechanistically, activated GSK3 $\beta$ -induced CRY1 phosphorylation at S280/S281 residues facilitated FBXL3-mediated CRY1 degradation, resulting in elevated HGP. Collectively, these findings suggest that the dysregulation of CRY1 protein stability through GSK3 $\beta$ -dependent CRY1 degradation would be one of the etiological features of hyperglycemia.

FBXL3-mediated CRY1 polyubiquitination appears to be important for CRY1 protein stability in the regulation of circadian rhythms [138]. Recently, it has been demonstrated that FBXL3 is involved in various cellular processes beyond circadian rhythm, including cell proliferation, cell cycle progression, and cancer cell metabolism by manipulating CRY1 protein stability [149, 150]. In hepatocytes, I found that FBXL3 modulates

CRY1 protein stability by promoting polyubiquitination and proteasomal degradation. Given that CRY1 suppresses HGP through repression of FOXO1 levels, I hypothesized that FBXL3-dependent CRY1 degradation in hepatocytes might elevate the level of FOXO1, leading to enhanced HGP. In WT hepatocytes, FBXL3 overexpression stimulated HGP and the levels of FOXO1 protein and gluconeogenic gene expression, which was abolished in CRY1 KO hepatocytes, indicating that FBXL3-dependent CRY1 degradation stimulates FOXO1-mediated HGP. Here, I found that hepatic FBXL3 expression was elevated in diabetic animals. Although further studies are needed to determine which factors upregulate hepatic FBXL3 in diabetic animals, current data suggest that aberrantly increased FBXL3 would contribute to excessive HGP and metabolic disorders.

The FBXL3-containing SCF complex is important for recognizing and degrading phosphorylated substrate proteins [151]. I observed that the level of hepatic CRY1 protein phosphorylation was increased in diabetic animals, implying that FBXL3-dependent CRY1 degradation might be augmented by CRY1 phosphorylation. To date, it is unclear which kinase(s) are involved in the regulation of CRY1 protein stability in diabetic animals. *In silico* analysis revealed that CRY1 protein might be phosphorylated by several kinases. Among them, it is likely that hepatic GSK3 $\beta$  negatively modulates CRY1 protein stability. I also found that phosphorylation of CRY1 at S280/S281 residues by GSK3 $\beta$  promoted FBXL3-dependent CRY1 polyubiquitination. It is of interest to note that the reduction in CRY1

protein induced by FBXL3 overexpression was attenuated by GSK3 $\beta$  inhibition, proposing that CRY1 phosphorylated by GSK3 $\beta$  is a preferential target for FBXL3-dependent degradation. Furthermore, the enzymatic activity of hepatic GSK3 $\beta$  is elevated in obese and diabetic animals [142, 143]. In this regard, I suggest that GSK3 $\beta$  could operate as a rheostat of hepatic CRY1 protein stability in response to pathological cues by modulating the level of CRY1 phosphorylation, leading to FBXL3-dependent degradation in diabetes.

GSK3 $\beta$  has been implicated in inactivating glycogen synthase and regulating gluconeogenic gene expression in glucose metabolism [152]. In addition, GSK3 inhibitors have been shown to be effective in normalizing blood glucose levels in animal models of type 2 diabetes [153], and their effects appear to occur primarily through an increase in hepatic glycogen synthesis and a decrease in HGP [154]. However, the mechanism by which GSK3 $\beta$  inhibition confers HGP suppression is not thoroughly understood. In this study, I propose that CRY1 would be a crucial node in the inhibitory effect of GSK3 $\beta$  suppression on hyperglycemia. FOXO1 protein in WT hepatocytes was decreased by GSK3 $\beta$  repression, concomitantly with increased CRY1 protein levels, which was not largely observed in CRY1 KO hepatocytes. Consistently, the effect of GSK3 $\beta$  inhibitors on decreased FOXO1 protein expression was abolished in CRY1 2SA-expressing hepatocytes. Moreover, GSK3 $\beta$  suppression alleviated excessive HGP and

improved hyperglycemia through CRY1-mediated FOXO1 degradation. Nevertheless, I cannot exclude the possibilities that other GSK3 $\beta$  targets and/or related signaling pathways might be involved in HGP. Because GSK3 $\beta$  suppression marginally alleviated excessive HGP in CRY1 KO. Furthermore, it has been reported that other GSK3 $\beta$  targets, such as CREB, FOXO1,  $\beta$ -catenin, and c-MYC [155-158], would be involved in HGP.

It has been reported that HGP accounts for large portion of endogenous glucose production [159]. One of the prominent phenotypes of CRY1 KO mice was enhanced HGP accompanied by increased expression of FOXO1 and gluconeogenic genes. In diabetic animals, restoring CRY1 protein by suppression of hepatic FBXL3 or GSK3 $\beta$  mitigated hyperglycemia with reduced HGP. However, hepatic GSK3 $\beta$  suppression had little effects on HGP in CRY1 KO mice. In addition, the level of glucose production was higher in CRY1 KO primary hepatocytes than in WT primary hepatocytes in a cell-autonomous manner. These *in vivo* and *in vitro* data imply that CRY1 would play crucial roles in HGP under physiological and pathological conditions. As I analyzed whole-body CRY1 knockout mice, it is feasible that confounding effects of CRY1 deletion in other tissues would also affect HGP and systemic glucose metabolism. Thus, it needs to be further investigated with hepatocyte-specific knockout animal models.

In conclusion, I show that hepatic GSK3 $\beta$ -dependent CRY1

degradation plays a key role in modulating HGP (Fig. 37). In diabetic animals, elevated hepatic FBXL3 facilitates CRY1 degradation via GSK3 $\beta$ -induced phosphorylation, resulting in aberrant FOXO1 accumulation and hyperglycemia. Also, restoring the level of CRY1 protein by inhibiting GSK3 $\beta$  alleviated excessive HGP and ameliorated hyperglycemia. Collectively, these data suggest that the hepatic GSK3 $\beta$ -CRY1-FBXL3 axis would be one of the potential therapeutic targets in diabetes.

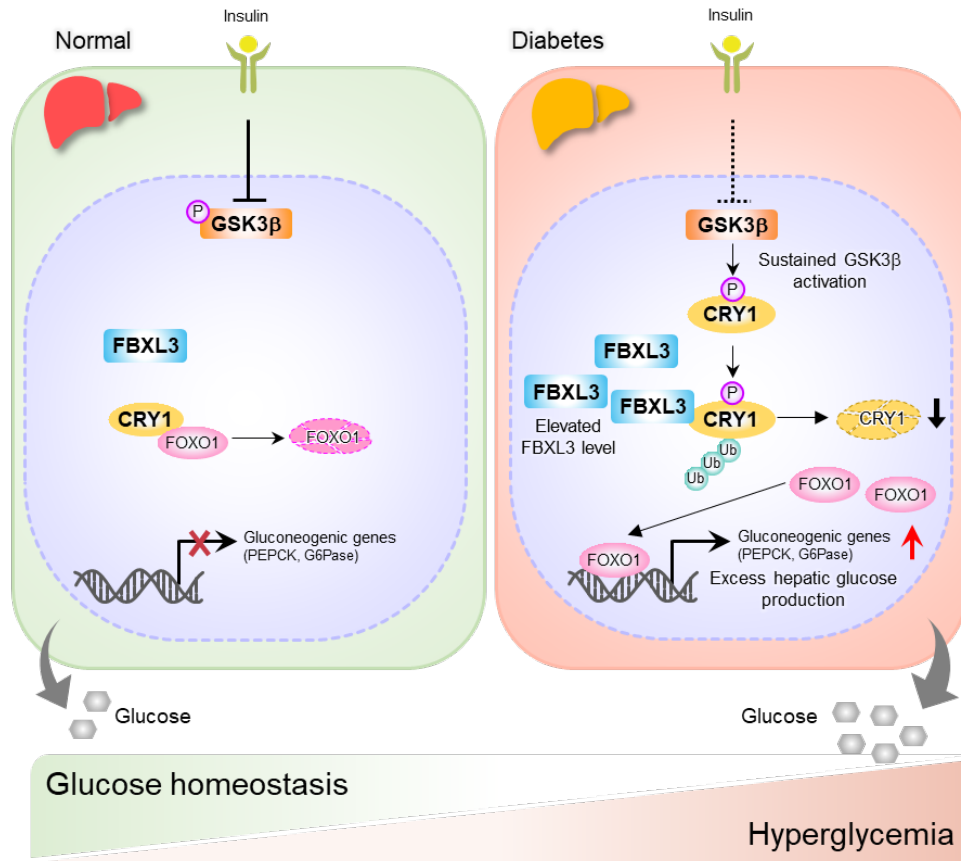


**Figure 37. Proposed model.**

Hepatic CRY1 protein stability is tightly regulated to govern glucose homeostasis through the suppression of FOXO1-mediated HGP. In diabetic animals, elevated FBXL3 promotes hepatic CRY1 degradation, leading to the accumulation of FOXO1. GSK3 $\beta$ -induced CRY1 phosphorylation potentiates FBXL3-dependent CRY1 degradation in hepatocytes. These findings suggest that facilitated hepatic CRY1 degradation is involved in inducing excessive HGP, contributing to hyperglycemia in diabetes. Ub, ubiquitin.

## **CHAPTER TWO:**

# **Cryptochrome 1 (CRY1) participates in mitochondria quality control for thermogenesis in BAT**

## 1. Abstract

Mitochondria are indispensable organelles that possess diverse roles depending upon cell type. For instance, mitochondria are crucial for thermogenic activity in brown adipocyte. Temperature change, one of the zeitgebers (cues) of peripheral circadian clocks, alters circadian rhythms in brown adipose tissue (BAT), a key organ for thermogenesis. However, the roles of circadian regulator(s) on thermogenic activity control in BAT are largely unknown. Here, I demonstrate the role of circadian regulator Cryptochrome 1 (CRY1) in mitochondrial homeostasis and its implications in thermogenesis. I found that CRY1 deficiency causes abnormal mitochondrial features and fitness. Compared to wild type (WT) mice, CRY1-deficient mice exhibited an increased frequency of mitophagy, leading to a decrease in mitochondrial abundance. Furthermore, CRY1 knockout (KO) mice impaired thermogenic activity due to reduced mitochondrial abundance and accumulation of damaged mitochondria. Collectively, these findings suggest that CRY1 would be an important player in maintaining healthy mitochondrial pool and function, leading to regulation of thermogenic activity in BAT.

## 2. Introduction

Mitochondria are essential organelles with multifaceted properties across tissues and cell types, conferring tissue-specific functions [160]. BAT is a highly metabolic organ that consumes high amounts of energy sources through abundant mitochondria for adaptive thermogenesis [90, 161, 162]. In BAT, mitochondria are equipped with an exclusive uncoupling protein 1 (UCP1), which induces proton leakage across the mitochondrial inner membrane, resulting in heat production [163]. In brown adipocyte, dynamic alterations in mitochondrial structure and their increase occur in response to cold stimuli, leading to maximizing thermogenic activity with UCP1 [164]. As mitochondria are critical for thermogenic and metabolic roles in BAT, maintaining mitochondrial homeostasis is important for preserving healthy BAT functions.

Circadian rhythms govern a wide variety of physiological and metabolic functions in most organisms [165]. Unlike central clock in brain, which is mainly regulated by light, peripheral clocks in adipose tissue, liver, and muscle are influenced by various external stimuli, including temperature, feeding/fasting cycles, hormones, physical activity, and metabolic byproducts [166, 167]. This peripheral clock is responsible for autonomous circadian rhythms in each tissue and necessary for regulating energy homeostasis [12, 168]. Among circadian regulators, it has been reported that Cryptochrome 1 (CRY1) plays dynamic roles in energy homeostasis in

metabolic organs [56, 57, 75]. Although BAT is one of the key thermogenic and metabolic organs highly responsive to temperature alterations, the roles of circadian regulator CRY1 in BAT are largely unknown.

Even though emerging evidence has proposed a potential link between changes in circadian clock and mitochondrial abundance and bioenergetics according to various stimuli [33, 34], the physiological roles of circadian regulators in mitochondria in brown adipocytes and their underlying mechanisms have not been thoroughly understood. Herein, I aimed to decipher the roles of CRY1 on mitochondrial homeostasis in BAT. I analyzed in-depth CRY1 in mitochondria features and behaviors using high-resolution approaches such as transmission electron microscopy (TEM) and fluorescence-based assay to assess mitochondria function. In addition, modulating CRY1 expression in BAT revealed that it is likely to fulfill a critical role in thermogenesis by restoring mitochondrial abundance. Collectively, these data propose a novel role of CRY1 in mitochondrial quality control for preserving thermogenic activity in BAT.

### **3. Materials and methods**

#### **Animal Experiments**

CRY1 KO mice were appreciatively provided by Dr. Sancar Aziz from the University of North Carolina. All animals were maintained under a 12-h/12-h light/dark cycle in a pathogen-free animal facility. For the cold tolerance test, 8~12 week-old male mice were placed in a cold room at 6°C. Cold-exposure studies are performed within climate-controlled rodent incubators (Environmental Cabinet, DBL CO.). For thermoneutral and cold-exposure experiments, 8~12 week-old male mice were placed at 30 °C for 7 days and then these mice were exposed to cold environments (6 °C). Rectal temperature was measured using a thermal probe (Testo925, Testo inc.). The surface temperature of the mice was imaged using an infrared camera (CX320 Thermal Imaging Camera; COX Co.). Dissected tissue specimens were immediately stored at –80 °C until analysis. For BAT-specific CRY1 overexpression, 5 µg of plasmid was directly injected into BAT of WT male mice using In Vivo-JetPEI® (201-10G, Polyplus) according to the manufacturer's protocol. For BAT-specific CRY1 rescue experiments, 14~15 week-old male mice were directly injected with adenoviruses encoding green fluorescent protein (GFP) (Ad-MOCK) or CRY1 (Ad-CRY1) into BAT (adenoviral dose of  $1 \times 10^9$  viral particles per mouse). After 10 days, mice were subjected to the cold tolerance test and analyzed. All animal experiments were approved by the Seoul National University Institutional Animal Care and Use Committee.

## **Cell Culture**

Immortalized murine brown adipocytes (BAC) were kindly provided by Dr. Kai Ge (National Institutes of Health). BAC preadipocytes were grown in Dulbecco's modified Eagle's medium (DMEM) supplemented with 10% FBS to confluence and then incubated in induction medium consisting of DMEM, 10% FBS, 20 nmol/L insulin, 10 nmol/L 3,3,5-triiodo-L-thyronine (T3), 125 µmol/L indomethacin, 0.5 mmol/L isobutylmethylxanthine, and 5 µmol/L dexamethasone. After 2 days, the cells were treated with differentiation medium (DMEM, 10% FBS, 20 nmol/L insulin, and 10 nmol/L T3) for 2 days, and then the medium was changed with DMEM containing 10% FBS. Primary MEFs were extracted from E13.5 embryos. Briefly, embryos are sterilized with ethanol, washed with PBS and triturated with razor blades with 0.25% trypsin-EDTA. Cells were then incubated in DMEM supplemented with 10% FBS and 1% MEM non-essential amino acid during 6 hours at 37 °C and 5% CO<sub>2</sub>. After 6hr, cultured cells were washed. Finally, MEFs were incubated at 37 °C and 5% CO<sub>2</sub> and used for the corresponding experiments.

## **Electron microscopy**

The dissected tissues fixed with 2% glutaraldehyde and 2% paraformaldehyde in 0.05 M cacodylate solution (pH 7.0) overnight at 4 °C. After washing with 0.05 M cacodylate solution, the samples were post-fixed with 1% osmium tetroxide at 4 °C for 1.5 hours, followed en bloc in 0.5% uranyl acetate overnight and dehydrated with graded ethanol series. The

samples were then embedded with a spurr's resin and polymerized in oven at 70 °C. The polymerized samples were section in 70 nm with an ultramicrotome (UC7; Leica Microsystems, Germany), and the sections were mounted on copper mesh grids. Sections were stained with uranyl acetate for 20 minutes and lead citrate 5 minutes. The samples were observed on a JEM-1010 transmission electron microscope at 80kV (JEOL, Japan).

### **Immunoblotting**

All tissues and cells were lysed on ice with RIPA buffer containing, and a protease inhibitor cocktail(#P3100, GeneDEPOT). Protein lysates were boiled and subjected to SDS-polyacrylamide gel electrophoresis. The separated proteins were transferred onto polyvinylidene fluoride membranes. Antibodies against MYC (Cell Signaling, 2276, 1:1000 dilution), OXPHOS (Abcam, ab110413, 1;1000 dilution), Actin (Sigma-Aldrich, A5316, 1:2000 dilution), UCP1 (Abcam, ab10983, 1:1000 dilution), TOM20 (Milipore, ST1705, 1:1000 dilution), PMP70 (Abcam, ab3421, 1:1000 dilution), Calreticulin , CRY2 (Invitrogen, PA5-13125, 1:1000 dilution), Bmal1 (Abcam, ab230822, 1:1000 dilution), Per2 (Abcam, ab227727, 1:1000 dilution), GAPDH (LabFrontier Co., LF-PA0018, 1:1000 dilution), VDAC (Cell Signaling, 4661, 1:1000 dilution), NRF1 (Abcam, ab47517, 1:1000 dilution), Vinculin (Cell signaling, 4650S, 1:1000 dilution), PGC1 $\alpha$  (NOVUS, NBP1-04676, 1:1000 dilution), LaminB1 (Abcam, ab16048, 1:1000 dilution), phosphor-PINK1 ser228 (Thermo fisher, PA5-

105356, 1:1000 dilution), phospho-Parkin Ser65 (Thermo fisher, PA5-114616, 1:1000 dilution), Parkin (Cell signaling, 2132S, 1:1000 dilution), ubiquitin (Cell signaling, 3936S, 1:1000 dilution), PINK (Abcam, 23707, 1:1000 dilution) and CRY1 (Abcam, 104736, 1:1000 dilution; lab-made antibody obtained from Dr. Aziz Sancar [135], 1:500 dilution) were used. MYC-CRY1 was cloned into the pcDNA3.1 vector.

### **Indirect calorimetry**

Indirect calorimetry was performed using PhenoMaster (TSE Systems) according to the manufacturer's protocol. Ten-week-old male mice were placed in a calorimetric chamber for 48 hours prior to measurements of  $VO_2$ ,  $VCO_2$ , and energy expenditure. To activate  $\beta_3$ -adrenergic signaling, mice were intraperitoneally injected with CL-316,243 (1 mg/kg). The experiments were performed at the Korea Mouse Phenotyping Center (KMPC), SNU, Seoul, Korea.

### **Quantification of mitochondrial DNA**

Mitochondrial DNA copy number analysis was performed as described [169]. DNA was isolated from all cells and tissues using phenol-chloroform extraction. mtDNA abundance was measured by qPCR using mitochondrial genomic primers to indicate genes. The nuclear *Hk2* gene was used for normalization. The sequences of the primer used for qPCR are listed in Table 5.

### **RT-qPCR**

Total RNA was isolated from tissues or cells using TRIzol Reagent (RiboEx,

GeneAll) and subjected to cDNA synthesis using the ReverTra Ace qPCR RT Kit (Toyobo). Relative mRNA levels were detected using the CFX96™ Real-Time System (Bio-Rad Laboratories). RT-qPCRs were run using SYBR Green Master Mix (DQ384-40h, Biofact). Target gene expression levels were normalized to cyclophilin gene expression levels. The primers used for RT-qPCR are listed in Table 5.

### **Evaluation of mitochondrial membrane potential**

The  $\Psi_m$ -sensitive fluorescent probe JC-1 and TMRE were utilized, and cells were analyzed either by flow cytometry or confocal analysis. Briefly, cells were incubated with 10  $\mu$ M JC-1 or 200 nM TMRE at 37 °C for 30 minutes and either viewed using a confocal microscope or quantified using the FACS Canto instrument (BD Bioscience). For FACS analysis, gates were set with unstained cells and CCCP (sigma Aldrich C2759)-treated controls (20  $\mu$ M) and quantified emission filters appropriated for PE and FITC. JC-1 ratio measurements were calculated in Diva as the FITC/PE ratio.

### **Mitophagy analysis**

Mitophagy was measured using mt-Keima and mitophagy detection kit according to manufacturer's protocol (MT02, Dojindo Molecular Technologies, Inc., Kumamoto, Japan). For the green (mt-Keima in mitochondria) signal, we used a 488-nm laser and our emission collection window was set from 570–690 nm. For the red (mt-Keima in lysosomes) signal we used a 552-nm laser and the emission collection window was

similar to that of the green signal (570–690 nm). Cells were washed with PBS and then stained 100 nM Mtpagy dye with serum-free medium for 30 minutes. Then, cells were washed with PBS twice and 20 mM CCCP treated for 4 hours. After 4 hours incubation, 50-100 nM lysotracker Green DND-26 was added to the cells and incubated for 10 minutes. In each experiment, all images were captured within 1 hour. Fluorescence was quantified using ImageJ software.

### **Cell and whole-mount tissue imaging**

Cell and whole-mount tissue imaging was performed as previously described [170]. Cells and whole or minced BAT were washed with PBS and then stained with Hoechst33342, MitoTracker Green, TMRE, JC-1 or MitoTracker Deep-Red for 15 minutes. Samples were observed using a CQ1 confocal microscope (Yokogawa) and Coherent anti-Stokes Raman Scattering Microscopy (CARS) microscopy (TCS SP8 CARS microscope, Leica Microsystems).

### **Statistical analyses**

Data are presented as the mean  $\pm$  standard deviation (s.d.). For comparison between two groups, a two-tailed Student's t-test was used. For comparison between more than two groups, one-way ANOVA with multiple comparisons was used followed by Tukey's post hoc test. For comparison between two independent variables, two-way ANOVA with multiple comparisons was used followed by Sidak's multiple comparisons test. To compare repeated measures, repeated measure ANOVA was used followed

by Sidak's multiple comparisons test. Statistical analyses were performed using GraphPad Prism (GraphPad Software).

Table 5. Primers used for qRT-PCR in Chapter two

Gene (mouse)	Forward	Reverse
Atp6	TGGCATTAGCAGTCCGGCTT	ATGGTAGCTGTTGGTGGGCT
Bmal1	AAATCCACAGGATAAGAGGG	ATAGTCCAGTGGAAAAGGAATG
Clock	AATGACTCATTAACCCCTG	CTATGTGTGCGTTGTATAGTTC
Cox1	ACACAACCTTTCTTTGATCCCG	AGAATCAGAACAGATGCTGG
Cox2	ATAATCCCAACAAACGACCT	CTCGGTTATCAACTTCTAGCA
Cox3	CTTACCATCTCCAAGCTTCA	AGTCCATGGAATCCAGTAGCCAT
Cox5a	TGTCTGTTCCATTGCTGCTATTC	TTACGCAATCCCAGGCATCAATG
Cox7a1	AAAACCGTGTGGCAGAGAAG	CCAGCCCAAGCAGTATAAGC
Cox8a	TGCGAAGTTCACAGTGGTTC	TGCTGCGGAGCTCTTTTTAT
Cry1	TGAGGCAAGCAGACTGAATATTG	CCTCTGTACCGGGAAAAGCTG
Cry2	CTGGCGAGAAGGTAGAGTGG	GACGCAGAATTAGCCTTTGTC
Cytb	CCTTCATGTCGGACGAGGCTT	TGCTGTGGCTATGACTGCGAA
Dio2	CAGTGTGGTGCACGTCTCCAATC	TGAACCAAAGTTGACCACCAG
Dloop1	AATCTACCATCTCCGTGAAACC	TCAGTTTAGCTACCCCAAGTTTAA
Dloop2	CCCTCCCCATTGGTCT	TGGTTTCACGGAGGATGG
Elov13	ATGCAACCTATGACTTCGAG	ACGATGAGCAACAGATAGACG
Hk2	GGGACGACGGTACACTCAAT	GCCAGTGGTAAGGAGCTCTG
Nd1	CTAGCAGAAACAAACCGGG	CCGGCTGCGTATTCTACGTT
Nd2	GCCTGGAATTCAGCCTACTAGC	GGCTGTTGCTTGTGTGACGA
Nd4L	CTCACCATAGCCTTCTCAC	CGTAATCTGTTCCGTACGTG
Nd6	GGGATGTTGGTTGTGTTTGGGA	CTACCCCAATCCCTCCTTCC
Ndufb10	TGGAGCAGTTCACCAAAGTG	TTCCAGCATTCTCTGCTTCT
Ndufs3	TTATGGCTTCGAGGGACATC	ATTCTTGTGCCAGCTCCACT
Nfe2l2	GAGAGGTAAGAATAAAGTCGC	GTAGATGGAGGTTTCTGTCTG
Nrf1	TGAATGTGGCTTTCGCTCC	GTGAAGTAATTGTCCAGGTCTATGC
Per1	CCCAGCTTACCTGCAGAAG	ATGGTCGAAAGGAAGCCTCT
Per2	TGTGCGATGATGATTCTGTA	GGTGAAGGTACGTTTGGTTTGC
Ppargc1a	CCCTGCCATTGTTAAGACC	TGCTGCTGTTCTGTTTTTC
Sdha	GGAACACTCCAAAAACAGACCT	CCACCACTGGGTATTGAGTAGAA
Sdhb	AATTTGCCATTTACCGATGGGA	AGCATCCAACACCATAGGTCC
Tbp	GGGAGAATCATGGACCAGAA	CCGTAAGGCATCATTGGACT
Tfam	CGCATCCCCTCGTCTATCAGTC	TAAATTTGGGTAGCTGTTCTGTGG (
Tfb2m	GGAAACGCAATGCCCAATA	CCTCCGGGCAGTAGTCATAG
Ucp1	TCTGCATGGGATCAAACCCC	ACAGTAAATGGCAGGGGACG

## 4. Results

### **CRY1 deficiency causes abnormal mitochondrial characteristics**

To investigate roles of CRY1 in BAT mitochondria, I first obtained electron microscopic (EM) images from WT and CRY1 KO mice, which provided clues to evaluate BAT mitochondrial ultrastructure. Compared to WT BAT, CRY1 KO BAT severely exhibited swollen mitochondria and prominent loss of cristae density (Fig. 38). To understand key molecular characteristics of mitochondrial phenotypes, I examined mitochondrial protein abundance and mitochondrial DNA (mtDNA) copies. The levels of mitochondrial proteins, such as OXPHOS system and TOM20, and number of mtDNA copies, were significantly reduced in BAT of CRY1 KO mice (Fig. 39A, B). By contrast, CRY1 depletion in BAT did not influence the expression of other organelle marker proteins including peroxisome marker protein PMP70 and ER marker proteins calreticulin (Fig. 39A). To monitor mitochondrial contents, I stained with the mitochondria-specific dye MitoTracker. As shown in Fig. 39C, overall intensity of mitochondrial staining was markedly reduced in BAT of CRY1 KO mice, indicating that CRY1 deficiency in BAT would downregulate mitochondrial contents. In accordance with these, the levels of mitochondrial proteins and amounts of mtDNA were decreased in various tissues in CRY1 KO mice (Fig. 40A, B). These data suggest that CRY1 deficiency would downregulate intact mitochondria and impair mitochondrial features in BAT, probably, as well as other tissues.

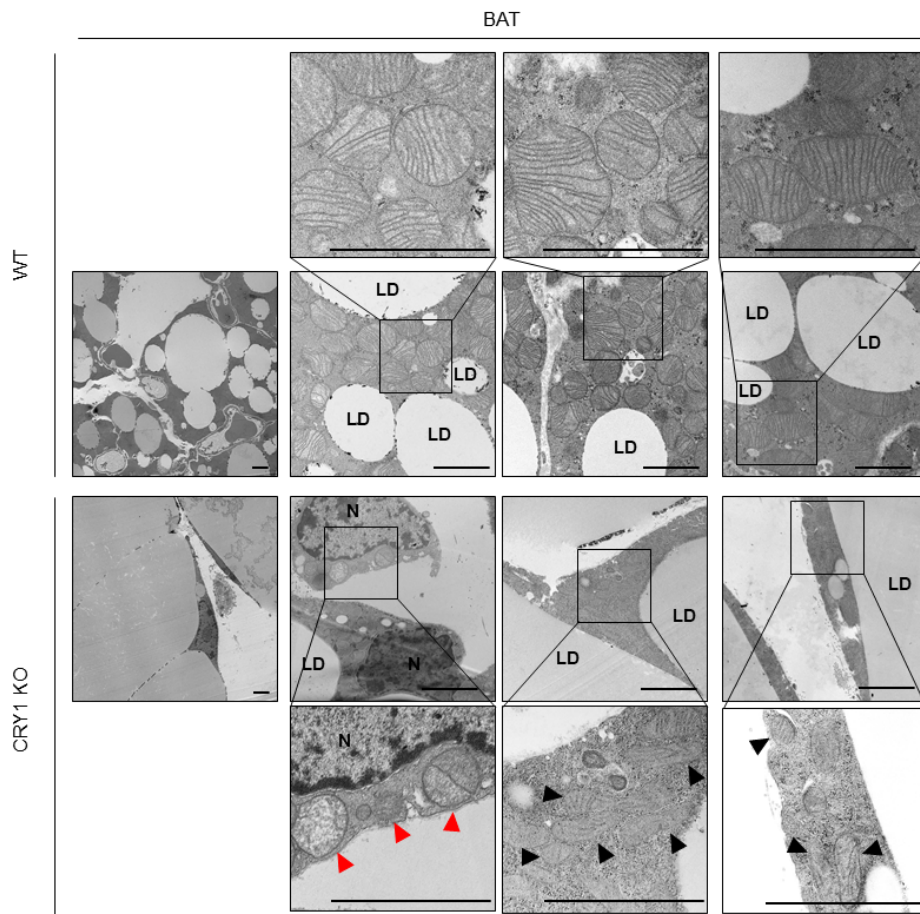


**Figure 38. Deficiency of CRY1 in BAT results in morphological mitochondrial defects**

Representative electron micrographs of BAT of 12-week-old WT and CRY1 KO mice housed at room temperature (RT). Red arrowheads point to swollen mitochondria and black arrowheads point to low-density and disrupted mitochondria. Scale bar, 2  $\mu$ m.

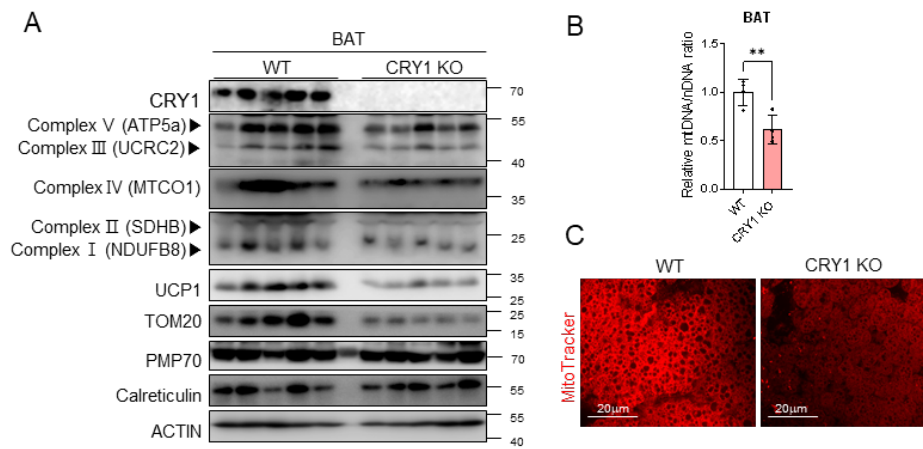


**Figure 39. Deficiency of CRY1 in BAT decreases expression of mitochondrial proteins and downregulated mitochondrial contents**

A: Western blotting analysis of BAT from WT and CRY1 KO mice housed at RT B: mtDNA(Dloop2) contents normalized to nuclear DNA(HK2) in BAT of WT and CRY1 KO mice. C: Representative wholemount MitoTracker Red staining images of BAT of WT and CRY1 KO mice housed at RT. Scale bar, 20  $\mu$ m. Data are mean  $\pm$ S.D. **\*\*** $P < 0.01$ .

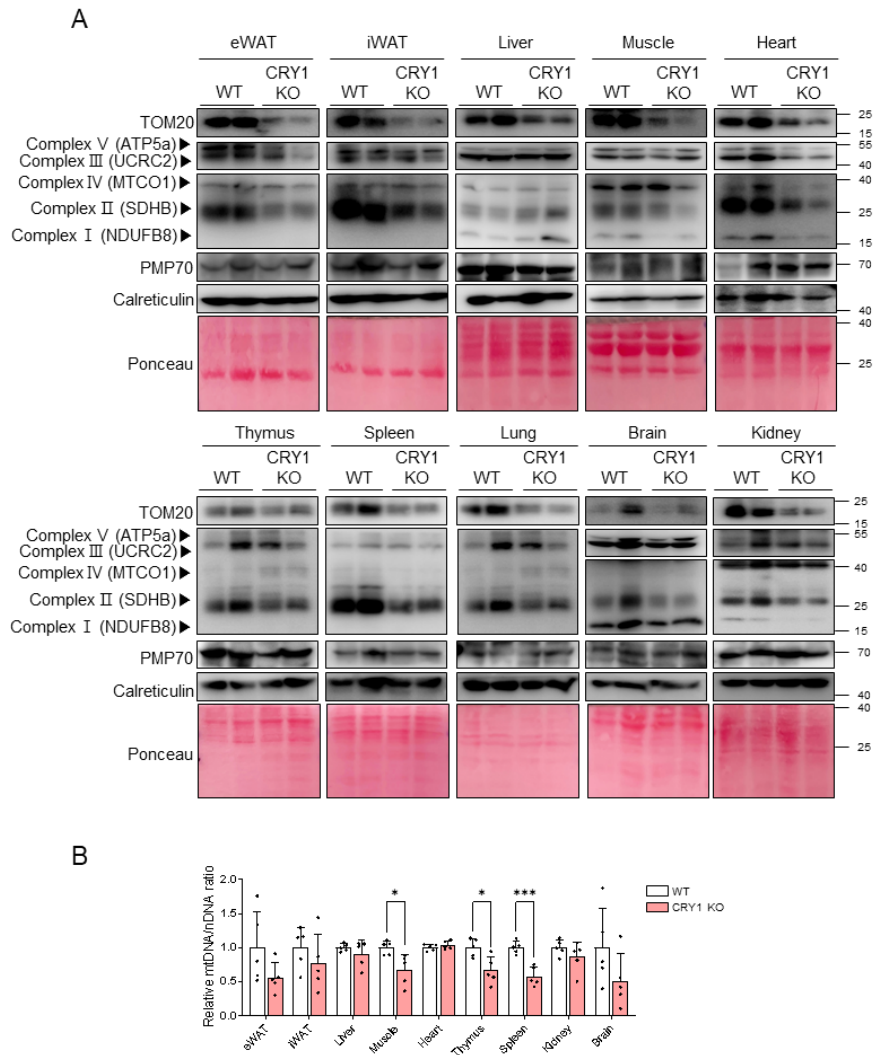


**Figure 40. Deficiency of CRY1 shows a tendency to reduce OXPHOS protein and mitochondrial contents in various tissues**

A: Western blotting analysis of indicated tissues from WT and CRY1 KO mice housed at RT B: mtDNA(Dloop2) contents normalized to nuclear DNA (HK2) in indicated tissues of WT and CRY1 KO mice. Data are mean  $\pm$  S.D. n.s., not significant. \*\* $P < 0.01$  vs. WT mice by multiple Student's *t*-test.

### **CRY1 regulates mitochondrial abundance and fitness.**

To comprehend whether CRY1 might be involved in mitochondrial biology, I decided to establish CRY1 KO mouse embryonic fibroblast (MEF), which would be invaluable subjects to test (Fig. 41A, B). In CRY1 KO MEF, the level of CRY2 protein appeared to be slightly increased, while the levels of other circadian regulators were not largely affected by CRY1 deficiency (Fig. 41A). Similar to BAT of CRY1 KO mice (Fig. 42A), CRY1 KO MEF decreased the levels of most mitochondrial proteins, whereas that of ER protein calreticulin was not different from that in WT MEF. Moreover, CRY1 KO MEF showed reduced mitochondria quantity and decreased abundance of mtDNA copies (Fig. 42B, C). To further investigate mitochondrial bioenergetics in CRY1 KO MEF, I analyzed mitochondrial membrane potential by using JC-1 assay in WT and CRY1 KO MEF. By combining confocal microscopy with flow cytometry, I observed a significant decrease in the red-to-green ratio in CRY1 KO MEF (Fig. 43), implying that CRY1 defect would impair mitochondrial membrane potentials. Consistent with these, formation of mitochondrial electrochemical gradient (TMRE intensity) per unit of mitochondrial mass (MitoTracker Green intensity) was significantly compromised in CRY1 KO MEF (Fig. 44). Therefore, these data suggest that CRY1 depletion in MEF would promote defects in mitochondrial fitness.

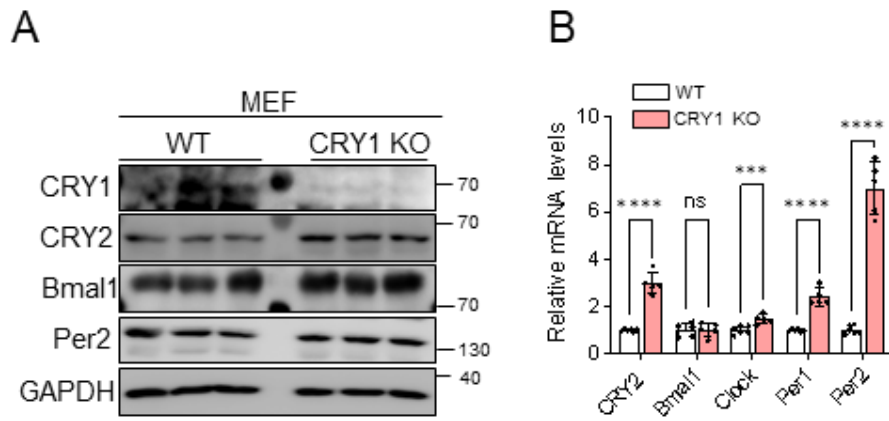


**Figure 41. MEF cells are established from WT and CRY1 KO mouse embryos**

A: western blotting analysis of MEF from WT and CRY1 KO. B: qRT-PCR analysis of genes related to circadian regulators in MEF of WT and CRY1 KO mice. Data are mean  $\pm$ S.D. n.s., not significant. \*\*\* $P < 0.001$  vs. WT MEF by multiple Student's  $t$ -test.

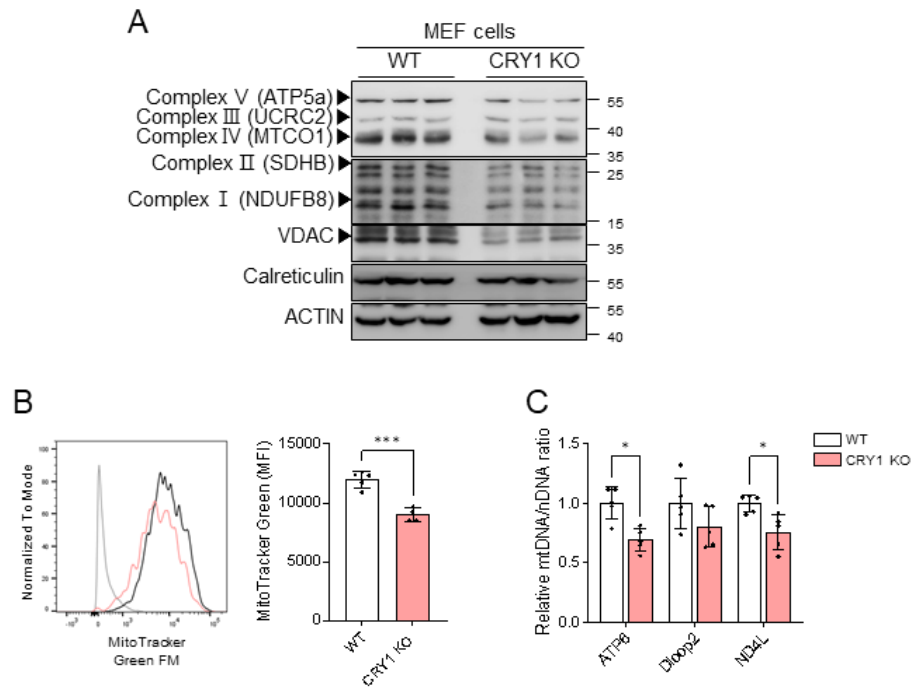


**Figure 42. CRY1-deficient MEF shows downregulated OXPHOS and mitochondrial proteins abundances and mitochondrial contents**

A: Western blotting analysis of MEF from WT and CRY1 KO. B: Flow cytometry analysis of MitoTracker Green FM mitochondrial staining in MEF of WT and CRY1 KO. C: mtDNA contents normalized to nuclear DNA in MEF of WT and CRY1 KO. Data are mean  $\pm$  S.D. \* $P < 0.05$ , \*\*\* $P < 0.001$ .

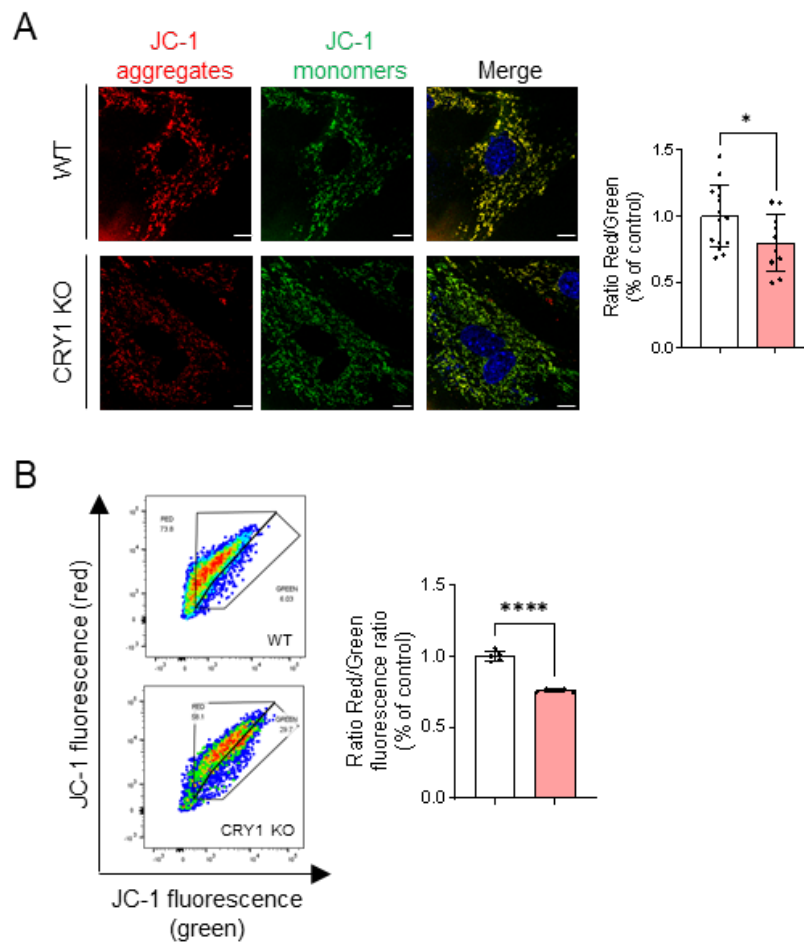


**Figure 43. CRY1 deficiency in MEF is associated with dysfunctional mitochondria**

A: Representative images of mitochondrial staining of JC-1 (red for JC-1 forms aggregate in healthy mitochondria; green for JC-1 forms monomers) and Hoechst 33342 (blue for nucleus) in MEF of WT and CRY1 KO (left). Quantification of average fluorescence intensity of ratio of red to green (right). Scale bar, 10  $\mu$ m. B: Flow cytometry analysis of JC-1 mitochondrial membrane potential staining in MEF of WT and CRY1 KO. Data are mean  $\pm$ S.D. \* $P$ <0.05, \*\*\* $P$ < 0.001.

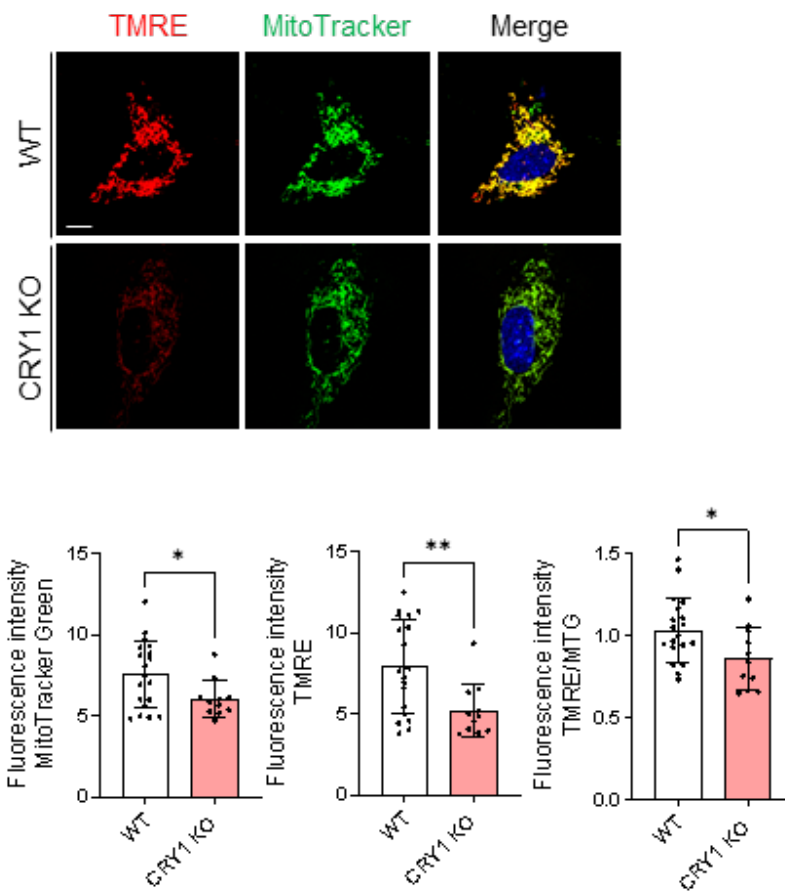


**Figure 44. CRY1-deficient MEF exhibits defective mitochondrial function**

Representative images of mitochondrial staining of TMRE (red for mitochondrial membrane potential) and MitoTracker Green FM (green for mitochondrial mass) and Hoechst 33342 (blue for nucleus) in MEF from WT and CRY1 KO. Scale bar, 10  $\mu$ m. Quantification of average fluorescence intensity. Data are mean  $\pm$  S.D. \* $P$  < 0.05, \*\* $P$  < 0.01, \*\*\* $P$  < 0.001.

**In CRY1-deficient MEF is decreased mitochondrial contents is associated with mitophagy**

Mitochondrial population is maintained through a balance between mitochondrial biogenesis and mitophagy, which could regulate mitochondrial contents [103, 171]. This balance helps to prevent cellular damage accumulation by preserving a population of healthy mitochondria. To test whether a decrease in mitochondrial contents in CRY1 MEF might be associated with mitochondrial biogenesis, I firstly evaluated the expression of key regulators of mitochondrial biogenesis in WT and CRY1 KO MEF. The levels of key regulators of mitochondrial biogenesis peroxisome proliferator-activated receptor gamma coactivator 1-alpha (PGC1 $\alpha$ ) and nuclear respiratory factor 1 (NRF1) were comparable between WT and CRY1 KO MEF (Fig. 45A). In addition, the levels of their target gene expression and OXPHOS complex were not largely altered by CRY1 deficiency in MEF (Fig. 45B, C), implying that CRY1 deficiency might not influence in mitochondrial biogenesis.

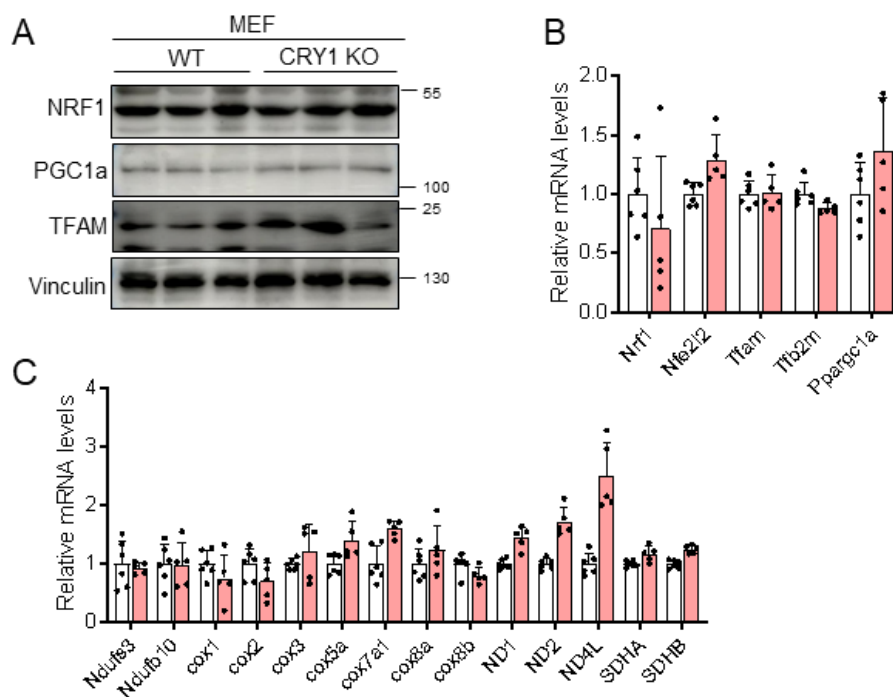


**Figure 45. Mitochondrial biogenesis gene expression in MEF is comparable between WT and CRY1 KO**

A: Western blotting analysis of MEF from WT and CRY1 KO. B: qRT-PCR analysis of key regulators of mitochondrial biogenesis genes in MEF of WT and CRY1 KO. C: qRT-PCR analysis of mitochondrial genes in MEF of WT and CRY1 KO. Data are mean  $\pm$  S.D.

Next, I aimed to study whether decreased mitochondria abundance through CRY1 deficiency might be associated with mitophagy. I utilized Carbonyl Cyanide 3-ChloroPhenyl-hydrazone (CCCP), a mitochondrial inner membrane ionophore, to induce mitophagy by depolarizing mitochondrial membrane [172]. As shown in Fig. 46, the intensity of mtphagy dye fluorescence was expectedly enhanced by CCCP treatment, resulting from mitophagic flux to lysosomes. Interestingly, this CCCP effect was accelerated in CRY1 KO MEF compared to WT (Fig. 46). To investigate mt-Keima distribution in mitochondria and lysosomes after mitophagic flux (green versus red mt-Keima, respectively), mt-Keima plasmid was ectopically expressed in WT and CRY1 KO MEF. As shown in Fig. 47, without CCCP, mt-Keima emitted predominantly green fluorescence in WT MEF, indicating mitochondrial localization. However, the majority of mt-Keima emitted red fluorescence in the presence of CCCP, indicating the mitophagic flux to lysosomes in WT MEF (Fig. 47). Compared to WT, CRY1 KO MEF mt-Keima potently emitted red fluorescence the with or without CCCP, implying that CRY1 KO MEF would be activated in the aspect of mitophagic flux. Together, these results suggest that a decrease in mitochondrial contents in CRY1-deficient MEF might be caused by elevated mitophagy.

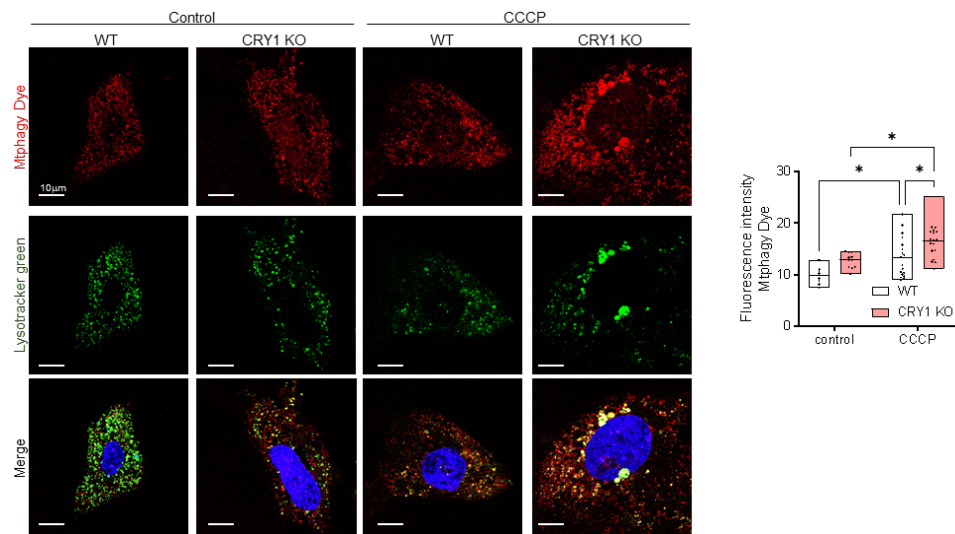


**Figure 46. CRY1 deficiency in MEF is associated with induced mitophagy**

Representative images of mitophagy using Mtpagy dye (red), Lysotracker green (green) and Hoechst 33342 (blue) in MEF of WT and CRY1 KO (left). Cells were treated with either DMSO or CCCP (20  $\mu$ M) for 2 hours. Scale bar, 10  $\mu$ m. Quantification of average fluorescence intensity of Mtpagy dye (right). Data are mean  $\pm$ S.D. \* $P$ <0.05 indicated control group by two-way ANOVA followed by Tukey post hoc test.

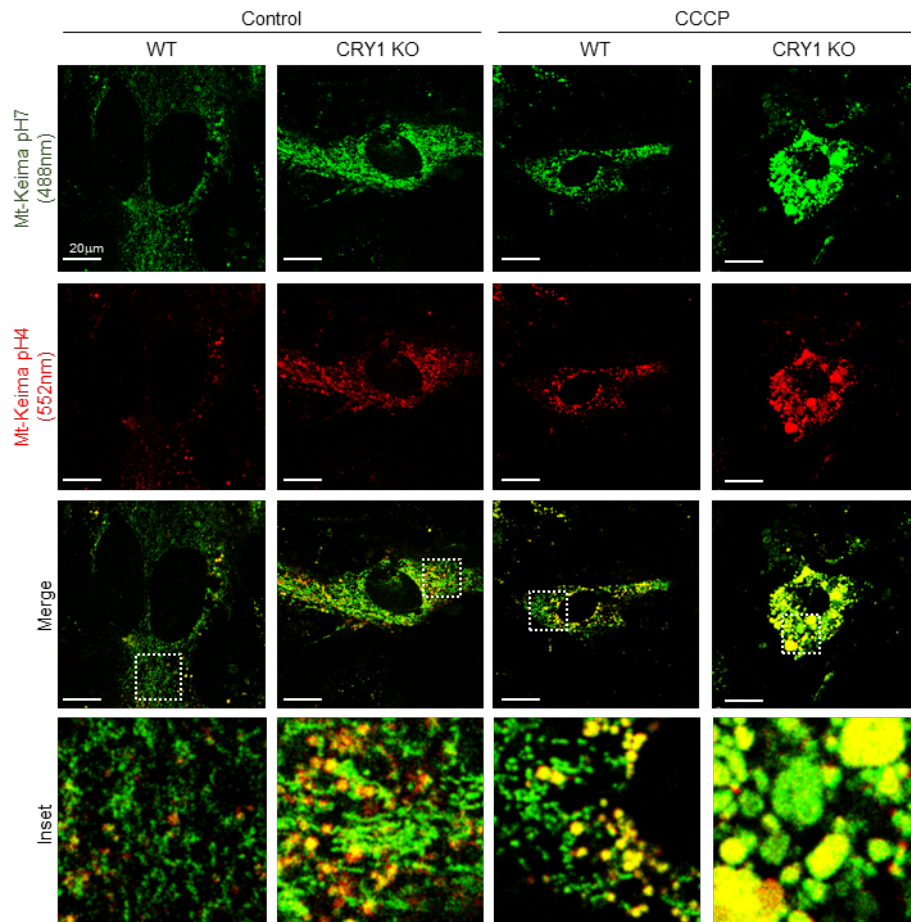


**Figure 47. CRY1 deficiency in MEF is associated with induced mitophagy**

Representative images of mitophagy using Mt-Keima probe in MEF of WT and CRY1 KO. The probe emitted green fluorescence when excited at 488-nm and red fluorescence when excited at 552-nm. MEF cells were transduced with mt-Keima-encoding plasmids for 2 days and then treated with either DMSO or CCCP (20  $\mu$ M) for 2 hours. Scale bar, 20  $\mu$ m.

### **In BAT, CRY1 is elevated upon cold exposure**

To verify whether CRY1 might be linked to BAT function through mitochondrial activity control, I examined its expression levels in BAT of mice exposed to room temperature (RT) (22°C) or cold temperatures (6°C). As shown in Fig. 48A, C, the levels of CRY1 mRNA and protein in BAT were gradually elevated upon cold exposure. Compared to other circadian regulators, cold-induced CRY1 expression was quite prominent in BAT (Fig. 48C). In addition, publicly available data of transcriptome profiles of BAT from mice exposed to RT or cold revealed that CRY1 expression was distinctively elevated in BAT upon cold exposure (Fig. 48B). To investigate further whether CRY1 in other thermogenic adipose tissue such as inguinal white adipose tissue (iWAT) might show similar patterns in BAT, I examined the levels of CRY1 mRNA and protein in iWAT. In WT mice, CRY1 proteins were elevated in iWAT upon long-term cold. In contrast to BAT, CRY1 mRNA expression was not greatly affected by cold exposure (Fig. 49A, B), implying that CRY1 would be activated in thermogenic adipose tissues in response to cold.

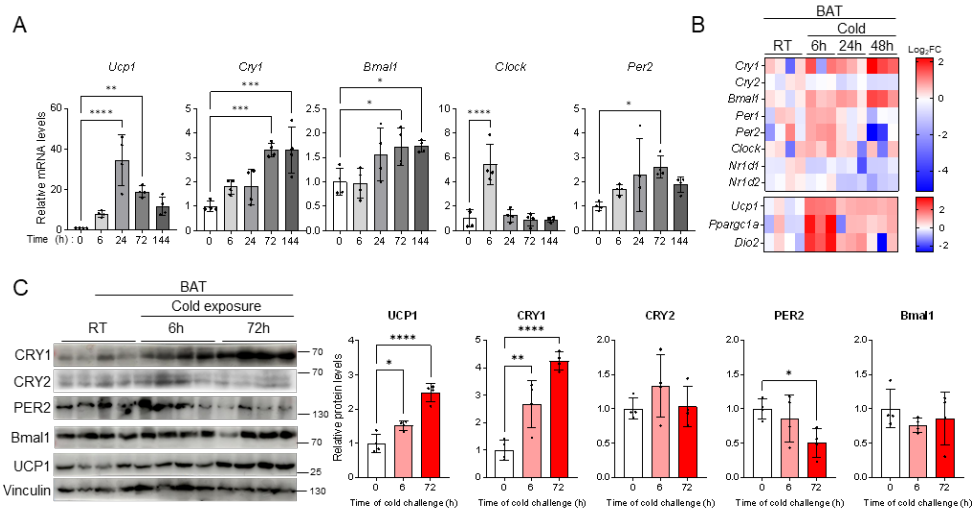


**Figure 48. In BAT, the expression of CRY1 is increased by cold exposure**

A: qRT-PCR analysis of CRY1 and indicated genes in BAT of WT and CRY1 KO. B: Heat map of gene expression associated with circadian genes in BAT from RT or cold-exposed mice (GSE 119452[173]). C: Western blotting analysis of CRY1 protein in BAT from WT and CRY1 KO. Data are mean  $\pm$  S.D. Mean of the band intensities was calculated from independent experiments using Image J. \* $P < 0.05$ , \*\* $P < 0.01$ , \*\*\* $P < 0.001$  vs. RT group by one-way ANOVA followed Tukey post hoc test.

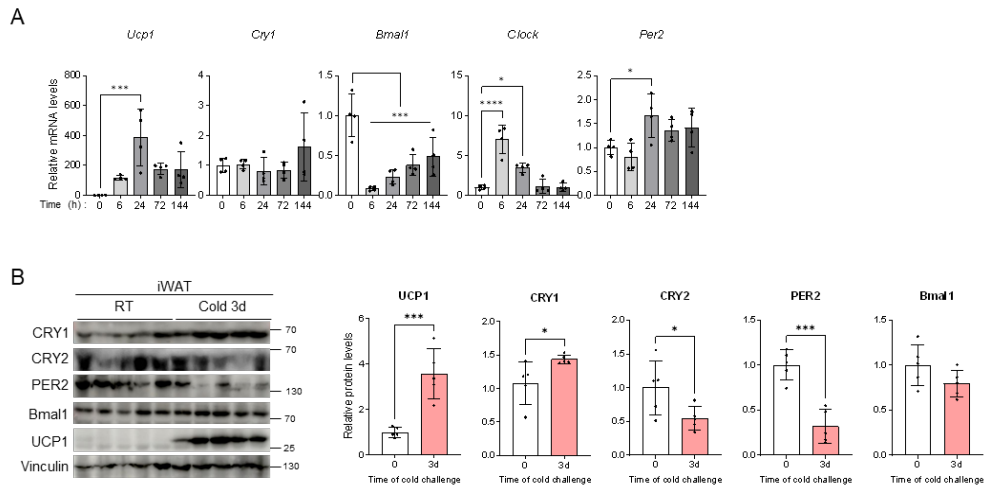


**Figure 49. In iWAT, the expression of CRY1 is increased by cold exposure**

A: qRT-PCR analysis of CRY1 and indicated genes in iWAT of WT and CRY1 KO. B: Western blotting analysis of CRY1 protein in iWAT from WT and CRY1 KO. Data are mean  $\pm$ S.D. Mean of the band intensities was calculated from independent experiments using Image J. \* $P < 0.05$ , \*\*\* $P < 0.001$  vs. RT group by one-way ANOVA followed Tukey post hoc test.

## **CRY1 KO mice show impaired BAT thermogenesis and energy expenditure in response to cold or $\beta$ -adrenergic activation**

To investigate the physiological relevance of CRY1 in BAT *in vivo*, I decided to compare thermogenic activity in WT and CRY1 KO mice. Compared to WT mice, CRY1 KO mice were cold intolerant (Fig. 50A, B). Additionally, histological analysis revealed that BAT of CRY1 KO mice showed larger adipocytes with bigger lipid droplets (Fig. 50C). In contrast, there were no significant differences in iWAT and eWAT between the two genotypes (Fig. 50D, E). Furthermore, when metabolic activities of WT and CRY1 KO mice were evaluated, CRY1 KO mice displayed decreased oxygen consumption and energy expenditure upon  $\beta$ 3-adrenergic agonist CL316,243 (CL) (Fig. 51). Nonetheless, there was no significant difference in the expression of thermogenic marker genes such as *Ucp1*, *Ppargc1a*, *Dio2*, and *Elovl3* between the two genotypes (Fig. 52).

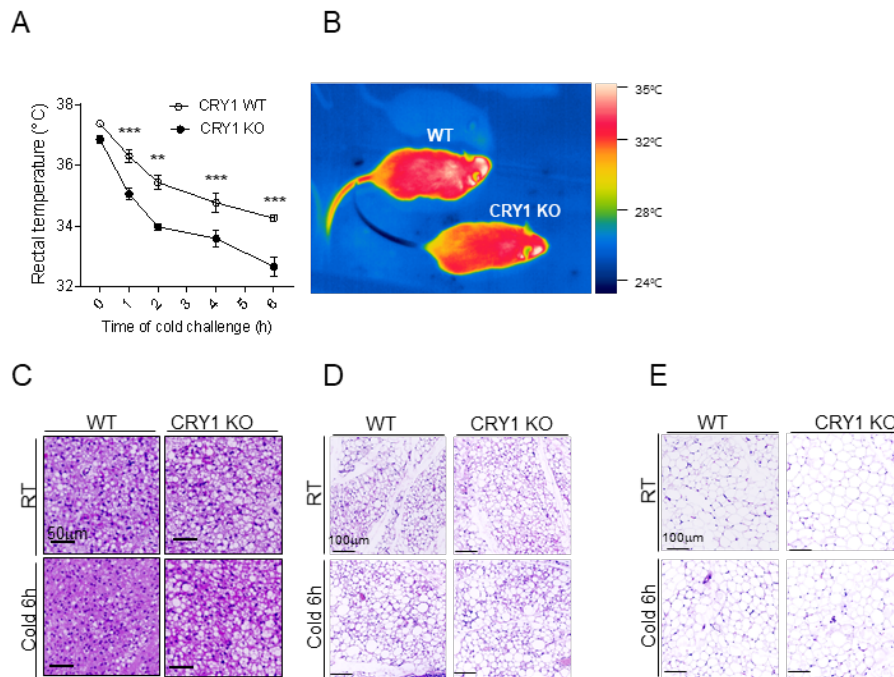


**Figure 50. CRY1 KO mice show impaired heat generation**

A: Rectal temperature of WT and CRY1 Ko mice upon cold exposure.  $**P < 0.01$ ,  $***P < 0.001$ . vs. WT group with repeated-measures ANOVA by Sidak post hoc test. B: Representative infrared images of mice upon cold exposure for 6 hours. C-E: Representative H&E images of BAT (C), iWAT (D), and eWAT (E) from WT and CRY1 KO mice exposed to cold for 6 hours. Data are represented as mean  $\pm$  S.D.

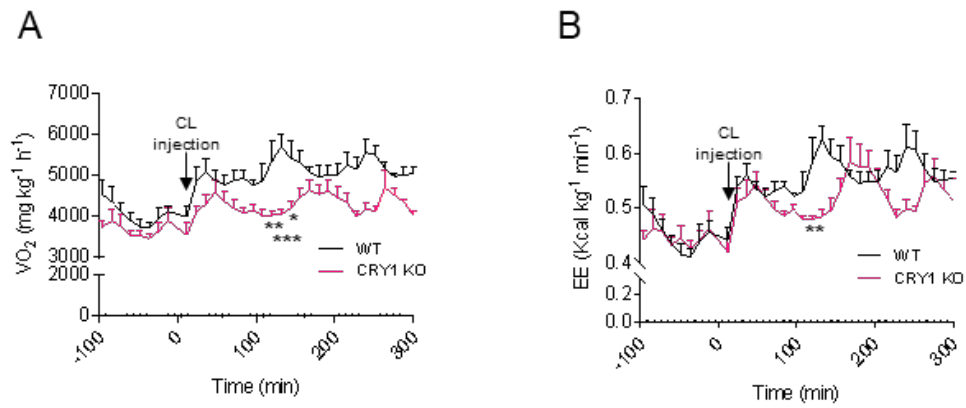


**Figure 51. CRY1 KO mice exhibit decreased energy expenditure upon  $\beta$ 3-adrenergic agonist CL316,243 injection**

A and B:  $VO_2$  (A) and energy expenditure (EE) (B) of WT and CRY1 KO mice before and after CL316,243 (1 mg/kg body wt) injection. \* $P < 0.05$ , \*\* $P < 0.01$ , \*\*\* $P < 0.001$  vs. WT group with repeated-measures ANOVA by Sidak post hoc test.

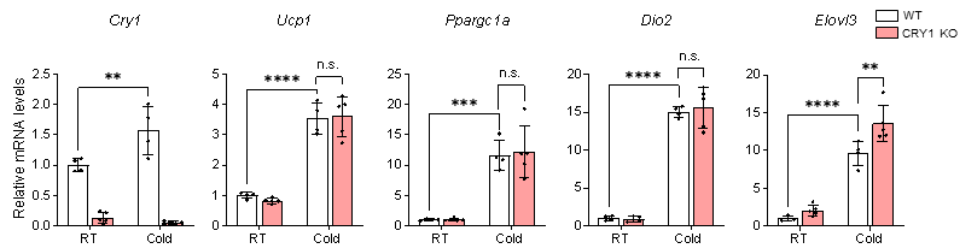


**Figure 52. Thermogenic gene expression in BAT is comparable between WT and CRY1 KO**

qRT-PCR analysis of thermogenic genes of BAT from WT and CRY1 KO mice exposed to RT or 6 hours cold conditions. \*\* $P < 0.01$ , \*\*\* $P < 0.001$  vs. indicated control group by two-way ANOVA followed by Tukey post hoc test.

Given that the regulation of mitochondrial abundance via CRY1 might affect thermogenesis, I investigated mitochondrial contents of BAT upon cold. In Fig. 53A, B, BAT of CRY1 KO mice decreased mitochondrial DNA contents and expression of OXPHOS system and TOM20 compared to that of WT mice upon cold exposure. These data implied that CRY1 might affect mitochondrial contents rather than regulate nuclear thermogenic gene expression, eventually resulting in decreased BAT thermogenic activity. The findings that CRY1-deficient MEF would potentiate mitophagic flux (Fig. 46, 47) led me to ask whether CRY1 deficiency in BAT might accelerate mitophagy during cold exposure, leading to reduced mitochondrial abundance. To address this, I examined the effect of CRY1 deficiency on mitophagy or autophagy in BAT using TEM imaging. It is of interest to note that swollen mitochondria were greatly accumulated and the degree of mitophagy was highly induced in CRY1 KO MEF (Fig. 54). Next, I investigated whether the PINK-Parkin axis could contribute to this process in BAT [174]. Compared to WT mice, phosphorylation of PINK and Parkin was upregulated in BAT of CRY1 KO mice (Fig. 55). Consistently, it seemed that overall degree of polyubiquitination in mitochondrial proteins was upregulated in BAT of CRY1 KO mice, indicating that Parkin-dependent mitophagy would be augmented in BAT of CRY1 KO. Collectively, these data proposed that elevated mitophagic flux in CRY1 ablation could decrease mitochondrial abundance in BAT, resulting in reduced thermogenic activity.

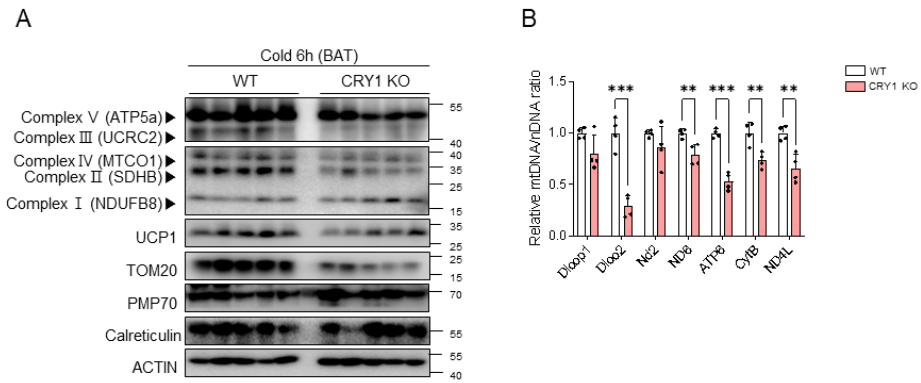


**Figure 53. In BAT, deficiency of CRY1 decreases expression of mitochondrial proteins and mitochondrial contents after cold exposure**

A: Western blotting analysis of BAT from WT and CRY1 KO mice after 6 hours cold exposure B: mtDNA contents normalized to nuclear DNA in BAT of WT and CRY1 KO mice after 6 hours cold exposure. Data are mean  $\pm$  S.D. \*\* $P < 0.01$ , \*\*\* $P < 0.001$ .

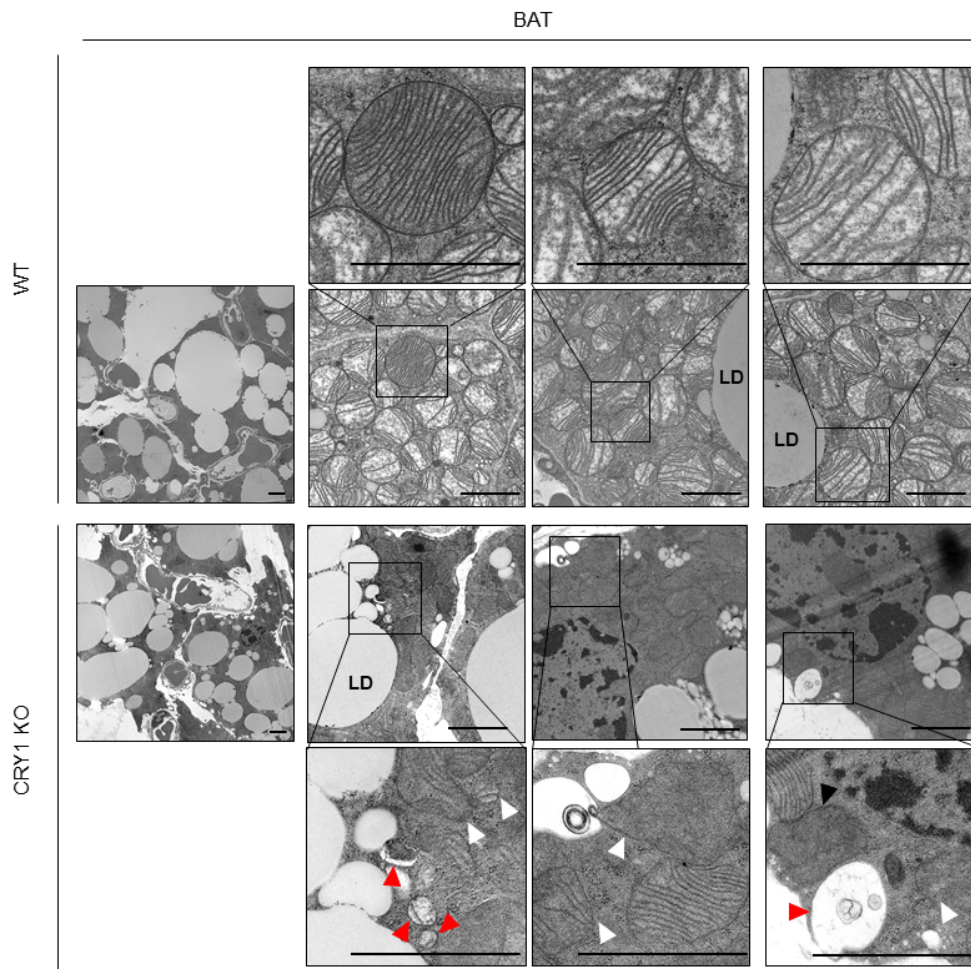


**Figure 54. Deficiency of CRY1 in brown adipose tissue shows morphological defects in mitochondria upon cold exposure**

Representative electron micrographs of BAT of 12-week-old WT and CRY1 KO mice after 6 hours of cold exposure. Red arrowheads point to mitophagosome and swollen mitochondria and white arrowheads point to low-density and disrupted mitochondria. Scale bar, 2  $\mu$ m.

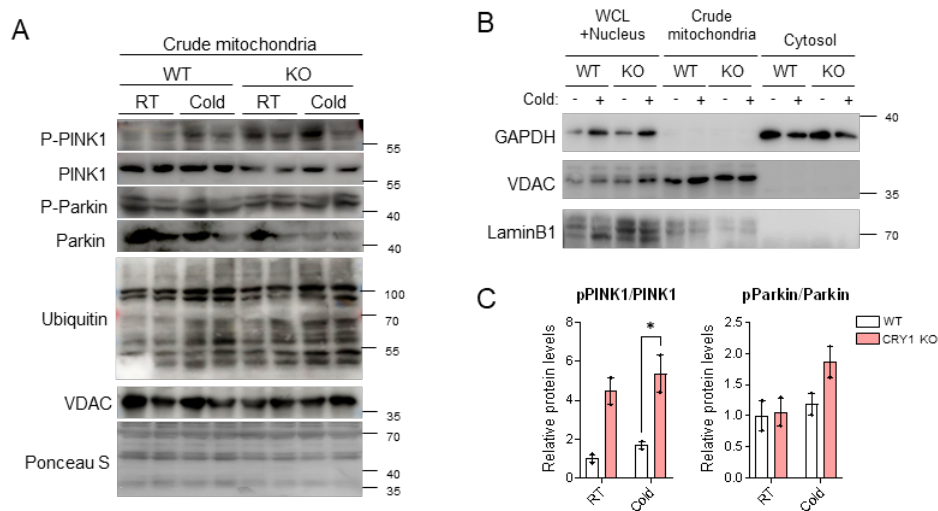


**Figure 55. PINK-Parkin pathway is activated in BAT of CRY1 KO mice after cold exposure**

A-B: Western blotting analysis of crude mitochondria fractions (A) in BAT of WT and CRY1 KO mice exposed to RT or 6 hours cold exposure. BAT was lysed and separated into mitochondrial (A), nucleus (whole cell lysates, WCL), and cytosolic fractions (B). C: Quantification of band intensities for each represented blot was performed using ImageJ. Data are represented as mean  $\pm$  S.D. Mean of the band intensities was calculated from independent experiments using Image J. \* $P < 0.05$  vs. indicated control group by two-way ANOVA followed by Tukey post hoc test.

**BAT-specific CRY1 overexpression potentiates thermogenic activity upon cold stimuli.**

Next, to address the question of whether BAT-specific CRY1 increase might affect body temperature during cold exposure, CRY1 was selectively overexpressed in BAT of WT mice. In contrast the data from whole-body CRY1 KO mice, body temperature was upregulated by BAT-specific CRY1 overexpression (OE) (Fig. 56A) without bodyweight changes (Fig. 56B). Simultaneously, CRY1 OE in BAT potentiated small lipid droplet formation (Fig. 56C). Moreover, CRY1 OE in BAT marginally increased mitochondrial DNA contents and expression of OXPHOS system and TOM20 in BAT upon cold exposure (Fig 57).

Then, I asked whether the increased mitochondrial fitness by increasing CRY1 levels would confer thermogenic activity. To address this, the adenovirus containing CRY1 gene was directly injected into BAT of CRY1 KO mice. Upon cold exposure, ectopic OE of CRY1 in BAT of CRY1 KO mice showed higher body and BAT temperature compared to MOCK-treated CRY1 KO mice (Fig. 58 A, B). In addition, BAT of ectopic OE of CRY1 displayed smaller LDs compared to BAT of MOCK-treated CRY1 KO mice (Fig. 58C). In line with these, the levels of mitochondrial DNA contents and expression of OXPHOS system, TOM20, and UCP1 in BAT were partially, but substantially, rescued by CRY1 OE (Fig. 58D, 59). Collectively, these data suggest that CRY1 in BAT would potentiate thermogenic activity by regulating mitochondrial fitness.

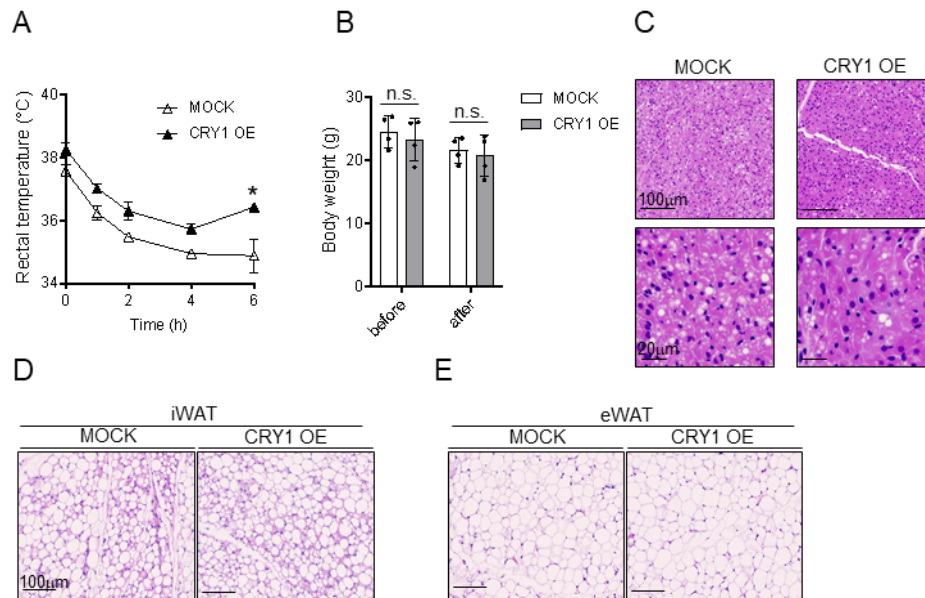


**Figure 56. Mice with BAT-specific CRY1 overexpression potentiate thermogenic capacity**

A: Rectal temperature of MOCK and CRY1 OE mice upon cold exposure. \* $P < 0.05$  vs. MOCK group with repeated-measures ANOVA by Sidak post hoc test. B: body weight of MOCK and CRY1 OE mice before and after 6 hours of cold exposure C-E: Representative H&E images of BAT (C), iWAT (D), and eWAT (E) from MOCK and CRY1 OE mice exposed to cold for 6 hours. Scale bar, 100  $\mu\text{m}$ , 20  $\mu\text{m}$ . Data are represented as mean  $\pm$  S.D. n.s. non-significant

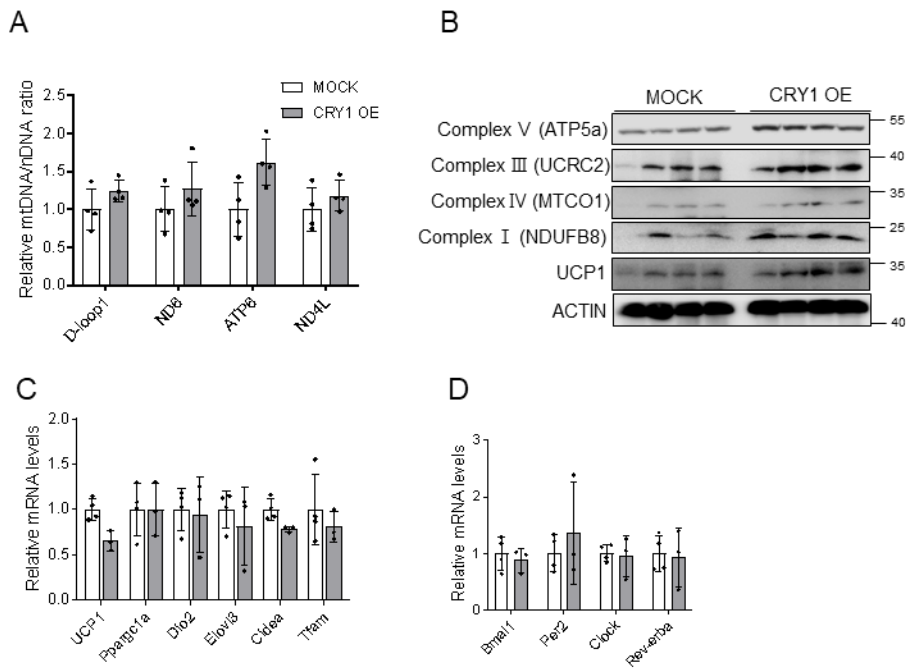


**Figure 57. Mice with BAT-specific CRY1 overexpression exhibit increased mitochondrial contents and protein abundance upon cold**

A: Mitochondrial DNA contents normalized to nuclear DNA in BAT from MOCK and CRY1 OE mice upon cold exposure for 6 hours. B: Western blotting analysis of BAT from MOCK and CRY1 OE mice. C-D: qRT-PCR analysis of thermogenic (C) and circadian regulators (D) genes in BAT from MOCK and CRY1 OE mice. Data are represented as mean  $\pm$  S.D.

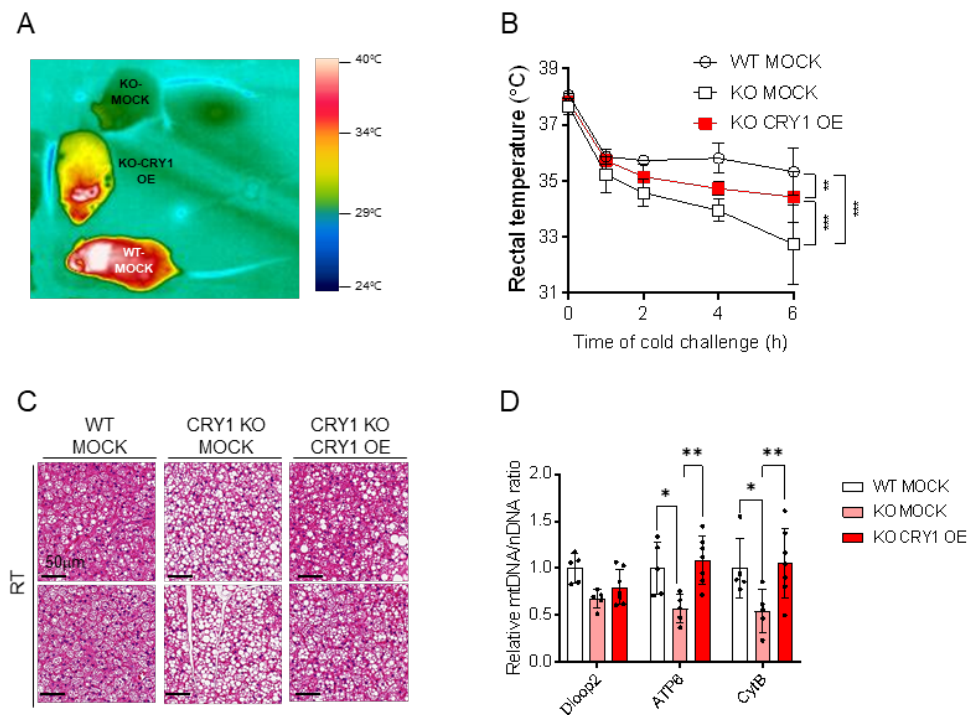


**Figure 58. BAT-specific CRY1 restoration results in enhanced heat generation and mitochondria DNA contents**

A-D: Empty vectors were injected into BAT of WT (WT-MOCK) and CRY1 KO (KO-MOCK) mice, while CRY1-expressing plasmids were injected into BAT of CRY1 KO (KO-CRY1 OE) mice. A: Representative infrared images of WT-MOCK, KO-MOCK and KO-CRY1 OE mice. B: Rectal temperature of WT-MOCK, KO-MOCK and KO-CRY1 OE mice.  $**P < 0.01$ ,  $***P < 0.001$  vs. indicated group two-way ANOVA by Tukey post hoc test. C: Representative H&E images of BAT from WT-MOCK, KO-MOCK and KO-CRY1 OE mice. Scale bar, 50  $\mu\text{m}$ . D: Mitochondrial DNA contents normalized to nuclear DNA in BAT from WT-MOCK, KO-MOCK and KO-CRY1 OE mice.  $*P < 0.05$ ,  $**P < 0.01$  vs. indicated group two-way ANOVA by Tukey post hoc test. Data are represented as mean  $\pm$  S.D.

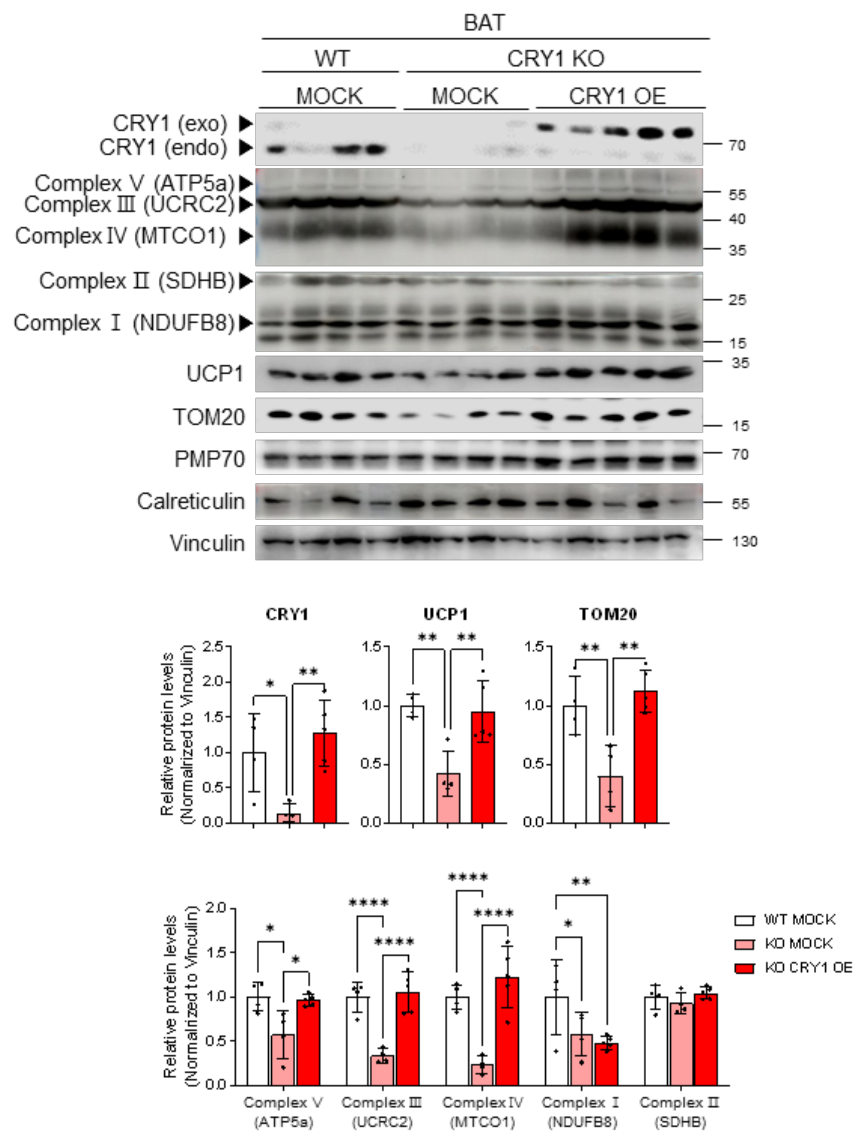


**Figure 59. BAT-specific CRY1 OE increases mitochondrial protein abundance**

Western blotting analysis of BAT from WT-MOCK, KO-MOCK and KO-CRY1 OE mice. \* $P < 0.05$ , \*\* $P < 0.01$ , \*\*\* $P < 0.001$  vs. indicated group one-way ANOVA by Tukey post hoc test. Data are represented as mean  $\pm$  S.D.

## 5. Discussion

The maintenance of mitochondrial abundance and integrity for efficient UCP1 activity fulfills pivotal roles in thermogenesis in BAT [104, 114]. Although temperature change is one of representative zeitgebers of peripheral clock, it remains largely unknown how circadian regulator(s) in BAT might contribute to mitochondrial homeostasis. In this study, I found that CRY1 would be a crucial factor for mitochondrial quality control for preserving thermogenic functions in BAT. Several lines of evidence support this idea. First, CRY1 deficiency impaired mitochondrial abundance and fitness in BAT. Second, mitophagic flux was elevated in CRY1-deficient MEF and BAT, which was further augmented upon mitochondrial stress and cold exposure. Third, CRY1 KO mice were cold intolerant, probably, due to a decrease in mitochondrial contents. Moreover, BAT-specific overexpression of CRY1 rescued mitochondrial contents and bioenergetics for BAT thermogenic activity in CRY1 KO mice.

Mitochondrial quality control is essential for conserving a healthy mitochondrial population and is crucial to meet metabolic demands [175]. For this, mitophagy is a dynamic process by selectively removing damaged or excessive mitochondria in response to metabolic stress, which could help prevent the accumulation of damaged mitochondria and excess ROS, leading to systemic energy abnormalities. In BAT, thermogenesis is a highly energy-demanding process that exposes mitochondria to metabolic stress

and oxidative damage [6]. Notably, I found that CRY1 deficiency in BAT impaired mitochondrial abundance and fitness, leading to mitophagy. Moreover, increased mitochondrial fitness by restoring CRY1 levels in CRY1 KO mice, in turn enhanced thermogenic activity. In CRY1 KO mice, I also found that mitochondrial contents were downregulated in various tissues including muscle (Fig. 40). Interestingly, CRY1 KO mice showed reduced exercise capacity in the voluntary wheel performance and grip strength test (Fig. 60). Even though further investigations with tissue-specific KO animal models are needed in future studies, current data suggest that CRY1 appears to be one of key mediators to preserve mitochondrial bioenergetics, which could play key roles in physiological functions.

Mammalian CRY1 has been shown to have various molecular regulatory functions beyond its known roles in canonical transcriptional regulation. For instance, one of CRY1 functions includes acting as a scaffold protein, participating in DNA repair, and contributing to cellular processes such as tumorigenesis, glucose metabolism, autophagy, and inflammation [69, 71, 72, 167]. In BAT, I found that CRY1 would involve in mitochondrial quality control. Although the absence of large changes in expression of thermogenic, mitochondrial biogenesis, and mitochondria regulatory genes, CRY1 deficiency resulted in decreased mitochondrial fitness and abundance. These observations clearly indicate that the change in mitochondrial contents upon CRY1 deficiency would reflect non-canonical roles of CRY1 other than transcriptional regulation. Given that

CRY1 is involved in proteasomal degradation pathway by interactions with E3 ligases [57, 70, 149], I raised the hypothesis that CRY1 might be involved in the regulation of mitochondrial proteostasis and/or PINK-Parkin-mediated mitophagy. Interestingly, mitophagic flux was enhanced in CRY1-deficient MEF and BAT (Fig. 46, 47, 54). In addition, proteomic analysis and subcellular fraction revealed that CRY1 could be enriched in mitochondria upon cold or  $\beta$ -adrenergic activation (Fig. 61). Although it remains to be investigated whether CRY1 protein enriched in mitochondria could involve in the regulation of mitochondrial proteostasis and/ or mitophagy, current data suggest that CRY1 would act as a key regulator of mitochondrial homeostasis beyond its canonical roles as a transcriptional regulator.

In conclusion, the present study herein provides new knowledge of CRY1 function in mitochondrial quality control. In BAT, CRY1 positively contributes to thermogenic activity by preserving mitochondrial features upon cold stimulation (Fig. 62). Given that CRY1, as a circadian regulator, plays pivotal roles in maintaining healthy mitochondrial fitness, it seems that these findings shed light on the multifaceted roles of CRY1 beyond its canonical function as transcriptional regulation of circadian rhythm.

### **Limitation of Study**

This study explores the relationship between CRY1 and mitophagy, as well as the influence of CRY1 on thermogenesis in BAT. However,

further study is needed to elucidate the underlying mechanism(s) in which signaling pathways could be involved in mitochondrial quality control by CRY1 and relationship between CRY1 and mitophagy. Firstly, it is required to investigate whether CRY1 could be enriched in mitochondria, thereby regulating mitochondrial quality control rather than transcriptional regulation in the nucleus. Further, the identification of interacting partners of CRY1 in the mitochondria that contribute to the regulation of mitophagy needs to be elucidated. Additionally, since I analyzed whole-body CRY1 KO mice, it is feasible to speculate that confounding effects of CRY1 deletion in other tissues are also involved in heat production during cold exposure. Thus, it is important to analyze brown adipocyte-specific KO animal models to elucidate the brown adipose-specific roles of CRY1.

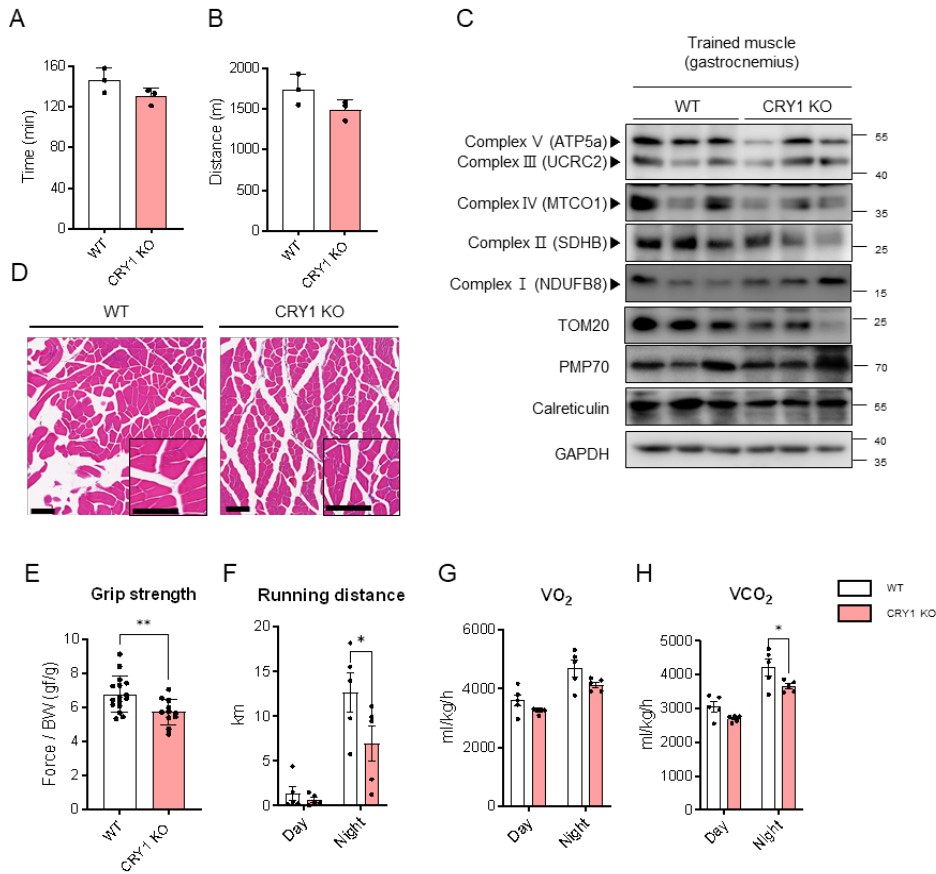


**Figure 60. CRY1 deficiency downregulates the ability to perform the exercise**

A-D: 10-week-old male WT and CRY1 KO mice were subjected to forced treadmill performance until exhaustion, and time (A) and distance (B) were recorded. C: western blotting analysis of trained gastrocnemius muscle of WT and CRY1 KO mice. D: Representative H&E images of gastrocnemius muscle of WT and CRY1 KO mice. Scale bar, 100  $\mu$ m. E: Fore-/hindlimb grip strength assessment of WT and CRY1 KO mice.  $**P < 0.01$ . F-H: 12-week-old male WT and CRY1 KO mice were subjected to voluntary wheel performance and distance (F),  $VO_2$  (G),  $VCO_2$  (H) were recorded.  $*P < 0.05$  vs. WT two-way ANOVA by Tukey post hoc test. Data are represented as mean  $\pm$  S.D.

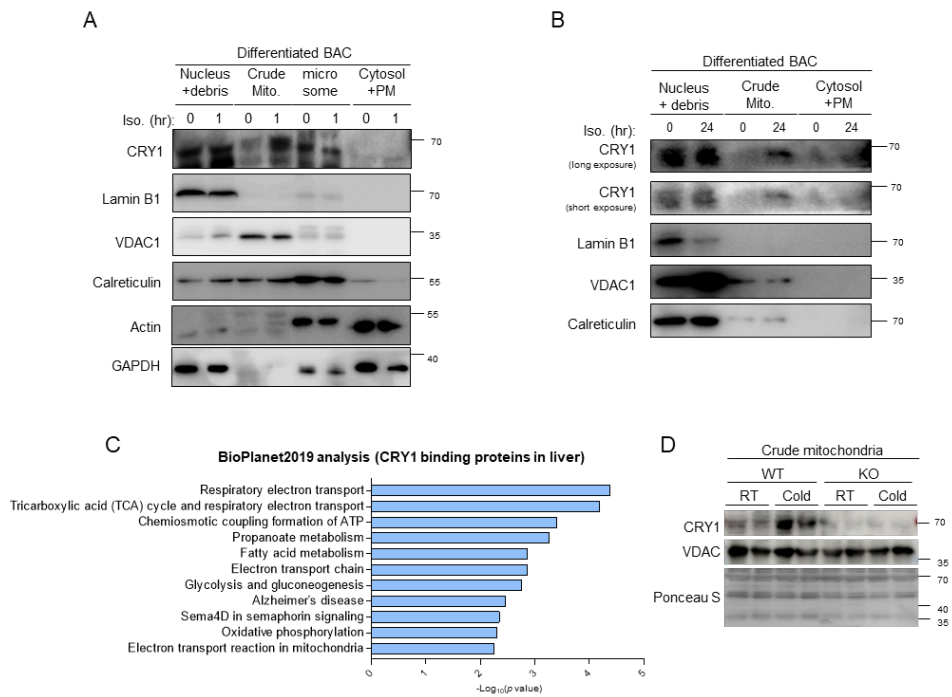


**Figure 61. CRY1 is enriched to mitochondria upon cold and  $\beta$ -adrenergic stimulation**

A-B: Western blotting analysis of differentiated BAC treated to isoproterenol (Iso. 1  $\mu$ M) for 1 hour (A), 24 hours (B). Cells were lysed and separated into mitochondrial, nucleus (whole cell lysates, WCL), cytosolic fractions, and/or microsomes. C: BioPlanet 2019 pathway enrichment of CRY1 binding proteins in liver lysates [57] D: Western blotting analysis of crude mitochondria fractions in BAT of WT and CRY1 KO mice exposed to RT or 6 hours cold exposure.

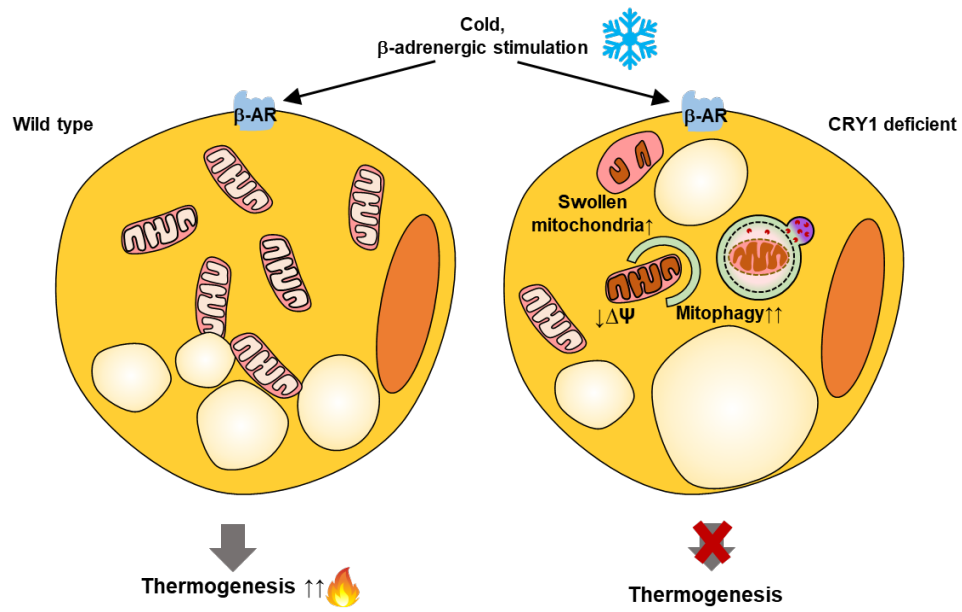


**Figure. 62. Proposed model**

CRY1 plays a crucial role in maintaining mitochondrial homeostasis in BAT. CRY1 deficiency leads to an increase in mitophagy, resulting in reduced mitochondrial abundance. Overall, these findings suggest that CRY1 is an important factor in maintaining thermogenic activity in brown adipocytes through regulating mitochondrial quality control.

# CONCLUSION

Circadian clocks, consisting of a central clock (suprachiasmatic nucleus) and peripheral clocks in peripheral tissues such as liver, adipose tissue, and muscle, regulate physiological rhythms and molecular processes throughout diurnal cycle. Peripheral circadian clocks are influenced by external cues including hormonal signals, temperature changes, feeding/fasting cycle, and physical activity, and are involved in maintaining metabolic homeostasis. It has been demonstrated that disruption of peripheral circadian clocks is tightly associated with various metabolic disorders, such as obesity, diabetes, and cardiovascular disease [176]. Also, recent studies have shown a correlation between circadian rhythm and mitochondrial dynamics for its functions such as respiration and ATP production, and reactive oxygen species production to maintain mitochondrial homeostasis [35]. Nevertheless, the underlying mechanism(s) by which the molecular clocks could cause metabolic disease and regulate mitochondrial homeostasis is still unknown.

In this dissertation, I would like to propose that the circadian regulator CRY1 plays numerous roles in whole-body energy homeostasis. In chapter one, I demonstrated the importance of precise regulation of hepatic protein stability through the GSK3 $\beta$ -FBXL3 axis for systemic glucose homeostasis. In chapter two, I elucidated the novel role of CRY1 in thermogenesis in BAT by fine-tuning mitochondrial homeostasis. Taken

together, current data reveal that CRY1 could serve as a cellular and molecular hub for circadian regulation and metabolism.

## **1.CRY1 and hepatic glucose production in diabetes**

Dysregulated hepatic glucose production is a key contributor to hyperglycemia in type 2 diabetes, resulting from the failure of insulin to effectively suppress FOXO1. In liver, CRY1 downregulates hepatic glucose production by promoting MDM2-mediated nuclear FOXO1 degradation upon insulin [56]. Although decreased hepatic CRY1 protein appeared to be linked to hyperglycemia in diabetic animals, the molecular mechanisms by which hepatic CRY1 dysregulation induces excessive hepatic glucose production in diabetes have not been properly addressed.

Here, I demonstrated that elevated E3 ligase FBXL3 potentiated proteasomal degradation of hepatic CRY1 protein in diabetic mice. Furthermore, I discovered that GSK3 $\beta$ -induced CRY1 phosphorylation at S280/S281 plays a key role in FBXL3-mediated CRY1 degradation. Phospho-dead mutant CRY1 protein potently diminished hepatic glucose production, accompanied by downregulated gluconeogenic gene expression. In addition, restoration of CRY1 protein through suppression of FBXL3 or GSK3 $\beta$  alleviated excessive hepatic glucose production and improved hyperglycemia in diabetic mice.

In liver, CRY1 functions as a negative regulator of hepatic glucose

production via downregulation of FOXO1 [177]. In diabetes, reduced hepatic CRY1 confers excessive FOXO1 accumulation. Also, several human studies have shown that single-nucleotide polymorphisms (SNPs) of CRY1 genes are associated with hyperglycemia, insulin resistance, and diabetes risk [147, 148]. In this study, I suggest that aberrantly increased FBXL3 would contribute to excessive hepatic glucose production and metabolic disorders. Given that hepatic GSK3 $\beta$  enzymatic activity is increased in diabetic animals, I propose that GSK3 $\beta$  would function as a regulator of hepatic CRY1 protein stability in response to pathological signals by controlling the degree of CRY1 phosphorylation, ultimately resulting in FBXL3-mediated degradation in diabetes. Although above idea needs to be verified further, publicly available chromatin immunoprecipitation followed by sequencing (ChIP-seq) data [178] and several experimental data have suggested that the potential role(s) of NF- $\kappa$ B and/or TNF $\alpha$  might be increased hepatic FBXL3 expression in diabetes. Thus, it will be interesting to investigate its upstream regulatory roles in detail.

Taken together, these findings highlight the important underlying mechanisms of the modulation of CRY1 protein stability in the regulation of hepatic glucose production, which might provide clues to understanding the relationship between circadian rhythm dysregulation and the pathogenesis of type 2 diabetes.

## **2. CRY1 and mitochondrial quality control**

BAT is a highly metabolic tissue that uses energy sources for adaptive thermogenesis and contains a large number of mitochondria. The efficient thermogenesis of BAT during cold exposure relies on the maintenance of mitochondrial abundance and integrity. The peripheral clock significantly contributes to regulating energy metabolism in response to various environmental stimuli, including temperature changes. While there is an emerging idea that diurnal changes in mitochondria might be linked to circadian rhythms [33], the effects of circadian regulators on mitochondria in brown adipocytes and their underlying mechanisms are largely unknown.

In this study, I demonstrated that CRY1 would be required for maintenance of mitochondrial homeostasis to preserve thermogenic functions in BAT. CRY1 deficiency impaired the ability to maintain optimal levels of mitochondria and compromised their fitness, which might have negative effects on various cellular processes, including thermogenesis in BAT. Further, CRY1-deficient MEF and BAT exhibited increased frequency of mitophagy, leading to a decrease in mitochondrial abundance. Upon cold exposure, CRY1 KO mice exhibited cold intolerance, whereas BAT-specific CRY1 OE resulted in activation of thermogenesis through restoration of mitochondrial contents.

Although the N-terminus of CRY1 is a well-conserved region of photolyase homology, its C-terminal tail is highly diverse and determines its

cellular location and unique function, which would be crucial in future studies [179, 180]. It has been reported that CRY1 protein is distributed in nucleus and cytoplasm [181-183]. Further, CRY1 has multiple roles depending on cellular compartments [179, 180]. For instance, CRY1 protein was found in mitochondria [184]. Also, proteomics data revealed that CRY1 might interact with a range of mitochondrial proteins (Fig. 61). Furthermore, it appeared that CRY1 protein in BAT is translocated to mitochondria upon cold stimuli. Thus, it is plausible to speculate that CRY1-enriched mitochondria could affect mitochondrial functions upon stimuli. In the future, it will be interesting to elucidate the underlying mechanism(s) by which spatial regulation of CRY1 in BAT affects mitochondrial quality control and thermogenic activity. These results provide insights into the relationship between circadian regulators, mitochondrial homeostasis, and BAT function.

In conclusion, current study elucidates a novel role of CRY1 in maintaining mitochondrial homeostasis. Thus, it seems that CRY1, as a circadian regulator, has broader roles beyond its canonical function in regulating whole-body energy metabolism.

## ACKNOWLEDGEMENTS

Chapter one in this thesis study was published in *Diabetes* (2022) Vol. 71 Issue 7 pp. 1373-1387. In addition, parts of chapter two were presented in abstract form at the Korean Society for Molecular and Cellular Biology Winter Conference, Pyeong Chang Alpensia, Pyeong Chang, 22–24 February 2023. Also, parts of this thesis were be published in *Nature Metabolism* (2023) Vol. 5 Issue 5 pp.735-759. This study was supported by the National Research Foundation, funded by the Korean government (Ministry of Education; 2020R1A6A3A1307212511) and Basic Science Research Program through the National Research Foundation of Korea (NRF) funded by the Ministry of Education (2022R1A6A3A13070991).

## REFERENCES

1. Reppert, S.M. and D.R. Weaver, *Coordination of circadian timing in mammals*. *Nature*, 2002. **418**(6901): p. 935–941.
2. Zhang, R., et al., *A circadian gene expression atlas in mammals: Implications for biology and medicine*. *Proceedings of the National Academy of Sciences*, 2014. **111**(45): p. 16219–16224.
3. Dibner, C., U. Schibler, and U. Albrecht, *The mammalian circadian timing system: organization and coordination of central and peripheral clocks*. *Annual review of physiology*, 2010. **72**: p. 517–549.
4. Stenvers, D.J., et al., *Nutrition and the circadian timing system*. *Progress in brain research*, 2012. **199**: p. 359–376.
5. Lowrey, P.L. and J.S. Takahashi, *Mammalian circadian biology: elucidating genome-wide levels of temporal organization*. *Annu. Rev. Genomics Hum. Genet.*, 2004. **5**: p. 407–441.
6. Storch, K.-F., et al., *Extensive and divergent circadian gene expression in liver and heart*. *Nature*, 2002. **417**(6884): p. 78–83.
7. Zvonic, S., et al., *Characterization of peripheral circadian clocks in adipose tissues*. *Diabetes*, 2006. **55**(4): p. 962–970.
8. Reddy, A.B., et al., *Circadian orchestration of the hepatic proteome*. *Current Biology*, 2006. **16**(11): p. 1107–1115.
9. Panda, S., et al., *Coordinated transcription of key pathways in the mouse by the circadian clock*. *Cell*, 2002. **109**(3): p. 307–320.
10. Hoyle, N.P. and J.S. O'Neill, *Circadian rhythms: hijacking the cyanobacterial clock*. *Curr Biol*, 2013. **23**(23): p. R1050–2.
11. Gamble, K.L., et al., *Circadian clock control of endocrine factors*. *Nat Rev Endocrinol*, 2014. **10**(8): p. 466–75.
12. Mohawk, J.A., C.B. Green, and J.S. Takahashi, *Central and peripheral circadian clocks in mammals*. *Annual review of neuroscience*, 2012. **35**: p. 445–462.
13. Buhr, E.D. and J.S. Takahashi, *Molecular components of the Mammalian circadian clock*. *Circadian clocks*, 2013: p. 3–27.
14. Solt, L.A., D.J. Kojetin, and T.P. Burris, *The REV-ERBs and RORs: molecular links between circadian rhythms and lipid homeostasis*. *Future medicinal chemistry*, 2011. **3**(5): p. 623–638.
15. Gallego, M. and D.M. Virshup, *Post-translational modifications regulate the ticking of the circadian clock*. *Nat Rev Mol Cell Biol*, 2007. **8**(2): p. 139–48.
16. Mason, I.C., et al., *Impact of circadian disruption on glucose metabolism: implications for type 2 diabetes*. *Diabetologia*, 2020. **63**(3): p. 462–472.
17. Kalsbeek, A., S. la Fleur, and E. Fliers, *Circadian control of glucose metabolism*. *Mol Metab*, 2014. **3**(4): p. 372–83.
18. Maury, E., H.K. Hong, and J. Bass, *Circadian disruption in the pathogenesis of metabolic syndrome*. *Diabetes Metab*, 2014. **40**(5): p. 338–46.

19. Vetter, C., et al., *Night shift work, genetic risk, and type 2 diabetes in the UK biobank*. *Diabetes care*, 2018. **41**(4): p. 762-769.
20. Stokkan, K.-A., et al., *Entrainment of the circadian clock in the liver by feeding*. *Science*, 2001. **291**(5503): p. 490-493.
21. Krishnaiah, S.Y., et al., *Clock regulation of metabolites reveals coupling between transcription and metabolism*. *Cell metabolism*, 2017. **25**(4): p. 961-974. e4.
22. Rudic, R.D., et al., *BMAL1 and CLOCK, Two Essential Components of the Circadian Clock, Are Involved in Glucose Homeostasis*. *PLOS Biology*, 2004. **2**(11): p. e377.
23. Lamia, K.A., K.F. Storch, and C.J. Weitz, *Physiological significance of a peripheral tissue circadian clock*. *Proc Natl Acad Sci U S A*, 2008. **105**(39): p. 15172-7.
24. Peek, C.B., et al., *Circadian clock interaction with HIF1 $\alpha$  mediates oxygenic metabolism and anaerobic glycolysis in skeletal muscle*. *Cell metabolism*, 2017. **25**(1): p. 86-92.
25. Jacobi, D., et al., *Hepatic Bmal1 regulates rhythmic mitochondrial dynamics and promotes metabolic fitness*. *Cell metabolism*, 2015. **22**(4): p. 709-720.
26. Macauley, M., et al., *Diurnal variation in skeletal muscle and liver glycogen in humans with normal health and Type 2 diabetes*. *Clinical Science*, 2015. **128**(10).
27. Wehrens, S.M., et al., *Meal timing regulates the human circadian system*. *Current Biology*, 2017. **27**(12): p. 1768-1775. e3.
28. Gliniak, C.M., J.M. Brown, and N. Noy, *The retinol-binding protein receptor STRA6 regulates diurnal insulin responses*. *J Biol Chem*, 2017. **292**(36): p. 15080-15093.
29. Delezie, J., et al., *The nuclear receptor REV-ERB $\alpha$  is required for the daily balance of carbohydrate and lipid metabolism*. *The FASEB Journal*, 2012. **26**(8): p. 3321-3335.
30. Shostak, A., J. Meyer-Kovac, and H. Oster, *Circadian regulation of lipid mobilization in white adipose tissues*. *Diabetes*, 2013. **62**(7): p. 2195-2203.
31. Feneberg, R. and B. Lemmer, *Circadian rhythm of glucose uptake in cultures of skeletal muscle cells and adipocytes in Wistar-Kyoto, Wistar, Goto-Kakizaki, and spontaneously hypertensive rats*. *Chronobiology international*, 2004. **21**(4-5): p. 521-538.
32. Loboda, A., et al., *Diurnal variation of the human adipose transcriptome and the link to metabolic disease*. *BMC medical genomics*, 2009. **2**: p. 1-16.
33. Ezagouri, S. and G. Asher, *Circadian control of mitochondrial dynamics and functions*. *Current Opinion in Physiology*, 2018. **5**: p. 25-29.
34. Aguilar-López, B.A., et al., *Mitochondria: An Integrative Hub Coordinating Circadian Rhythms, Metabolism, the Microbiome, and Immunity*. *Frontiers in Cell and Developmental Biology*, 2020. **8**.
35. Schmitt, K., et al., *Circadian control of DRP1 activity regulates mitochondrial dynamics and bioenergetics*. *Cell metabolism*, 2018.

- 27(3): p. 657–666. e5.
36. Kohsaka, A., et al., *The circadian clock maintains cardiac function by regulating mitochondrial metabolism in mice*. PLoS One, 2014. **9**(11): p. e112811.
  37. Aviram, R., et al., *Lipidomics analyses reveal temporal and spatial lipid organization and uncover daily oscillations in intracellular organelles*. Molecular cell, 2016. **62**(4): p. 636–648.
  38. Peek, C.B., et al., *Circadian clock NAD<sup>+</sup> cycle drives mitochondrial oxidative metabolism in mice*. Science, 2013. **342**(6158): p. 1243417.
  39. Chen, W.W., et al., *Absolute quantification of matrix metabolites reveals the dynamics of mitochondrial metabolism*. Cell, 2016. **166**(5): p. 1324–1337. e11.
  40. Ramsey, K.M., et al., *Circadian clock feedback cycle through NAMPT-mediated NAD<sup>+</sup> biosynthesis*. Science, 2009. **324**(5927): p. 651–654.
  41. Asher, G., et al., *SIRT1 regulates circadian clock gene expression through PER2 deacetylation*. Cell, 2008. **134**(2): p. 317–328.
  42. Nakahata, Y., et al., *The NAD<sup>+</sup> -dependent deacetylase SIRT1 modulates CLOCK-mediated chromatin remodeling and circadian control*. Cell, 2008. **134**(2): p. 329–340.
  43. Turek, F.W., et al., *Obesity and Metabolic Syndrome in Circadian Clock Mutant Mice*. Science, 2005. **308**(5724): p. 1043–1045.
  44. Oishi, K., et al., *Disrupted fat absorption attenuates obesity induced by a high-fat diet in Clock mutant mice*. FEBS Letters, 2006. **580**(1): p. 127–130.
  45. Kennaway, D.J., et al., *Metabolic homeostasis in mice with disrupted Clock gene expression in peripheral tissues*. American Journal of Physiology–Regulatory, Integrative and Comparative Physiology, 2007. **293**(4): p. R1528–R1537.
  46. Marcheiva, B., et al., *Disruption of the clock components CLOCK and BMAL1 leads to hypoinsulinaemia and diabetes*. Nature, 2010. **466**(7306): p. 627–631.
  47. Shostak, A., J. Husse, and H. Oster, *Circadian regulation of adipose function*. Adipocyte, 2013. **2**(4): p. 201–206.
  48. Kennaway, D.J., et al., *Global Loss of Bmal1 Expression Alters Adipose Tissue Hormones, Gene Expression and Glucose Metabolism*. PLOS ONE, 2013. **8**(6): p. e65255.
  49. Paschos, G.K., et al., *Obesity in mice with adipocyte-specific deletion of clock component Arntl*. Nature medicine, 2012. **18**(12): p. 1768–1777.
  50. Grimaldi, B., et al., *PER2 Controls Lipid Metabolism by Direct Regulation of PPAR $\gamma$* . Cell Metabolism, 2010. **12**(5): p. 509–520.
  51. Schmutz, I., et al., *The mammalian clock component PERIOD2 coordinates circadian output by interaction with nuclear receptors*. Genes & development, 2010. **24**(4): p. 345–357.
  52. Zhao, Y., et al., *Loss of mPer2 increases plasma insulin levels by enhanced glucose-stimulated insulin secretion and impaired insulin clearance in mice*. FEBS Letters, 2012. **586**(9): p. 1306–1311.

53. Zani, F., et al., *PER2 promotes glucose storage to liver glycogen during feeding and acute fasting by inducing Gys2 PTG and G L expression*. Mol Metab, 2013. **2**(3): p. 292–305.
54. Lamia, K.A., et al., *Cryptochromes mediate rhythmic repression of the glucocorticoid receptor*. Nature, 2011. **480**(7378): p. 552–556.
55. Barclay, J.L., et al., *High-fat diet-induced hyperinsulinemia and tissue-specific insulin resistance in Cry-deficient mice*. American Journal of Physiology–Endocrinology and Metabolism, 2013. **304**(10): p. E1053–E1063.
56. Jang, H., et al., *SREBP1c-CRY1 signalling represses hepatic glucose production by promoting FOXO1 degradation during refeeding*. Nat Commun, 2016. **7**: p. 12180.
57. Kim, Y.Y., et al., *Hepatic GSK3beta-Dependent CRY1 Degradation Contributes to Diabetic Hyperglycemia*. Diabetes, 2022. **71**(7): p. 1373–1387.
58. Cho, H., et al., *Regulation of circadian behaviour and metabolism by REV-ERB- $\alpha$  and REV-ERB- $\beta$* . Nature, 2012. **485**(7396): p. 123–127.
59. Delezie, J., et al., *The nuclear receptor REV-ERB $\alpha$  is required for the daily balance of carbohydrate and lipid metabolism*. The FASEB Journal, 2012. **26**(8): p. 3321–3335.
60. Griffin, E.A., Jr., D. Staknis, and C.J. Weitz, *Light-independent role of CRY1 and CRY2 in the mammalian circadian clock*. Science, 1999. **286**(5440): p. 768–771.
61. Kume, K., et al., *mCRY1 and mCRY2 are essential components of the negative limb of the circadian clock feedback loop*. Cell, 1999. **98**(2): p. 193–205.
62. van der Horst, G.T., et al., *Mammalian Cry1 and Cry2 are essential for maintenance of circadian rhythms*. Nature, 1999. **398**(6728): p. 627–30.
63. Koike, N., et al., *Transcriptional Architecture and Chromatin Landscape of the Core Circadian Clock in Mammals*. Science, 2012. **338**(6105): p. 349–354.
64. Vitaterna, M.H., et al., *Differential regulation of mammalian period genes and circadian rhythmicity by cryptochromes 1 and 2*. Proceedings of the National Academy of Sciences, 1999. **96**(21): p. 12114–12119.
65. Anand, S.N., et al., *Distinct and separable roles for endogenous CRY1 and CRY2 within the circadian molecular clockwork of the suprachiasmatic nucleus, as revealed by the Fbxl3(Afh) mutation*. J Neurosci, 2013. **33**(17): p. 7145–53.
66. Zhu, H., F. Conte, and C.B. Green, *Nuclear localization and transcriptional repression are confined to separable domains in the circadian protein CRYPTOCHROME*. Current Biology, 2003. **13**(18): p. 1653–1658.
67. Khan, S.K., et al., *Identification of a novel cryptochrome differentiating domain required for feedback repression in circadian clock function*. Journal of Biological Chemistry, 2012. **287**(31): p. 25917–25926.

68. Chaves, I., et al., *Functional evolution of the photolyase/cryptochrome protein family: importance of the C terminus of mammalian CRY1 for circadian core oscillator performance*. *Molecular and cellular biology*, 2006. **26**(5): p. 1743-1753.
69. Shafi, A.A., et al., *The circadian cryptochrome, CRY1, is a pro-tumorigenic factor that rhythmically modulates DNA repair*. *Nature Communications*, 2021. **12**(1): p. 401.
70. Correia, S.P., et al., *The circadian E3 ligase complex SCF(FBXL3+CRY) targets TLK2*. *Sci Rep*, 2019. **9**(1): p. 198.
71. Narasimamurthy, R., et al., *Circadian clock protein cryptochrome regulates the expression of proinflammatory cytokines*. *Proceedings of the National Academy of Sciences*, 2012. **109**(31): p. 12662-12667.
72. Toledo, M., et al., *Autophagy Regulates the Liver Clock and Glucose Metabolism by Degrading CRY1*. *Cell Metab*, 2018.
73. Zhang, E.E., et al., *Cryptochrome mediates circadian regulation of cAMP signaling and hepatic gluconeogenesis*. *Nat Med*, 2010. **16**(10): p. 1152-6.
74. Lamia, K.A., et al., *Cryptochromes mediate rhythmic repression of the glucocorticoid receptor*. *Nature*, 2011. **480**(7378): p. 552-6.
75. Okano, S., et al., *Non-obese early onset diabetes mellitus in mutant cryptochrome1 transgenic mice*. *Eur J Clin Invest*, 2010. **40**(11): p. 1011-7.
76. Leszek, S., *Glucose Homeostasis*, in *Gluconeogenesis*, Z. Weizhen, Editor. 2017, IntechOpen: Rijeka. p. Ch. 2.
77. Rines, A.K., et al., *Targeting hepatic glucose metabolism in the treatment of type 2 diabetes*. *Nat Rev Drug Discov*, 2016. **15**(11): p. 786-804.
78. Postic, C., R. Dentin, and J. Girard, *Role of the liver in the control of carbohydrate and lipid homeostasis*. *Diabetes Metab*, 2004. **30**(5): p. 398-408.
79. Hatting, M., et al., *Insulin regulation of gluconeogenesis*. *Ann N Y Acad Sci*, 2018. **1411**(1): p. 21-35.
80. Ramnanan, C.J., et al., *Physiologic action of glucagon on liver glucose metabolism*. *Diabetes Obes Metab*, 2011. **13 Suppl 1**(Suppl 1): p. 118-25.
81. Oh, K.-J., et al., *Transcriptional regulators of hepatic gluconeogenesis*. *Archives of Pharmacal Research*, 2013. **36**(2): p. 189-200.
82. Brunet, A., et al., *Akt promotes cell survival by phosphorylating and inhibiting a Forkhead transcription factor*. *Cell*, 1999. **96**(6): p. 857-68.
83. Mihaylova, M.M., et al., *Class IIa histone deacetylases are hormone-activated regulators of FOXO and mammalian glucose homeostasis*. *Cell*, 2011. **145**(4): p. 607-21.
84. Accili, D. and K.C. Arden, *FoxOs at the crossroads of cellular metabolism, differentiation, and transformation*. *Cell*, 2004. **117**(4): p.

- 421-6.
85. Magnusson, I., et al., *Increased rate of gluconeogenesis in type II diabetes mellitus. A 13C nuclear magnetic resonance study.* J Clin Invest, 1992. **90**(4): p. 1323-7.
  86. Consoli, A., et al., *Predominant role of gluconeogenesis in increased hepatic glucose production in NIDDM.* Diabetes, 1989. **38**(5): p. 550-7.
  87. Rizza, R.A., *Pathogenesis of fasting and postprandial hyperglycemia in type 2 diabetes: implications for therapy.* Diabetes, 2010. **59**(11): p. 2697-707.
  88. Altomonte, J., et al., *Inhibition of Foxo1 function is associated with improved fasting glycemia in diabetic mice.* Am J Physiol Endocrinol Metab, 2003. **285**(4): p. E718-28.
  89. Valera, A., et al., *Transgenic mice overexpressing phosphoenolpyruvate carboxykinase develop non-insulin-dependent diabetes mellitus.* Proc Natl Acad Sci U S A, 1994. **91**(19): p. 9151-4.
  90. Cannon, B. and J. Nedergaard, *Brown adipose tissue: function and physiological significance.* Physiological reviews, 2004.
  91. Emont, M.P., D.I. Kim, and J. Wu, *Development, activation, and therapeutic potential of thermogenic adipocytes.* Biochim Biophys Acta Mol Cell Biol Lipids, 2019. **1864**(1): p. 13-19.
  92. Jeon, Y.G., et al., *Physiological and pathological roles of lipogenesis.* Nature Metabolism, 2023. **5**(5): p. 735-759.
  93. Lee, P., et al., *Temperature-Acclimated Brown Adipose Tissue Modulates Insulin Sensitivity in Humans.* Diabetes, 2014. **63**(11): p. 3686-3698.
  94. Chondronikola, M., et al., *Brown Adipose Tissue Improves Whole-Body Glucose Homeostasis and Insulin Sensitivity in Humans.* Diabetes, 2014. **63**(12): p. 4089-4099.
  95. Pagliarini, D.J. and J. Rutter, *Hallmarks of a new era in mitochondrial biochemistry.* Genes Dev, 2013. **27**(24): p. 2615-27.
  96. Willis, E.J., *The powerhouse of the cell.* Ultrastruct Pathol, 1992. **16**(3): p. iii-vi.
  97. Wang, X., *The expanding role of mitochondria in apoptosis.* Genes Dev, 2001. **15**(22): p. 2922-33.
  98. Green, D.R., L. Galluzzi, and G. Kroemer, *Mitochondria and the autophagy-inflammation-cell death axis in organismal aging.* Science, 2011. **333**(6046): p. 1109-12.
  99. Boudina, S. and T.E. Graham, *Mitochondrial function/dysfunction in white adipose tissue.* Exp Physiol, 2014. **99**(9): p. 1168-78.
  100. Enerbäck, S., *The origins of brown adipose tissue.* New England Journal of Medicine, 2009. **360**(19): p. 2021-2023.
  101. Forner, F., et al., *Proteome differences between brown and white fat mitochondria reveal specialized metabolic functions.* Cell Metab, 2009. **10**(4): p. 324-35.
  102. Nicholls, D.G., *Stoichiometries of proton translocation by mitochondria.* Biochem Soc Trans, 1977. **5**(1): p. 200-3.
  103. Picca, A., et al., *Mitochondrial quality control mechanisms as*

- molecular targets in cardiac ageing*. Nature Reviews Cardiology, 2018. **15**(9): p. 543–554.
104. Aquilano, K., et al., *Multifaceted mitochondrial quality control in brown adipose tissue*. Trends in Cell Biology, 2022.
  105. Lee, J.H., et al., *The Role of Adipose Tissue Mitochondria: Regulation of Mitochondrial Function for the Treatment of Metabolic Diseases*. Int J Mol Sci, 2019. **20**(19).
  106. Chouchani, E.T., et al., *Mitochondrial ROS regulate thermogenic energy expenditure and sulfenylation of UCP1*. Nature, 2016. **532**(7597): p. 112–116.
  107. Lettieri-Barbato, D., *Redox control of non-shivering thermogenesis*. Molecular metabolism, 2019. **25**: p. 11–19.
  108. Wikstrom, J.D., et al., *Hormone-induced mitochondrial fission is utilized by brown adipocytes as an amplification pathway for energy expenditure*. The EMBO journal, 2014. **33**(5): p. 418–436.
  109. Pisani, D.F., et al., *Mitochondrial fission is associated with UCP1 activity in human brite/beige adipocytes*. Molecular metabolism, 2018. **7**: p. 35–44.
  110. Mahdaviani, K., et al., *Mfn2 deletion in brown adipose tissue protects from insulin resistance and impairs thermogenesis*. EMBO reports, 2017. **18**(7): p. 1123–1138.
  111. Pereira, R.O., et al., *OPA1 deletion in brown adipose tissue improves thermoregulation and systemic metabolism via FGF21*. Elife, 2021. **10**: p. e66519.
  112. Bean, C., et al., *The mitochondrial protein Opa1 promotes adipocyte browning that is dependent on urea cycle metabolites*. Nature metabolism, 2021. **3**(12): p. 1633–1647.
  113. Quirós, P.M., et al., *Loss of mitochondrial protease OMA1 alters processing of the GTPase OPA1 and causes obesity and defective thermogenesis in mice*. The EMBO journal, 2012. **31**(9): p. 2117–2133.
  114. Lu, Y., et al., *Mitophagy is required for brown adipose tissue mitochondrial homeostasis during cold challenge*. Scientific Reports, 2018. **8**(1): p. 1–13.
  115. Yau, W.W., et al., *Chronic cold exposure induces autophagy to promote fatty acid oxidation, mitochondrial turnover, and thermogenesis in brown adipose tissue*. Iscience, 2021. **24**(5): p. 102434.
  116. Son, Y., et al., *Adipocyte-specific Beclin1 deletion impairs lipolysis and mitochondrial integrity in adipose tissue*. Molecular metabolism, 2020. **39**: p. 101005.
  117. Cai, J., et al., *Autophagy ablation in adipocytes induces insulin resistance and reveals roles for lipid peroxide and Nrf2 signaling in adipose-liver crosstalk*. Cell reports, 2018. **25**(7): p. 1708–1717. e5.
  118. Cairó, M., et al., *Parkin controls brown adipose tissue plasticity in response to adaptive thermogenesis*. EMBO reports, 2019. **20**(5): p. e46832.
  119. Lin, H.V. and D. Accili, *Hormonal regulation of hepatic glucose*

- production in health and disease*. Cell Metab, 2011. **14**(1): p. 9–19.
120. Summers, S.A. and M.J. Birnbaum, *A role for the serine/threonine kinase, Akt, in insulin-stimulated glucose uptake*. Biochem Soc Trans, 1997. **25**(3): p. 981–8.
121. Perry, R.J., et al., *The role of hepatic lipids in hepatic insulin resistance and type 2 diabetes*. Nature, 2014. **510**(7503): p. 84–91.
122. Lu, M., et al., *Insulin regulates liver metabolism in vivo in the absence of hepatic Akt and Foxo1*. Nat Med, 2012. **18**(3): p. 388–95.
123. Oishi, K., et al., *Disrupted fat absorption attenuates obesity induced by a high-fat diet in Clock mutant mice*. FEBS Lett, 2006. **580**(1): p. 127–30.
124. Gatfield, D. and U. Schibler, *Physiology. Proteasomes keep the circadian clock ticking*. Science, 2007. **316**(5828): p. 1135–6.
125. Reinke, H. and G. Asher, *Crosstalk between metabolism and circadian clocks*. Nat Rev Mol Cell Biol, 2019.
126. Tong, X., et al., *DDB1-Mediated CRY1 Degradation Promotes FOXO1-Driven Gluconeogenesis in Liver*. Diabetes, 2017. **66**(10): p. 2571–2582.
127. Jeon, Y.G., et al., *RNF20 Functions as a Transcriptional Coactivator for PPARgamma by Promoting NCoR1 Degradation in Adipocytes*. Diabetes, 2020. **69**(1): p. 20–34.
128. Krueger, F., *Trim galore*. A wrapper tool around Cutadapt and FastQC to consistently apply quality and adapter trimming to FastQ files, 2015. **516**(517).
129. Kim, D., B. Langmead, and S.L. Salzberg, *HISAT: a fast spliced aligner with low memory requirements*. Nat Methods, 2015. **12**(4): p. 357–60.
130. Pertea, M., et al., *Transcript-level expression analysis of RNA-seq experiments with HISAT, StringTie and Ballgown*. Nat Protoc, 2016. **11**(9): p. 1650–67.
131. Ritchie, M.E., et al., *limma powers differential expression analyses for RNA-sequencing and microarray studies*. Nucleic Acids Res, 2015. **43**(7): p. e47.
132. Xie, Z., et al., *Gene Set Knowledge Discovery with Enrichr*. Curr Protoc, 2021. **1**(3): p. e90.
133. Han, H., et al., *TRRUST v2: an expanded reference database of human and mouse transcriptional regulatory interactions*. Nucleic Acids Res, 2018. **46**(D1): p. D380–d386.
134. Cowen, L., et al., *Network propagation: a universal amplifier of genetic associations*. Nat Rev Genet, 2017. **18**(9): p. 551–562.
135. Ye, R., et al., *Dual modes of CLOCK:BMAL1 inhibition mediated by Cryptochrome and Period proteins in the mammalian circadian clock*. Genes Dev, 2014. **28**(18): p. 1989–98.
136. Park, J., et al., *Activation of invariant natural killer T cells stimulates adipose tissue remodeling via adipocyte death and birth in obesity*. Genes Dev, 2019. **33**(23–24): p. 1657–1672.
137. Ganz, M., et al., *Progression of non-alcoholic steatosis to steatohepatitis and fibrosis parallels cumulative accumulation of*

- danger signals that promote inflammation and liver tumors in a high fat-cholesterol-sugar diet model in mice.* J Transl Med, 2015. **13**: p. 193.
138. Busino, L., et al., *SCFFbx13 controls the oscillation of the circadian clock by directing the degradation of cryptochrome proteins.* Science, 2007. **316**(5826): p. 900-4.
139. Skaar, J.R., J.K. Pagan, and M. Pagano, *Mechanisms and function of substrate recruitment by F-box proteins.* Nature Reviews Molecular Cell Biology, 2013. **14**: p. 369.
140. Hornbeck, P.V., et al., *PhosphoSitePlus, 2014: mutations, PTMs and recalibrations.* Nucleic Acids Res, 2015. **43**(Database issue): p. D512-20.
141. Obenauer, J.C., L.C. Cantley, and M.B. Yaffe, *Scansite 2.0: Proteome-wide prediction of cell signaling interactions using short sequence motifs.* Nucleic Acids Res, 2003. **31**(13): p. 3635-41.
142. Tubbs, E., et al., *Mitochondria-associated endoplasmic reticulum membrane (MAM) integrity is required for insulin signaling and is implicated in hepatic insulin resistance.* Diabetes, 2014. **63**(10): p. 3279-94.
143. Wang, X.X., et al., *Effects of octreotide on hepatic glycogenesis in rats with high fat diet-induced obesity.* Mol Med Rep, 2017. **16**(1): p. 109-118.
144. Wang, C., et al., *GPS 5.0: an update on the prediction of kinase-specific phosphorylation sites in proteins.* Genomics, Proteomics & Bioinformatics, 2020. **18**(1): p. 72-80.
145. Kelly, M.A., et al., *Circadian gene variants and susceptibility to type 2 diabetes: a pilot study.* PLoS One, 2012. **7**(4): p. e32670.
146. Wang, C., et al., *GPS 5.0: An Update on the Prediction of Kinase-specific Phosphorylation Sites in Proteins.* Genomics Proteomics Bioinformatics, 2020.
147. Kelly, M.A., et al., *Circadian gene variants and susceptibility to type 2 diabetes: a pilot study.* PLoS One, 2012. **7**(4): p. e32670.
148. Dashti, H.S., et al., *CRY1 circadian gene variant interacts with carbohydrate intake for insulin resistance in two independent populations: Mediterranean and North American.* Chronobiol Int, 2014. **31**(5): p. 660-7.
149. Chan, A.B., A.L. Huber, and K.A. Lamia, *Cryptochromes modulate E2F family transcription factors.* Sci Rep, 2020. **10**(1): p. 4077.
150. Guo, X., et al., *miR-181d and c-myc-mediated inhibition of CRY2 and FBXL3 reprograms metabolism in colorectal cancer.* Cell Death Dis, 2017. **8**(7): p. e2958.
151. Reischl, S. and A. Kramer, *Kinases and phosphatases in the mammalian circadian clock.* FEBS Lett, 2011. **585**(10): p. 1393-9.
152. Cline, G.W., et al., *Effects of a novel glycogen synthase kinase-3 inhibitor on insulin-stimulated glucose metabolism in Zucker diabetic fatty (fa/fa) rats.* Diabetes, 2002. **51**(10): p. 2903-10.
153. Norman, P., *Emerging fundamental themes in modern medicinal chemistry.* Drug News Perspect, 2001. **14**(4): p. 242-7.

154. Cohen, P. and M. Goedert, *GSK3 inhibitors: development and therapeutic potential*. Nat Rev Drug Discov, 2004. **3**(6): p. 479–87.
155. Horike, N., et al., *AMP-activated protein kinase activation increases phosphorylation of glycogen synthase kinase 3beta and thereby reduces cAMP-responsive element transcriptional activity and phosphoenolpyruvate carboxykinase C gene expression in the liver*. J Biol Chem, 2008. **283**(49): p. 33902–10.
156. Liu, H., et al., *Wnt signaling regulates hepatic metabolism*. Sci Signal, 2011. **4**(158): p. ra6.
157. Riu, E., et al., *Overexpression of c-myc in the liver prevents obesity and insulin resistance*. Faseb j, 2003. **17**(12): p. 1715–7.
158. Rena, G., et al., *Two novel phosphorylation sites on FKHR that are critical for its nuclear exclusion*. Embo j, 2002. **21**(9): p. 2263–71.
159. Moore, M.C., et al., *Regulation of hepatic glucose uptake and storage in vivo*. Adv Nutr, 2012. **3**(3): p. 286–94.
160. Monzel, A.S., J.A. Enriquez, and M. Picard, *Multifaceted mitochondria: moving mitochondrial science beyond function and dysfunction*. Nature Metabolism, 2023. **5**(4): p. 546–562.
161. Kajimura, S., B.M. Spiegelman, and P. Seale, *Brown and beige fat: physiological roles beyond heat generation*. Cell metabolism, 2015. **22**(4): p. 546–559.
162. Kwok, K.H., K.S. Lam, and A. Xu, *Heterogeneity of white adipose tissue: molecular basis and clinical implications*. Experimental & molecular medicine, 2016. **48**(3): p. e215–e215.
163. Ricquier, D. and F. BOUILLAUD, *The uncoupling protein homologues: UCP1, UCP2, UCP3, StUCP and AtUCP*. Biochemical Journal, 2000. **345**(2): p. 161–179.
164. Saltykova, M.M., *Cold Adaptation as a Means of Increasing Antioxidant Protection*. Neuroscience and Behavioral Physiology, 2019. **49**(3): p. 323–330.
165. Reddy, A.B. and J.S. O'Neill, *Healthy clocks, healthy body, healthy mind*. Trends in Cell Biology, 2010. **20**(1): p. 36–44.
166. McGinnis, G.R. and M.E. Young, *Circadian regulation of metabolic homeostasis: causes and consequences*. Nat Sci Sleep, 2016. **8**: p. 163–80.
167. Stenvers, D.J., et al., *Circadian clocks and insulin resistance*, in *Nat Rev Endocrinol*. 2018.
168. Douma, L.G. and M.L. Gumz, *Circadian clock-mediated regulation of blood pressure*. Free radical biology and medicine, 2018. **119**: p. 108–114.
169. Huh, J.Y., et al., *TANK-Binding Kinase 1 Regulates the Localization of Acyl-CoA Synthetase ACSL1 to Control Hepatic Fatty Acid Oxidation*. Cell Metab, 2020. **32**(6): p. 1012–1027 e7.
170. Hwang, I., et al., *GABA-stimulated adipose-derived stem cells suppress subcutaneous adipose inflammation in obesity*. Proc Natl Acad Sci U S A, 2019. **116**(24): p. 11936–11945.
171. Ma, K., et al., *Mitophagy, Mitochondrial Homeostasis, and Cell Fate*. Front Cell Dev Biol, 2020. **8**: p. 467.

172. Narendra, D., et al., *Parkin is recruited selectively to impaired mitochondria and promotes their autophagy*. J Cell Biol, 2008. **183**(5): p. 795–803.
173. Li, Y., et al., *Secretin-Activated Brown Fat Mediates Prandial Thermogenesis to Induce Satiation*. Cell, 2018. **175**(6): p. 1561–1574.e12.
174. Geisler, S., et al., *PINK1/Parkin-mediated mitophagy is dependent on VDAC1 and p62/SQSTM1*. Nature Cell Biology, 2010. **12**(2): p. 119–131.
175. Benard, G., et al., *Mitochondrial bioenergetics and structural network organization*. Journal of cell science, 2007. **120**(5): p. 838–848.
176. Mason, I.C., et al., *Impact of circadian disruption on glucose metabolism: implications for type 2 diabetes*. Diabetologia, 2020. **63**(3): p. 462–472.
177. Jang, H., G. Lee, and J.B. Kim, *SREBP1c-CRY1 axis suppresses hepatic gluconeogenesis upon insulin*. Cell Cycle, 2017. **16**(2): p. 139–140.
178. Ngo, K.A., et al., *Dissecting the Regulatory Strategies of NF-kappaB RelA Target Genes in the Inflammatory Response Reveals Differential Transactivation Logics*. Cell Rep, 2020. **30**(8): p. 2758–2775 e6.
179. Wu, G. and E.P. Spalding, *Separate functions for nuclear and cytoplasmic cryptochrome 1 during photomorphogenesis of Arabidopsis seedlings*. Proc Natl Acad Sci U S A, 2007. **104**(47): p. 18813–8.
180. Liu, S., et al., *Differential photoregulation of the nuclear and cytoplasmic CRY1 in Arabidopsis*. New Phytologist, 2022. **234**(4): p. 1332–1346.
181. Liu, C., et al., *Molecular evolution and functional divergence of zebrafish (Danio rerio) cryptochrome genes*. Scientific Reports, 2015. **5**(1): p. 8113.
182. Liu, N. and E.E. Zhang, *Phosphorylation Regulating the Ratio of Intracellular CRY1 Protein Determines the Circadian Period*. Front Neurol, 2016. **7**: p. 159.
183. Yoo, S.H., et al., *Competing E3 ubiquitin ligases govern circadian periodicity by degradation of CRY in nucleus and cytoplasm*. Cell, 2013. **152**(5): p. 1091–105.
184. Kobayashi, K., et al., *Characterization of photolyase/blue-light receptor homologs in mouse and human cells*. Nucleic Acids Res, 1998. **26**(22): p. 5086–92.

## 국문 초록

말초조직의 생체시계는 다양한 외부 자극에 의해 조절되며, 각 조직 특이적인 생체리듬 생산 및 전신적 에너지 항상성을 유지하는 데 증추적인 역할을 수행한다. 일주기 생체리듬의 조절장애는 비만, 인슐린 저항성 및 심혈관 질환과 같은 대사증후군과 밀접하게 연관되어 있으며, 이에 대한 기전연구가 활발히 진행되고 있다. 최근, 다양한 자극에 의한 생체 리듬변화와 미토콘드리아의 양적 기능적 변화와의 상관관계가 보고되고 있다. 그럼에도 불구하고, 생체시계 조절인자에 의한 대사질환 발병 기전 및 미토콘드리아 항상성 조절 기전 연구는 부족한 상황이다.

본 연구에서 연구자는 생체시계 조절인자 중 하나인 Cryptochrome 1 (CRY1)의 말초 조직에서의 에너지 대사 조절 역할을 조사하였다. 1장에서는 간 조직 내 CRY1 단백질의 조절이상인 과도한 포도당 신생과정을 유발하여 고혈당증을 야기하며 당뇨병의 병인임을 규명하였다. CRY1은 섭식 및 인슐린에 반응하여 포도당 신생과정의 주요 전사인자인 forkhead box O1 (FOXO1) 분해를 촉진함으로써 간 조직에서 포도당 신생과정을 제어한다. 본 학위 논문연구 동안 본인은 당뇨병 동물모델에서 증가한 간 조직 내 F-box and leucine-rich repeat protein 3 (FBXL3) E3 유비퀴틴 라이게이즈는 CRY1의 분해를 촉진하여 과도한 포도당 신생과정을 유도함을 발견하였다. 또한, 당뇨병 생쥐 모델의 간조직에서 GSK3 $\beta$ 에 의한 CRY1 단백질 과잉 인산화는 FBXL3 의존적 CRY1 단백질 분해를 촉진함으로써 포도당 신생과정이 촉진되어 고혈당증을 초래하였다. 이러한 결과들은 GSK3 $\beta$ -CRY1-FBXL3 축이 CRY1 단백질 이상 조절 및 고혈당증의 원인 중 하나일 수 있음을 의미한다.

2장에서는 CRY1에 의한 미토콘드리아 항상성조절을 통한 갈색지방조

직의 열 생성 조절 기전을 연구하였다. CRY1 결핍된 배아 섬유아세포와 갈색지방조직에서 미토콘드리아의 양적 감소 및 기능 저하를 관찰하였다. 특히, CRY1 결손에 의한 손상 미토콘드리아의 자가포식 (mitophagy) 과정이 촉진됨을 발견하였다. 갈색지방조직에 CRY1을 과발현시킨 경우 미토콘드리아의 양이 증가하며 결과적으로 열 생성능이 증가됨을 관찰하였다. 이상의 결과들은 CRY1에 의한 미토콘드리아 항상성 조절이 갈색지방조직에서 열 생성능 유지에 필수적임을 제안한다.

이상의 연구를 종합하여 볼 때, CRY1은 간 조직의 포도당 신생과정 조절 및 갈색지방조직의 미토콘드리아 항상성 유지기전을 통해 체내 에너지 대사 조절에 중요한 조절인자임을 제안하며, 이들 결과는 생체시계 조절자인 CRY1이 생체리듬 조절 기능 외에 새로운 CRY1 기능을 제안함으로써 에너지 대사 대한 이해를 넓히는 지식의 초석이 될 수 있을 것이라 사료한다.

주요어: 에너지 항상성, 생체 시계, 생체 리듬, 포도당 신생과정, 갈색지방조직, 열생성, CRY1, 미토콘드리아 항상성.

학번: 2016-20377